D37799'81

IV

THE SPECTRA OF MANGANESE
AND ZIRCONIUM IN THE WAVELENGTH
REGION 0.8 μm - 2.6 μm

A THESIS SUBMITTED TO THE COUNCIL FOR
NATIONAL ACADEMIC AWARDS FOR THE
DEGREE OF DOCTOR OF PHILOSOPHY

BY

A.G. TAKLIF, M.Sc., M.Phil.

DEPARTMENT OF PHYSICS,

OCTOBER 1980   POLYTECHNIC OF NORTH LONDON.

THE SPECTRA OF MANGANESE AND ZIRCONIUM IN THE WAVELENGTH REGION 0.8 μm - 2.6 μm

A.G. TAKLIF

October, 1980

A B S T R A C T

Using electrodeless discharge tube sources, and a 1.5 m vacuum Ebert mounting spectrometer, the spectrum of manganese in the wavelength region 0.82 - 1.97 μm, and additional wavelengths of zirconium weak lines in spectral range of 0.8 - 2.7 μm have been measured.

The application of the equipment and instruments used are described. A general description of the Fabry-Perot interferometer as a calibrating system is given.

A description of the general method by which the electrodeless discharge tubes (EDT's) were manufactured is given. Some of the work has been concentrated on the preparation of the EDT's containing zirconium and manganese halides. Efforts were made on achieving new methods of preparing tubes containing less volatile elements such as manganese. This involved new design of material containers used inside the reaction line as well as some changes in the reaction system used in the preparation of the tube.

Investigations into the phenomenon of Zeeman effect are discussed, the results of which are then presented using zirconium electrodeless discharge tubes. In this investigation, Zeeman patterns were scanned using Fabry-Perot interferometer as a pressure-scanning spectrometer, and infrared Ebert mounting grating spectrometer as a monochromator. Values are given for 22 lines involving different multiplets.

218 manganese lines have been measured in the range 0.8 - 1.97 μm; of these, 84 have been identified by the transitions involving energy levels of neutral manganese atom.

Vacuum wavenumbers of 181 additional zirconium lines in the spectral range 0.78 - 1.36 μm and 1.77 - 2.7 μm have been measured. These have been compared with the predicted spectral lines from neutral zirconium energy levels and transitions assigned to 79 lines.

22 lines were studied for Zeeman effect; the analysis of the results confirmed the level 15932.10 cm^{-1} listed in MnI energy level list to be $^3P_1$ and not b^3P_2. A new level, 15624.31 cm^{-1}(b^3P_0) was also calculated and 5 new Landé g factors have been observed.

ACKNOWLEDGEMENT

My thanks to my supervisor, Dr. E.B.M. Steers, for his useful discussion during the course of this project and help in the production of the discharge tubes, and to Dr. M. Outred and to all those in the Physics Department. I would like to thank my fellow student Howard and my typist, Mrs. S. Conboy, for their help in the production of the thesis.

C O N T E N T S

vi.

LIST OF TABLES

LIST OF ILLUSTRATIONS

CHAPTER 1

INTRODUCTION AND LITERATURE SURVEY

1-1 Introduction

In 1976 a research project was carried out by the author to experimentally measure the infra-red spectrum of zirconium. 490 neutral zirconium lines were observed over the range 0.79 - 2.71 μm which are listed in the author's Thesis[1]. The measurements were then included in the infra-red tables of atomic lines for 10000 - 40000 $\mathring{A}$ region published by The National Bureau of Standards[2].

The above measured lines were compared with lines predicted from the known levels, and transitions assigned to two hundred and seventy-two lines. The majority agreed well with predicted values.

In the present project the same techniques were used to carry out preliminary measurements on the infra-red spectrum of manganese and to measure additional weaker lines in zirconium and, by a minor modification in the optical system, to observe zeeman effect on certain infra-red lines of zirconium spectrum.

1

1-2 Microwave-excited light sources

To obtain accurate result in wavelength measurements the line profiles should be as narrow as possible and symmetrical. This can be achieved by using a high resolution spectrometer, choosing a type of source which produces intense light with sharp lines, using a sensitive detecting instrument and introducing sharp and symmetric standard lines as a reference in the calibrating system.

This project has been carried out using microwave excited light sources as a modern source which promotes the emission of neutral atom radiation where it is used. The electrodeless discharge tubes (EDTs) were demonstrated by Meggers and Westfall in 1950[3] for mercury and by Corliss and Meggers in 1958[4] for hafnium. Meggers and Stanley[5] then measured the wavelengths of the lines in the thorium spectrum in region 3287.788 Å to 6989.656 Å emitted by a tube containing thorium iodide in 1958.

Electrodeless discharge tubes are intense[6], stable and long life light sources which can be constructed containing only a few milligram of the material under investigation. These tubes produce sharp lines specially important for observing first spectra in strong magnetic field and ideal for accurate measurement of wavenumbers in infra-red region.

2

Prior to 1950, before the introduction of electrodeless discharge tubes, d.c. arcs and high voltage sparks were the only conventional light sources used in the study of the atomic structure by observing the complex spectra of the atom. Arc has a high temperature and the high pressure and electric field associated with arc will cause considerable broadening and line shifting. These light sources may provide suitable sources when the procedure of recording is photographic but when a scanning procedure is in operation the arc wandering is a major problem in recording the signals. The strong background and continuous molecular band associated with arcs will mask the faint lines of interest.

Detail of tube preparation will be given in Chapter 2 and it will be fully discussed how the difficulties of manufacturing manganese halide tube were overcome. Manganese iodide is a less volatile material, and the sublimation of this halide during the procedure caused a great problem at the beginning, but with some alteration in the method of preparation it was possible to prepare manganese electrodeless discharge tube.

Zirconium iodide and thorium iodide tubes were prepared in the conventional way as discussed in Chapter 2. Fourteen zirconium tube, six manganese, and two thorium tube were prepared by Dr. Steers and the author to be used in present project.

3

1-3 Infra-red spectrum of manganese

The main interest in present measurement of the manganese spectrum in infra-red region is to extend the observations into spectral regions not covered by earlier work of the other investigators. The information obtained can be used to further the progress in the analysis of the MnI spectrum. The available information of manganese is based on the measurements made by different investigators using different dispersive devices. Therefore the available data has not been obtained in a uniform condition of experimental technique or a uniform condition of light source and hence the accuracy of the published term values may not be wholly consistent.

In 1949, a major advance in the analysis of MnI was reported by Olga Garcia-Riquelme[7] after assembling all known energy levels of MnI and compiling wavelength and intensity of manganese lines from spectroscopic papers by 15 different authors. Garcia-Riquelme found 58 new energy levels and 15 new terms for MnI. producing a total of 30 even terms (85 levels), 30 odd terms (124 levels). The permitted transitions between these levels account for 711 observed lines ranging in wavelength from 1876.48 Å to 17607.5 Å.

Earlier, Meggers (1933)[8] had detected one quartet and two sextet terms in observations of near infra-red spectra.

Randall and Barker (1919)[9] observed 16 infra-red lines in region 12900 Å to 17608 Å, emitted by arcs and detected with a thermopile detector. The observation by Randal and Barker covers only a limited number of very strong infra-red lines of manganese, since the technique used to detect the signals was not able to detect the weak lines. The method of detection (thermopile) was insensitive, therefore a wide open slit was needed in order to detect the signals, and a wide slit will reduce the resolving power of the dispersive instrument. The accuracy of these sixteen lines are low and whereas the wavenumbers are quoted to 0.1 cm^{-1} the error will exceed the value of 0.1 cm^{-1} and a value of 1 cm^{-1} may be present.

In 1952, the total number of even levels identified had increased to 118 and odd levels to 217, and the number of classified lines to 1500[10]. By 1962 the total number of levels had risen to 404 and the lines classified by Garcia-Riquelm[11] exceeded 2000.

The first spectrum of manganese, MnI, published by Catalon, Meggers, and Garcia-Riquelme (1964)[12], covers information for more than 2030 lines in wavelength from 1785 Å - 17608 Å. In 1977 the compilation of energy levels of the manganese atom in all of its stages of ionization by Corliss and Sugar[13] used the above data in its entirety for MnI levels.

The new data obtained in present observation of infra-red spectrum of manganese is tabulated in the line

5

list of Chapter 5. The line list represents about 220
new lines in region 0.82 to 1.97μ m. These have been
compared with predicted lines from the known energy levels
and transitions assigned to 84 lines. Eighty four new
lines were observed in region 1.29 to 1.97 μ m in
addition to 14 of the sixteen strong lines recorded
previously in this region of neutral manganese atom.
The number of lines assigned to the known energy levels
in this region are 39 for the new lines.

It is given in literature[12] that the relatively
light atomic weight of manganese and the high temperature
associated with the arc of this element may cause the
arc source of manganese to produce broad lines. In
present work the broadening of the lines was also apparent.
Manganese shows very pronounced multiplets with wide
range of fine structure intervals. There are many terms
with fine structure intervals of less than 1 cm^{-1} and
some levels show pronounced hyperfine structure which
may approach the same value giving a very complicated
structure which is difficult to resolve. Examples of
these lines are given in Chapter 5.

Meggers (1931)[14] gives an indication of band
appearance in the arc spectrum of manganese in region
8901 $\overset{o}{A}$ to 10561 $\overset{o}{A}$, which is expected from an arc source
at atmospheric pressure and high temperature to produce
a metalic oxide. In present work also a repeated pattern
of group of lines have been seen which are confined to
a limited spectrum band width of 23.2 nm in region

10260 Å to 10492.7 Å (vacuum wavelength), and there are
a suspicious of band structure which discussed in
Chapter 5.

The accuracy of the lines measured will be discussed
in Chapter 5. The transitions assigned confirmed strong
L – S coupling; the majority of the strong lines
involved no change in S; although a few lines have been
assigned to the transitions involving a change in spin,
these are almost weak lines and less certain. Two
complete multiplet arrays is given in Chapter 5 with
good agreements of multiplet intervals which supports
the accuracy of the measurements.

1-4 Infra-red spectrum of zirconium

In 1931 C.C. Kiess and H.K. Kiess[15] measured
1600 spectral lines of zirconium in range 2088.89 Å
and 9276.94 Å using an arc at atmospheric pressure as a
light source. These lines were used in the analysis of
neutral and first 3 ionized states of zirconium atom.
In 1932 Meggers and Kiess[16] extended the observation
to 10738.94 Å. Kiess and Lang[17] carried the analysis
of doubly and tribly ionized zirconium to the extreme
ultra violet. Harrison[18] observed the spectrum of
zirconium independently which, the results are given in
MIT tables of wavelength in the range 12233.48 Å to
12583.69 Å. Howe (1957)[19] remeasured the zirconium
spectrum in the range 6100 Å and 6497.92 Å and

7

contributed 224 new lines to the existing list of the zirconium lines. Howe used a microwave excited discharge tube (EDT's) as a source and existing measured arc lines of zirconium as standard lines.

The above measurements in the photographic region were the only existing data for the analysis of zirconium and no information in infra-red region was available before the author's observation in infra-red spectrum of zirconium in 1976[1].

In the current work, further measurements of the infra-red spectrum of zirconium were carried out for two reasons:-

1) to check the accuracy of the previous work in 1976, and to find out if any improvement can be achieved in present measurement.

2) to measure the wavenumber of the additional weak lines which were excluded from the previous results.

Some improvements have been made in the system of signal detection, the optical system of light source have been altered and fresh tubes have been prepared. The full details of these changes are given in Chapter 3 and of the preparation of the tubes is given in Chapter 2.

The discussion of measurement of infra-red spectrum of zirconium is given in Chapter 6 and the results obtained are listed in table 6-1 in the same Chapter. In this part of the work the zirconium light source and thorium light source (standard light source) were also interchanged in different recordings to investigate the effect of light collimation on the results.

1-5 Zeeman pattern of zirconium lines

The significance of zeeman effect was realised when the method of quantum theory was applicable in the interpretation of the effect. The important quantum numbers of both the levels involved in a given transition can be derived from the observation of zeeman effect for that transition, providing that all the components of the pattern are resolved. It is now apparent that the zeeman effect is almost vital importance in the analysis of more complex spectra.

The available information about analysis of zirconium is dating round 1932 in the photographic region. In 1931 C.C. Kiess and H.K. Kiess[20] carried out the observation of zeeman pattern to confirm the classification of the observed 1600 zirconium lines in spectrum between 2088.89 $\overset{o}{A}$ and 9276.94 $\overset{o}{A}$. P.M. Sancho (1932)[21] employed zeeman analysis to observe g values (magnetic splitting factor) of zirconium energy levels. No previous zeeman measurements have been made in the infra-

red region.

In present work a pressure scanning Fabry-Perot
interferometer (FPI) previously used by A. Reed for
line-width measurements in hollow cathodes was adapted
to record the zeeman pattern of selected infra-red lines
of zirconium spectrum. It has been used in this project
in conjunction with the grating instrument (1.5 m Ebert
mounting grating) as a monochromator. The monochromator
isolated the line being studied from the closest line of
comparable intensity emitted by the light source.
Jacquinot [22] has shown that the axially symmetric
interferometer used as spectrometer can have many times
the luminosity of grating spectrometer operating at the
same resolving power; alternatively a much higher
resolving power can be obtained with the same luminosity.
Luminosity is proportional to the area of the cross
section of the outgoing beam and the solid angle Ω
associated with the resolving power

$$\text{Luminosity} = S \, \Omega \, \tau \qquad (1\text{-}1)$$

where   S   is the surface area of the plates.

         Ω is the solid angle limited by the
                 focal diaphragm.

         τ is the transmission factor.

10

R. Beer and J. Ring in 1961[23] used a high
pressure scanning Fabry-Perot interferometer for the
investigation of isotope shifts from the 5254 cm^{-1} line
of U^{238} and hyperfine structure of some Am^{241} lines.
In this investigation they demonstrated that a gain in
luminosity of at least fifty was possible in the infra-
red region.

A large number of lines were listed to be studied in
the zeeman analysis, but most of these lines were above
1.45 μ and owing to restricted wavelength range for
high reflectivity with multilayer plates of the Fabry-
Perot, it was not possible to achieve a satisfactory
results for the lines above this wavelength. Metal
coated plates were first used to observe the zeeman
pattern but low reflectivity and high absorptivity led
to a low light through-put and only trends could be
observed. Later two sets of multilayer dielectric
coated plates with high reflectivity were available to
give an overall bandwidth of about 0.48 μ (0.97 – 1.25 μ
and 1.25 – 1.45 μ). Twenty-two lines were included
in this bandwidth which could be resolved into components
in a magnetic field. The number of lines recorded in
this bandwidth was limited by the available intensity
in the measured infra-red region. Values are given for
22 lines which involve different configurations and are
used to calculate Landé g-factors for the levels

involved to assign transitions and to identify levels.
Results and details of procedure are given in Chapter 7.

CHAPTER 2

ELECTRODELESS DISCHARGE TUBE

2-1 Introduction

Some of the work has been concentrated on the
preparation of the microwave excited electrodeless
discharge tubes (EDTs) containing materials under
investigation in present project. It was mentioned in
previous chapter this project consists of three differ-
ent investigations:

1) measurement of infra-red spectrum of manganese

2) re-measurement of infra-red spectrum of
   zirconium

3) application of pressure scanning of Fabry-Perot
   interferometer in zeeman effect investigation
   of certain infra-red lines of zirconium spectrum.

These investigations can only be carried out in
infra-red region if a suitable light source could be
provided. Microwave excited electrodeless discharge
tube is an intense[6] light source which emits narrow
spectra lines ideal for accurate measurements in this

13

region, particularly in zeeman effect investigation.

2-2 Preparation of the tube - Vacuum System

In 1957 Tomkins and Fred[19] successfully manufactured electrodeless discharge tubes containing metallic halide, and Allen in 1960[20] obtained tubes with iodide form of material which the procedure of preparation can be found in literature. In present manufacturing electrodeless discharge tubes, Dr. E.E.M. Steers adopted the Tomkins method[19] of introducing the halide into a previously outgassed tube, but the preparation of zirconium iodide or manganese iodide is to simply heat a mixture of pure metalic powder and iodine in an evacuated sealed tube, rather than double decomposition with aluminium iodide.

The vacuum system employed was capable of producing a pressure less than 10^{-5} Torr. The block diagram of the system is shown in Figure 2-1. Rough backing vacuum was obtained by use of a rotary pump and fine vacuum using a mercury diffusion pump. Helium, Neon or Argon gas could be introduced from prefilled glass bulbs connected to the vacuum system via two taps separated enough to accomodate 5 c.c of gas between the two taps. Ion and pirani gauges were connected into the system for low pressure reading. Between each section of the system pumps and the traps could be isolated by means of a tap on each trap part. This allowed each section to be

14

TAP

YOUNG
TAP

(DOTTED LINE SHOWS
CLOSED SIDE)

To TUBE UNDER
PREPARATION

AIR INLT FOR
GLASS BLOWING

SCHEMATIC DIAGRAM
OF VACUUM SYSTEM
FIG.2-1

To ROTARY
PUMP

15

isolated during trap cooling or warming. Before the use of the system, it was tested for leaks by a tesla spark source, and the reaction tube apparatus section outgassed while electrical heating tapes were wrapped around it.

2-3 Procedure

Approximately 20 mg zirconium powder and 100 mg iodine was carefully positioned inside a glass specimen tube of the form shown in Figure 2-2(a). Then the tube was placed in a glass reaction tube (Figure 2-2(b)), which was then drawn down to a capillary and sealed at the tip (Figure 2-2(c)). The glass reaction tube was then sealed to the vacuum system as in Figure 2-3(a). The outgassing to a pressure of nearly 2×10^{-5} Torr was done while the sample was kept condensed in the other end of the glass reaction tube by a wrapping of wet tissue and then solidified by liquid nitrogen. The capillary was sealed off at the constriction, and the glass reaction tube disconnected. A small piece of iron placed next to the reaction tube, behind the sealed constriction and the tube again evacuated to a pressure of nearly 10^{-3} Torr on an auxillary vacuum system, and sealed off. The capillary was then heated by a bunsen burner to form zirconium iodide.

Two small quartz blank lamps of 6 mm internal diameter and nearly six centimeters in length separated

FIG. 2-2

Specimen tube

6mm
4mm
~2.5cm
(a)

Glass reaction tube

9mm 7mm

~15cm
(b)

~12Cm
(c)

17
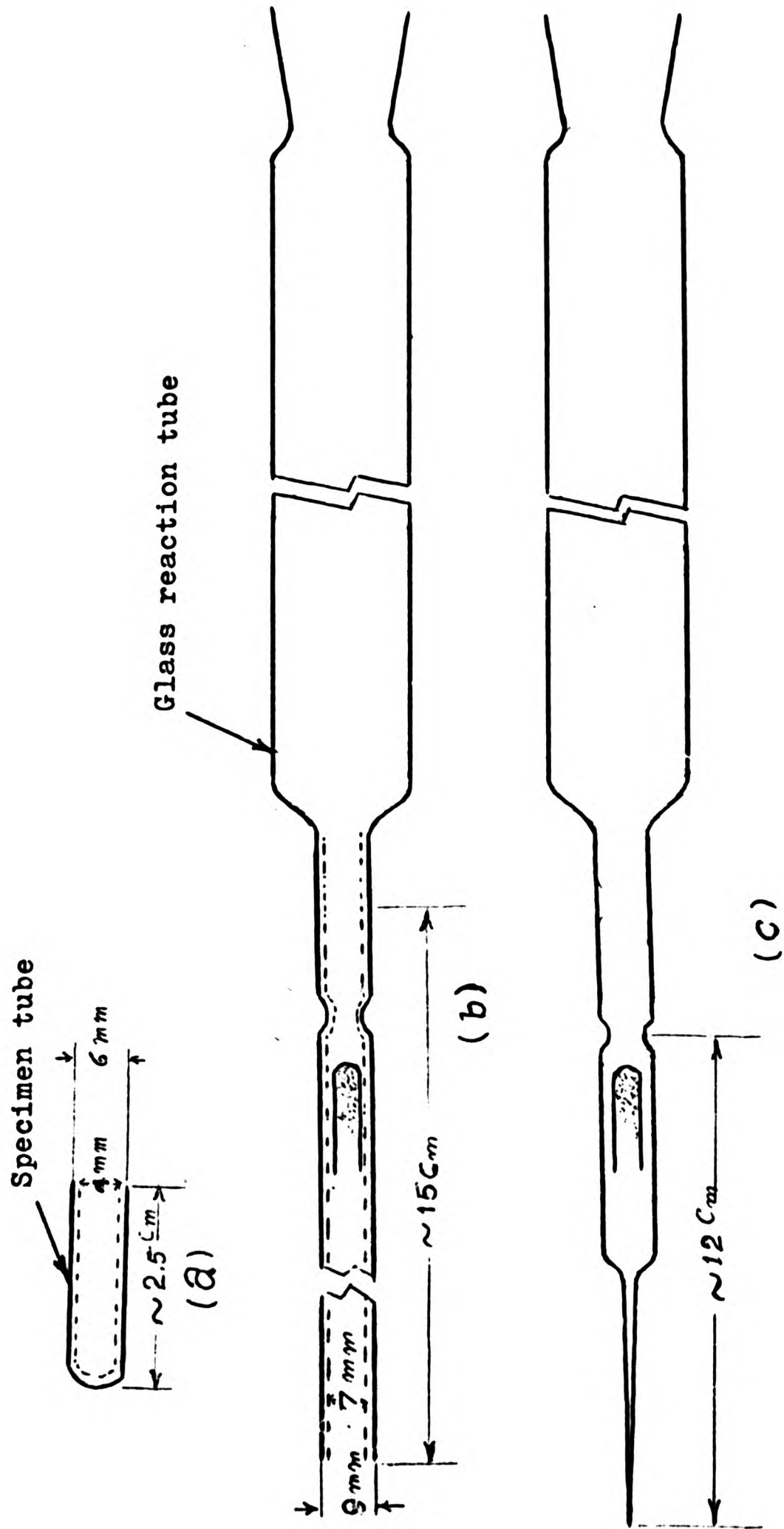
FIG.2-3
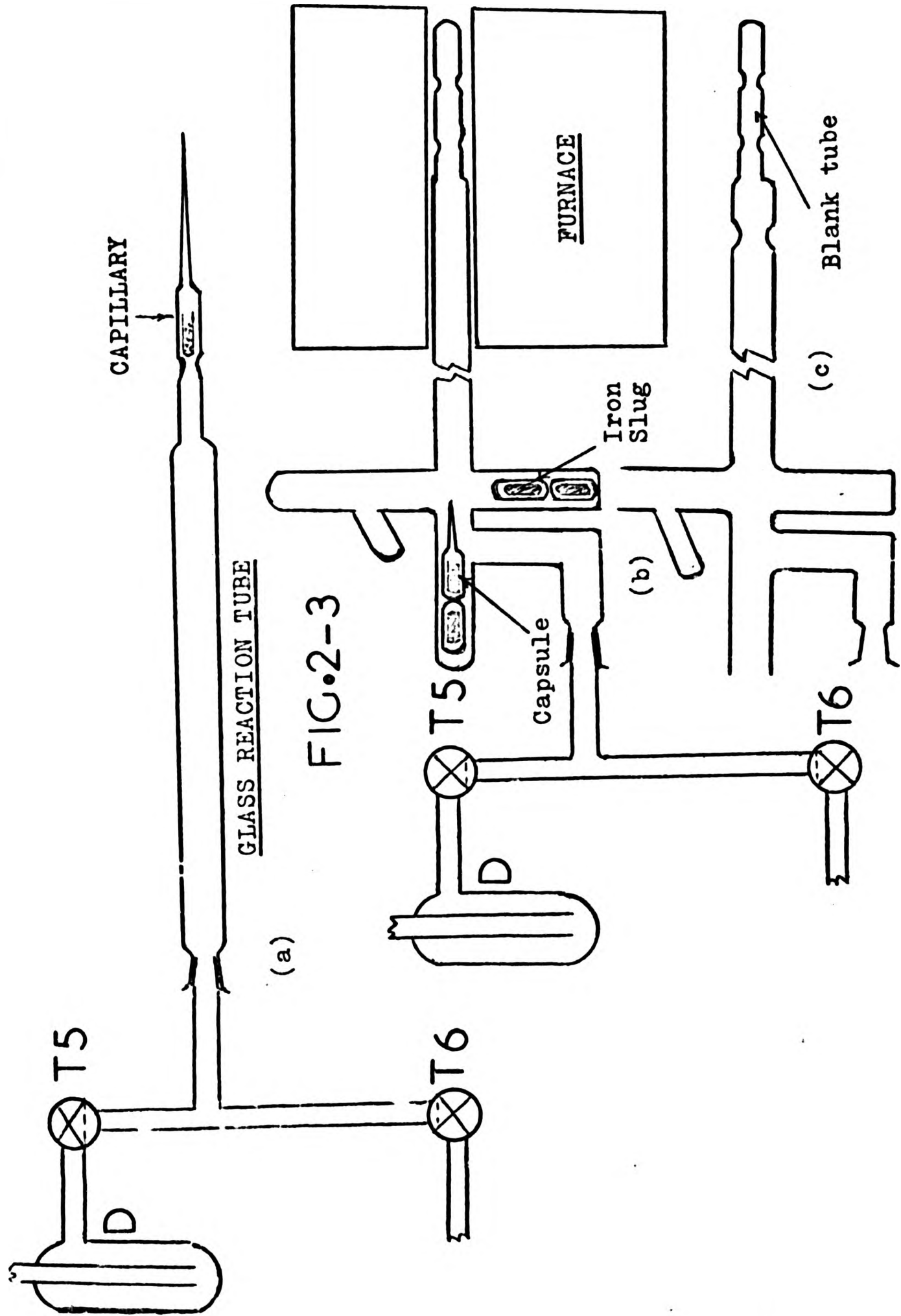
GLASS REACTION TUBE

by constriction and connected to line section of the
apparatus of the form shown in Figure 2-3(b) sealed on
in place of the reaction tube. The completed 'capsule'
containing zirconium iodide carrying an iron slug,
placed in the horizontal section of the apparatus
and also two glass covered iron slugs were placed in
the bottom of the vertical part of the apparatus and
the system sealed and pumped down. The two glass
covered iron slugs were placed in the system to provide
the instrumental tools of opening the tip of the
capillary by moving one of them by means of a magnet
over the vertical section of the apparatus and crashing
the tip by dropping and holding the other in position
under it as an anvil. A furnace placed over the
discharge tubes and that part of the system was heated
to 1100°C for more than two hours, while the system was
maintained under high vacuum ($\sim 3 \times 10^{-6}$ Torr).

It should be stressed that the degassing is one
of the most important steps of the procedure, particularly
for tubes used with material of low volatility which
requires operation at high temperature. The furnace
was then removed and the blank lamps were positioned in
a 2 in.diam. $\frac{3}{4}$ wavelength Broida Cavity 210L. A dose of
neon gas was admitted while the line section was
positioned in the Broida Cavity coupled to the microwave
power unit ready to be operated. The blank tubes and
the line section was excited using a tesla spark source.

19

The Cavity was tuned and the pressure of the neon gas
was reduced to nearly 2 Torr to minimise the reflected
power and the system was set to run for at least two
hours. This was to degas the tubes by bombarding the
tube wall. The light emitted by the tube was viewed
through a packet spectroscope to see if the neon spectrum
was free from any bands due to impurities (nitrogen band)
and if any trace of band was found, the system was slowly
evacuated and the microwave power was set off when the
discharge could no longer be maintained. A fresh
quantity of neon gas was then admitted and the procedure
was repeated until the neon spectrum was free from any
band. After two hours with a clean discharge the wall
bombardment by the neon gas was considered to be completed.
The tube and the line section was evacuated and the
power on the tube set off immediately after the light
went off. The isolating tap of the line section was
closed, then one of the iron slugs was vertically moved
in the vertical section of the line to a height enough
to crash the tip of the capsule by using a magnet. The
capsule was then moved horizontally to a distance where
the capillary tip was positioned under the slug, and
was crashed by dropping the iron slug from the top and
holding the other iron slug in position under the
capillary tip as an anvil. The capsule was then moved
through the line section to the constriction of the
blank tubes by using a magnet. The sample in the capsule
sublimed into the discharge tube by using a bunsen burner

collecting at the end of the tube which was cooled with
wet tissue solidified by liquid nitrogen. The capsule
was then removed, a dose of neon gas was admitted, the
tube was struck in the cavity for a minute or two and
the pressure reduced to the optimum value and the power
then was set off and the tubes were sealed. Running
the tube for one or two minutes is to remove the surplus
iodine in the tube before sealing the tubes off the
system. The prepared tube was then provided with a
piece of 5 mm diameter quartz rod attached to the sealed
off end.

2-4 Modification of the tube preparation for the
less volatile material

The technique chosen in preparation of zirconium
halide tube could not be fully applied to the manganese
halide tube.

1) Formation of manganese iodide took a long time
   and only a small amount of halide was obtained.

2) Sublimation of manganese iodide did not occur
   readily, and material could not be collected
   inside the blank tubes. It took a long time to
   sublime a small amount and that deposited on
   another portion of the inner wall of the capsule.

The preparation of the manganese tube began in
the same way as for zirconium tube. The glass reaction
tube was cleaned thoroughly by placing a few c.c. of
concentrated nitric acid in it. After an hour or so
the reaction tube was washed with distilled water for
three times, and then dried and positioned in the
furnace for half an hour with temperature below 400 $^{\circ}$c.
This was not only to extract the water vapour from
inside the glass reaction tube but also to extract any
gas trapped in the glass wall inside the tube. Then,
50 mg manganese powder and 150 mg iodine was carefully
positioned inside a specimen tube and the specimen tube
was placed inside the glass reaction tube which was then
drawn to a capillary and sealed off. The glass reaction
tube was then sealed to the vacuum system and outgassed
to a pressure of 2×10^{-5} and the capsule was sealed
off at the constriction in the same way as the preparation
of the zirconium capsule. It was then heated by a
bunsen burner to form manganese iodide. But the formation
of manganese iodide was run into difficulites. It took
hours of tedious work of heating the capsule with two
bunsen burners simultaneously, but only a trace of milky
coloured material was formed on the capsule wall, and
inside the capillary was covered with several patches of
black material which could easily be distinguished from
iodine. It was then decided to proceed with the
preparation of the manganese tube. The manganese capsule

22

was placed in the horizontal section of the apparatus
(Figure 2-3(b)), and two glass covered iron slugs were
placed in the bottom of the vertical part of the line,
and the system was sealed and pumped down. The furnace
placed over the blank tubes to heat the tubes to $1100^{\circ}C$
for two hours, neon gas admitted to the tubes and the
line and the tubes were struck in the cavity for two
hours under the operation of microwave power. Then
the capillary tip crashed by the iron slugs and the
capsule was moved to the blank tube constriction by a
magnet, and the sublimation was carried on. More than
three hours the capsule was heated by two bunsen burners
simultaneously, but nothing was gained, the only result
was the displacement of the small amount of milky colour
material inside the capsule and outside on the wall of
the capillary and there was no sign of material being
sublimed outside the capsule.

Later, the author suggested a new way of capsule
preparation to overcome the above problem. In this way,
the glass reaction tube was first drawn down to a
capillary and then the manganese powder and iodine was
carefully positioned inside the capillary without a
specimen tube. In this method, heat could more easily
be transferred to the material inside the capillary and
halide formation will be more successful, and sublimation
will be efficient.

This method was carried out in the preparation of the manganese tube, manganese iodide was obtained successfully, and the material sublimed and collected on the line wall close to the blank tube constriction, but did not pass through the constriction to be collected at the end of the blank tubes.

Dr. Steers suggested a further constriction on the quartz line as shown in Figure 2-3(c) just behind the collected material on the wall, and in due time be sealed off with the material restricted in a small part of the line connected to the blank tubes. This was done in the next procedure of the tube preparation, but again the material could not be sublimed into the blank tubes by heating. But when the manganese iodide was heated to sublime, it was seen that the material first changes into liquid and then changes to vapour form in a very short time and will deposit in a colder part of the line without passing the constriction. The melting condition of the manganese iodide by heat was indeed a new hope to obtain a manganese discharge tube. Dr. Steers suggested to make use of a small furnace and melt the material in the line while the blank tubes and the line are held vertically and let the manganese iodide liquid run into the blank tubes. The tubes and the part containing manganese iodide was held vertically by a stand and the small furnace was placed round the part of the line containing manganese iodide where the heat

24

could be transferred to the manganese iodide. The
furnace was set on and the current increased for
sufficient heat to melt the material. The halide
liquid gradually run down to the constriction and with
the aid of a bunsen burner the constriction was heated
enough to make the collection of the liquid halide
inside the blank tubes possible. This method of
manganese tube preparation was successful and four tubes
were obtained in this way.

2-5   Method of excitation - Cavities

The microwave cavity is used to couple the micro-
wave energy to the electrodeless discharge tubes. In
any cavity the resonant made may be identified as the sum
of two waves travelling opposite direction between
causes of reflection. These causes may be thought of
as short circuit like boundaries spaced $\lambda/2$ apart.
The electrodeless discharge tube is normally positioned
in the cavity at the point where an electric field
maximum is produced in the Un loaded cavity.

The 2 inch diameter Broida cavity gives a great
efficiency in the excitation of a tube. This cavity
provides great stability with their uniform field
configuration[24], may be water cooled by circulating
water through a $\frac{1}{4}$ inch brass tube soldered round the
cavity and the insulators (as in present project), to
stop the cavity from over heating when a higher power
is used. The one inch diameter Broida cavity (small
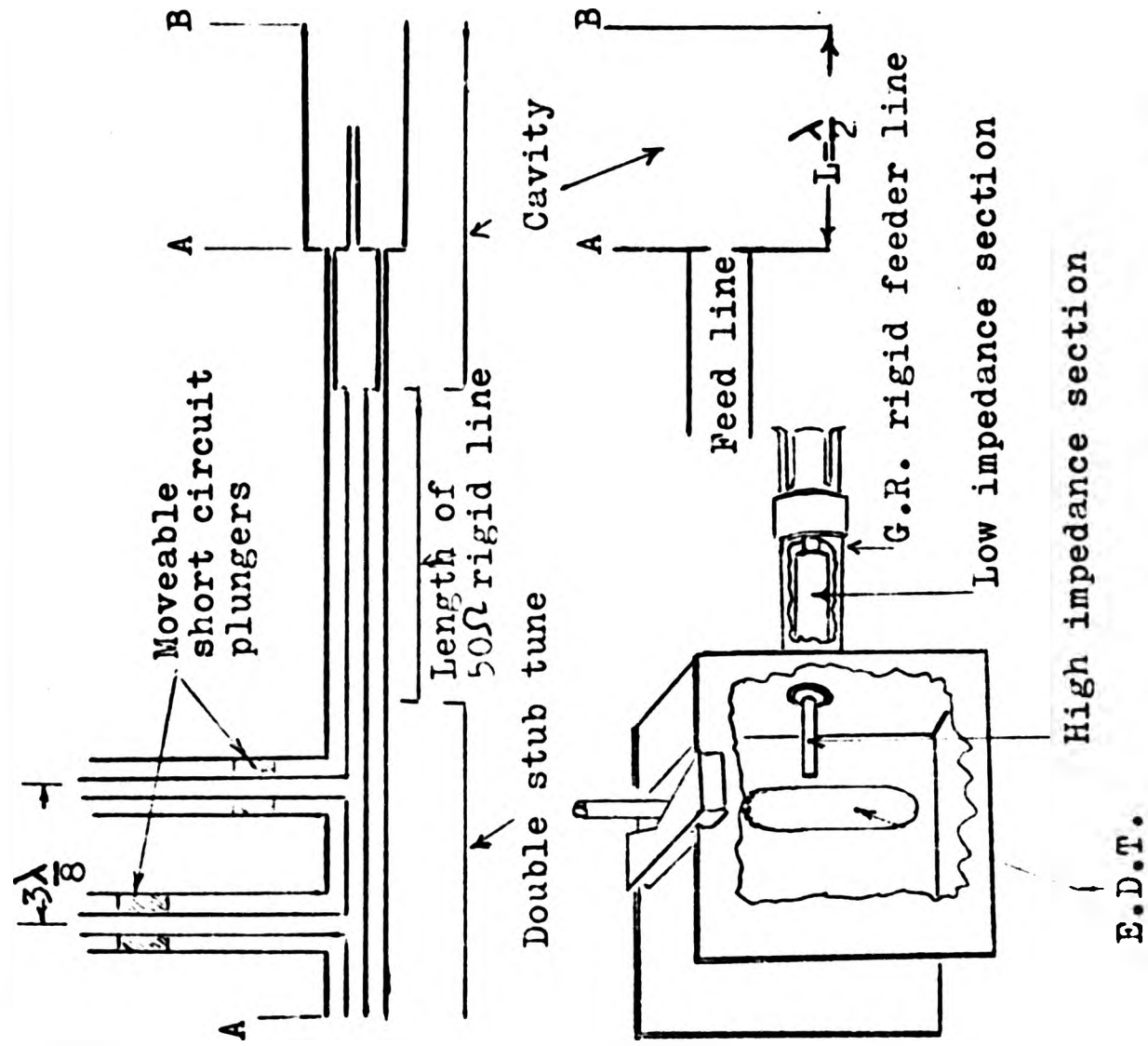
Fig 2-5: Slab line cavity
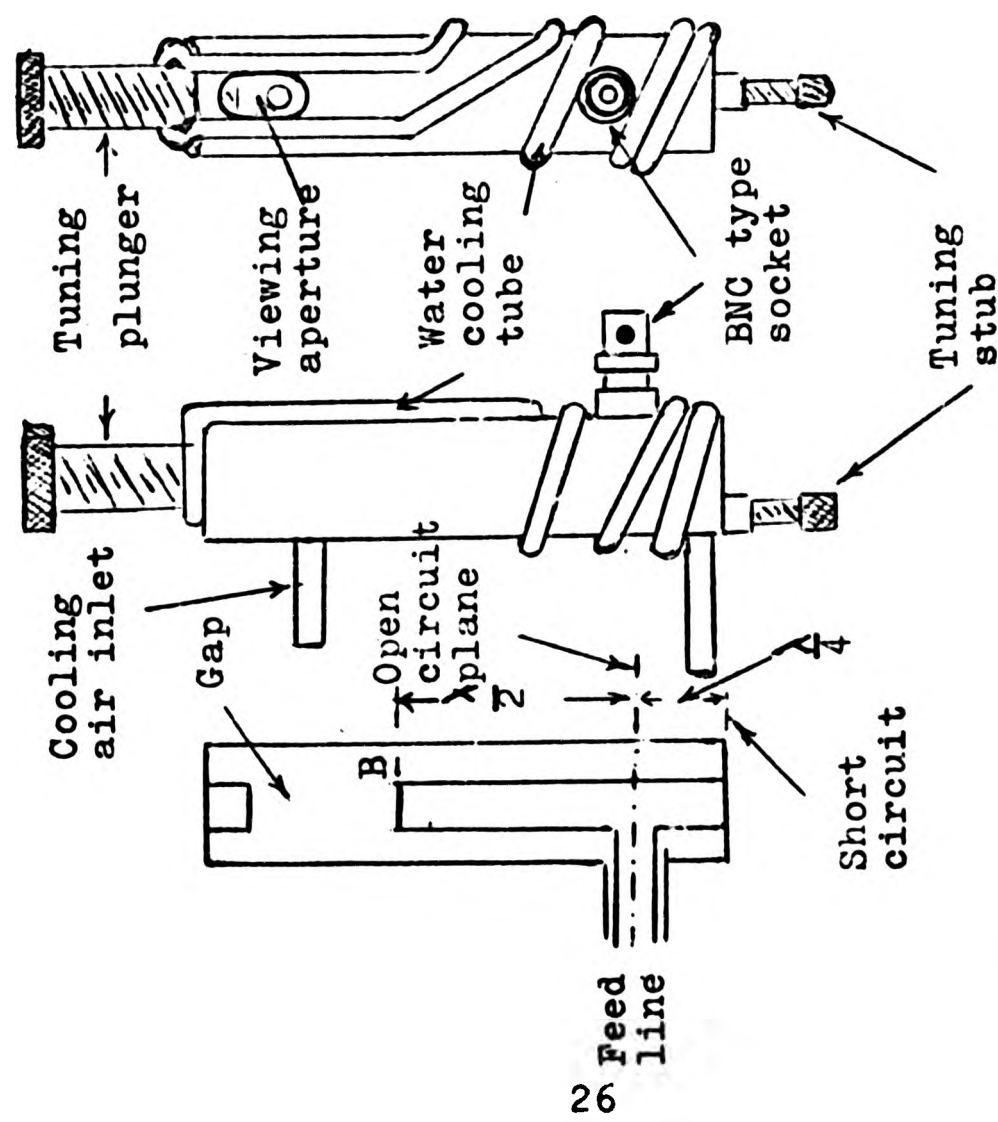
Fig 2-4: One-inch diameter Broida type cavity

cavity) is designed by Steers of PNL and supplied by EMS (Electro Medical Supply), (Figure 2-5). This small cavity provides more efficient excitation of the less volatile materials, and is readily tuned for low reflected power for most elements under operation inside the tubes.

A new cavity, called slab-line cavity has been recently developed by M. Outred and C.B. Hamand[25]. This cavity provides great stability under the low microwave power operation.

Internal tuning of the loaded Broida cavity is provided by means of one or more screws inserted into the cavity, which effectively alters the cavity dimensions. The slap line cavity has no internal tuning provision, but tuning is affected by a double stub tuner which may be inserted at any point[25] in the feed line from the microwave generator.

In figure 2-4 and 2-5 schematic diagram of Broida cavity and slab-line cavity are shown. In these diagrams, Broida cavity (Fig 2-4) may be represented by two open circuit boundaries $\lambda/2$ apart which provides resonance effect. But in practice the gap inside the cavity constitutes capacitive loading and the short circuit point is less than $\lambda/4$ from A. The coupling point in the Broida type cavity is near an open circuit plane where the field E would be maximum.

In slab line cavity, boundary B is an open circuit at a distance $\lambda/4$ from boundary A which provides the

27

electric field maximum and this is a convenient point
to place the tube.

2-6 Energy transfer in cavity

The output power of a magnetron, capable of giving
200 watts c.w. at a frequency of 2.45 GHz, is coupled
to the cavity to provide a high electric field across
the electrodeless discharge tube to assist in striking
the discharge, and provide maximum power transfer to
the tube under loaded condition. Most efficient trans-
fer of energy occurs when the output impedance of the
microwave power generator, the characteristic impedance
of the coaxial cable, and the load impedance (lamp
and the cavity) are equally matched. Before the tube
is struck, very little power is absorbed in the cavity,
and almost all the power is reflected back to the
magnetron. (To protect the magnetron, the power should
be kept as low as possible, and the tube struck
rapidly). Once the tube has been struck, the reflec-
ted power drops, and can be further reduced by using
tuning screws in Broida cavity or by double stub
tuner in slab line cavity. The amplitude and phase
of the reflected power can cause a variation in the
output power of the generator which in turn affects
the stability of the microwave excited discharge tube.

2-7 Performance of slab line cavity in exciting zirconium halide tube

The aim was to assess the suitability of the slab-line cavity for exciting EDTs containing metallic halides, particularly zirconium iodide, and compare its performance with that of Broida cavity. Previous investigations on slab-line cavity by Outred and Hamand have been limited to the inert gas tubes only.

A preliminary investigation was made of the intensity and line width of a typical zirconium line (587.98 nm) in the slab line and Broida cavities. The results are given in Appendix 3 in tables $A_3 - 1$, $A_3 - 2$, and $A_3 - 3$ for three different zirconium tubes. There was no immediate evidence of greatly enhanced intensity with the slab-line cavity which can be seen in Graph 2-1 for tube a, and it was decided to concentrate on the more convenient small diameter Broida cavity.
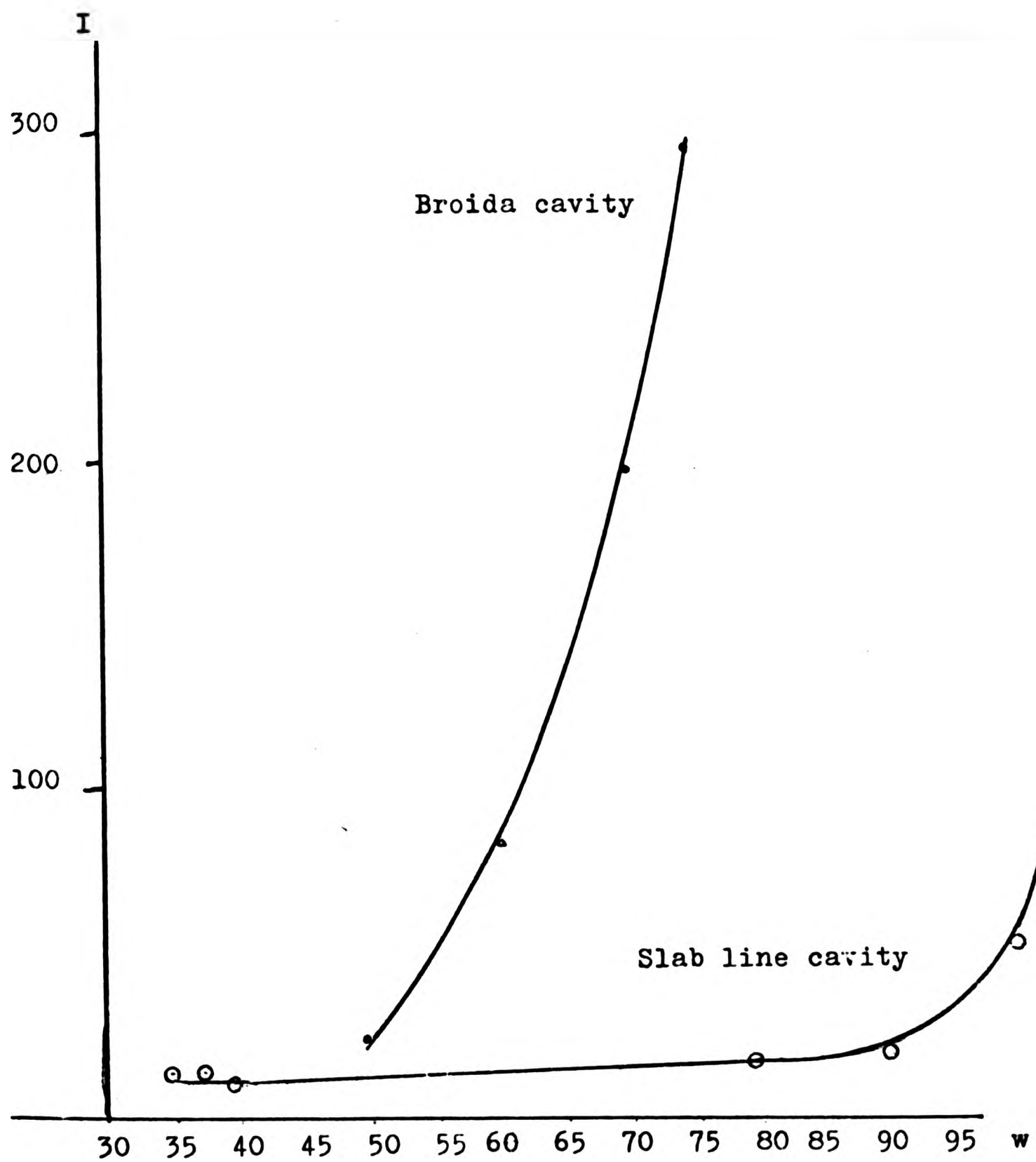
Graph 2-1: Intensity variation of zirconium line profile
587.98 nm vs. Microwave power in slab-line and
Broida cavities. The signals detected with a
photomultiplier voltage of 700 volts in Broida
cavity and with 670 volts in slab-line cavity.

CHAPTER 3

APPARATUS FOR INFRA-RED WAVELENGTH
MEASUREMENT

3-1 Ebert mounting spectrometer

The instrument used in this work was a 1.5 meter
Ebert mounting grating with 11.1 Å/mm dispersion in
the first order of 6000 Å. This was the same instru-
ment used for wavelength measurement on the infra-red
spectrum of zirconium by the author in 1976. The
detail of construction and the components with the
figures are given in the author's Thesis for the degree
of Master of Philosophy to the London University[1].
This instrument consisted of a plane grating, having
600 groove/mm over a ruled width 15 cm (12 x 15 cm),
and blazed for 1.2 - 1.8 μm to give the maximum inten-
sity to the spectral line in this region. The entrance
and exit slits are 2 cm high curved slits enclosed in
the main tank (Figure 3-1) but could easily be adjusted
from outside; curved slits are used to remove the effect
of astigmatism and image curvature and to increase the
energy flux passing at any given wavelength without
degrading the resolving power[26]. This spectrometer
was ideal for an accurate measurement of wavenumbers
of spectral lines. The optical arrangement of this
instrument (Figure 3-1) produces a perfect image as the

31

light rays travel the same distance from the entrance slit to the exit slit. The grating was driven by one of two electric motors shown in Figure 3-1 b. The instrument was easily reset by disengaging the slow scanning electric motor from the grating. The resetting electric motor was used as a wheel spindle in mesh with wormgear at the scanning time. The electric motors could be rotated in both directions by changing the phase of the current. The scanning speed could be easily changed by changing the position of two levers on the gear box. One of the levers was used to disconnect the slow scanning electric motor in order to reset the grating or achieving the proper speed by changing the position of the second lever. The same lever could be positioned down and could decrease the rotational speed of the scanning by half. The second lever could be positioned in three places: up, centre and down in order to achieve the overall scanning speed of: 40 Å/min, 10 Å/min, and 2.5 Å/min for the first lever positioned up, or 20 Å/min, 5 Å/min and 1.25 Å/min for the first lever positioned down in the first order of 600 nm wavelength. A locking screw could be withdrawn to allow the grating table to be manually turned to select the proper grating range, and then screwed in again by a locking screw. The grating instrument was enclosed in a cylindrical tank which could be evacuated to a pressure of 0.04 Torr.

The only change in the optical system which has taken place in the present work, is to make the instrument usable in the investigation of zeeman effect (Figure 7-1). This was done by joining additional optical bench to the system and replacing the concave mirror (CM Fig. 3-2) with a lens in front of the entrance slit of the spectrometer (Fig 3-1).

The replacement of concave mirror with a lens has two essential advantages:

1) improvement in the optical system by arranging all the components to have the same optical axis hence make the use of electromagnet for zeeman effect investigation possible in a limited space.

2) lenses can be prepared to have minimum off axis aberration compared with a concave mirror and improve the sharpness of the source image at the entrance slit and increase the grating luminosity.

But the disadvantage of the new arrangement is the inevitable variation of the focal length of the lens with the wavelength. The light of the source was refocussed on to the entrance slit of the spectrometer in each recording in different parts of the spectrum region, to minimise the effect of focal length variation on the

33

intensity of the recorded spectra lines.

The optical alignment of the system was performed
by using a laser beam and illuminating the centre of
the exit slit by passing the beam from the centre of
the lens in front of the photomultiplier horizontally.
The grating was positioned in zero order and the dia-
phragm in the relevant positions. The optical bench
was aligned parallel to the optical axis, so that
components could be moved along the optical axis.
The components adjusted until the laser beam was brought
through the centre of entrance slit to a focus at the
centre of the discharge tube between the electromagnet
poles.

3-2 Calibrating System

The recording of spectra lines are performed by
scanning the spectrum across the exit slit by rotating
the grating. The accuracy of the wavenumber of the lines
calculated depends on the smoothness and precision of
the mechanical drives which rotates the grating and
move the chart. In order to minimise the dependence on
the grating and the chart drives, it is necessary to
have as many closely spaced standards as possible.
Edser-Butler fringes recorded simultaneously with the
unknown spectrum provide an accurate, closely spaced
wavenumber scale (Figure 5-1 to 5-6). The optical
arrangement for calibration is represented in Figure 3-1.
Continuous radiation from a quartz tungsten halogen

34

Fig. 3-1 Optical System

EBERT SPECTROMETER

Scanning electric motor

Setting electric motor

Gearbox

Main tank

Infra-red detector

Photomultiplier

Fast scanning electric motor

Slow scanning electric motor

Gearbox levers

M_2

M_1 S_t L_1 D L_2 $F-P$ L_3 CB OX5

S Ln Ma S.Th

Main tank

(a)

(b)

35
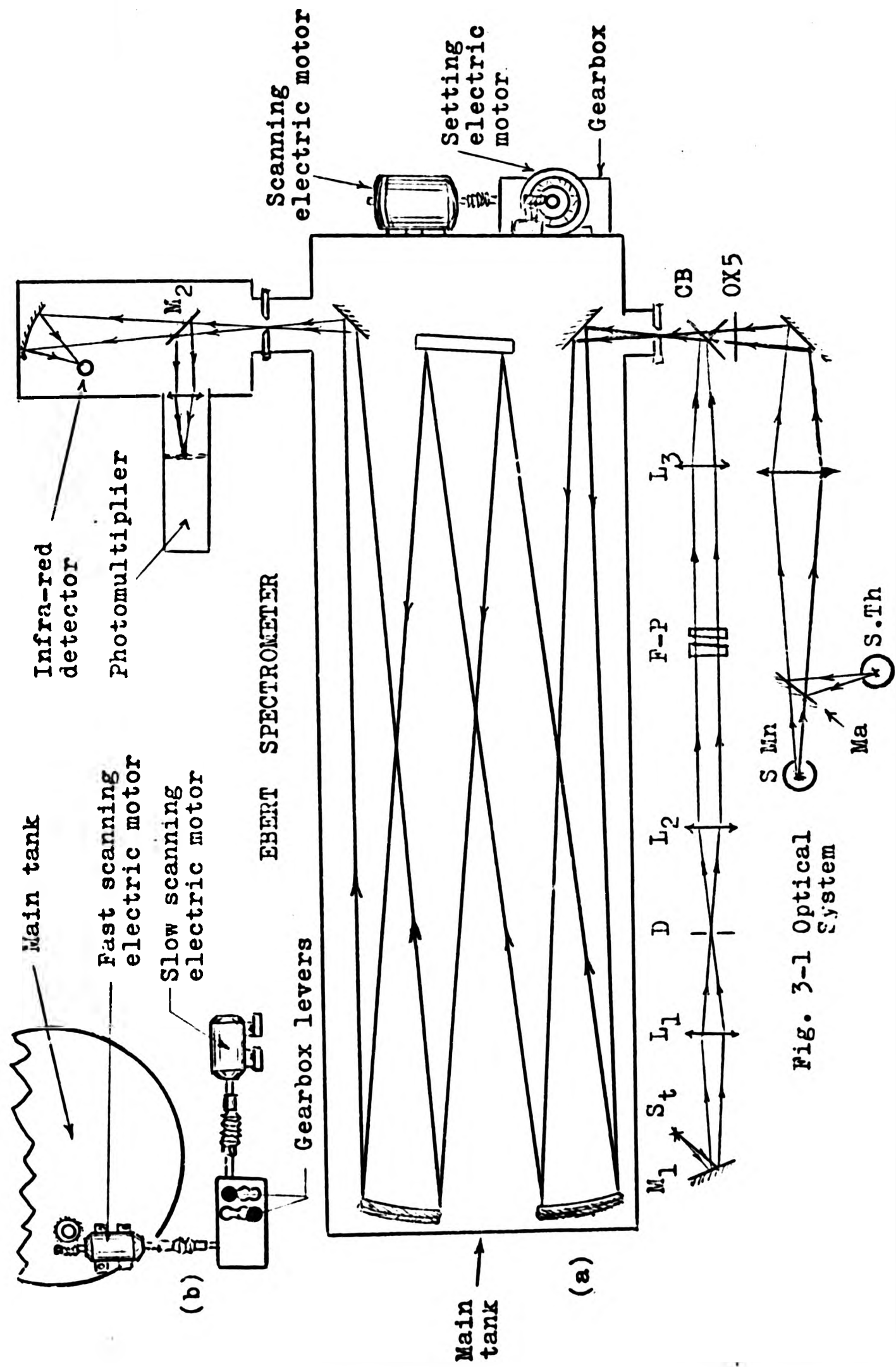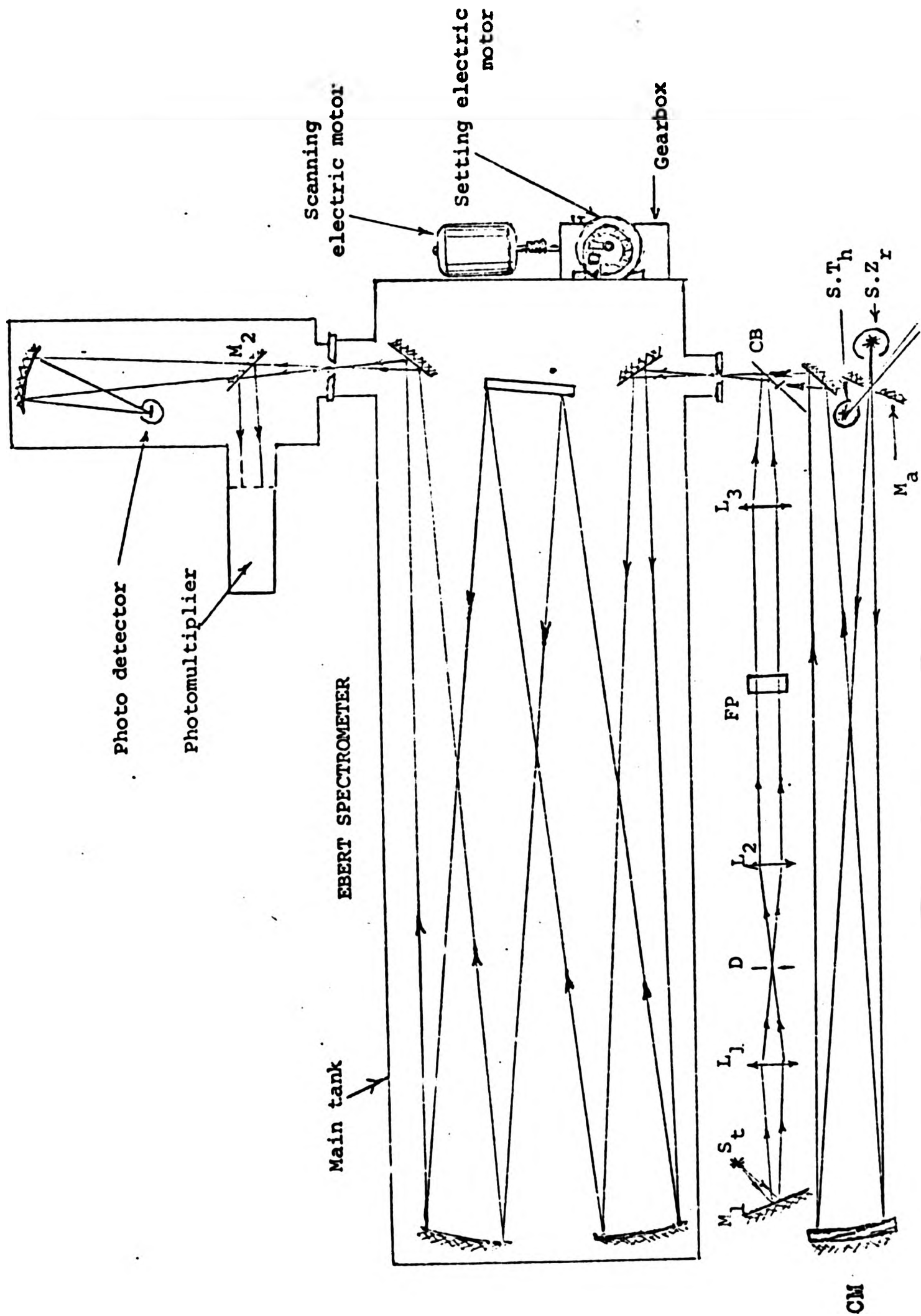
Fig. 3-2: OPTICAL SYSTEM.

lamp AI/215 (St) was focussed on the pin-hole diaphragm (D) by the lens L_1 after reflection from a cold mirror M_1 (Balzers - Kaltliehtspiegel 63/45, 53/2542). The cold mirror (M_1) was used next to the tungsten halogen lamp to filter the infra-red part of the continuous light which might disturb the infra-red spectrum of the manganese beam on the detector, and reflect the visible white light for the fringe system. The collimating lens L_2 directed a parallel beam on to the Fabry-Perot etalon (F.P). The radiation emerging from the etalon was focussed on the entrance slit by lens L_3, and by reflecting from the aluminised quadrants mounted on the chopper blade (CB) close to the entrance slit. From then on the fringe beam travelled with the manganese light beam inside the spectrometer, and was separated and directed to the photomultiplier by another cold mirror (M_2) behind the exit slit. The cold mirror (M_2) also transmits the incident infra-red spectrum of the main beam (manganese beam) to the detector, and the visible spectrum of the main beam was filtered by using a "chance" infra-red filter OX5 in front of the entrance slit which could only transmit the wavelength over 0.75μ m.

The accuracy of wavenumber calculation not only depends on the sharpness of the spectral line profile and sensitive detective instrument but also depends on the shape and sharpness of the Edser-Butler fringes as well.

A survey of Fabry-Perot instrumental function and
the merits of this interferometer is given in Chapter 1,
and the basic equations are discussed in Chapter 7, but
it is helpful to outline some important and effective
points on the sharpness of the fringe profile.

If the central region of the concentric fringes are
used for scanning (which actually is the case) then in
equation 7-1 $\theta = o$ and $\cos \theta \rightarrow 1$ and thus:

$$n = 2\mu t \sigma \qquad (3-1)$$

where n is the order of interference

           μ is the refractive index of the gas
                between the plates

           t is the distance between the plates

           σ is the wavenumber of the radiation
                transmitted with maximum intensity.

Considering the change in order to be one in equation
3-1 and setting for n, the distance between two orders,
i.e. the free spectral range $\Delta \sigma$ is given by

$$\Delta \sigma = \frac{1}{2\mu t} \qquad (3-2)$$

38

For a sharp fringe the halfwidth of the fringe profile $\delta\sigma$ is much less then $\Delta\sigma$ and $\Delta\sigma/\delta\sigma$ gives a finesse which depends on three factors: [27]

1) The flatness of the plates

2) The reflectivity of the plate coating (R)

3) The angular diameter of the fringe pattern isolated.

1) — The finesse, depending on flatness N_D is limited to m/2, if the plates are made smooth to within λ/m where λ is the wavelength of the radiation transmitted with maximum intensity and m is an integer.

2) — The finesse depending on the reflectivity of coating material is given by

$$N_R = \frac{\pi\sqrt{R}}{1-R} \qquad (3-3)$$

A graph of N_R variation versus R is given in Chapter 7, Figure 7-1.

3) — The finesse depending on angular diameter of the isolated fringe pattern is given by

39

$$N_A = \frac{2\pi}{n\Omega} \qquad\qquad (3\text{-}4)$$

where: Ω is the solid angle subtended by the limiting diaphragm at the camera lens

$$\Omega = \frac{\pi a^2}{f^2}$$

n is the order of interference.

a is the radius of the limiting diaphragm.

f is the focal length of the camera lens.

The glass etalon plates which were used by the author in 1976 was replaced by a pair of quartz metallic coated plates. The values for the reflectivity R, absorptivity A and transmissivity T for glass metallic coated and the quartz metallic coated plates were measured. Although the reflectivity of glass plates are higher than the quartz plates but the flatness and transmissivity of the quartz plates is much grater compared with the glass plates in visible region. From equation 7-8 in Chapter 7

$$I_{max} = \frac{Io}{(1 + A/T)^2}$$

Where I_{max} is the maximum transmitted light intensity

Io is the incident light intensity

a) For the glass plates and λ between 500-700 nm

$$R = 85\%, \quad A = 11.7\%, \quad T = 3.3\%$$

$$\frac{I_{max}}{I_o} \approx \frac{1}{20.66} \approx 4.8\%$$

b) For the quartz plates and λ between 500-700 nm

$$R = 77\%, \quad A = 15.4\%, \quad T = 7.6\%$$

$$\frac{I_{max}}{I_o} \approx \frac{1}{9.16} \approx 11\%$$

In practice the fringes were sharp, intense and symmetric as can be seen in Figure 5-1 to 5-6 for quartz plates.

A 6256B photomultiplier tube with small cathode, serial number 15634 was used to detect the fringe signals. This tube was sensitive towards the violet in visible region. It has 1 cm diameter quartz photocathode with high quantum efficiency and best signal to noise ratio. A lens of 5 cm focal length was positioned in front of photomultiplier to focus the fringe beam reflected from cold mirror (M_2) on to the photomultiplier cathode.

Where I_{max} is the maximum transmitted light intensity
Io is the incident light intensity

a) For the glass plates and λ between 500-700 nm

$$R = 85\%, \quad A = 11.7\%, \quad T = 3.3\%$$

$$\frac{I_{max}}{I_o} \approx \frac{1}{20.66} \approx 4.8\%$$

b) For the quartz plates and λ between 500-700 nm

$$R = 77\%, \quad A = 15.4\%, \quad T = 7.6\%$$

$$\frac{I_{max}}{I_o} \approx \frac{1}{9.16} \approx 11\%$$

In practice the fringes were sharp, intense and symmetric as can be seen in Figure 5-1 to 5-6 for quartz plates.

A 6256B photomultiplier tube with small cathode, serial number 15634 was used to detect the fringe signals. This tube was sensitive towards the violet in visible region. It has 1 cm diameter quartz photocathode with high quantum efficiency and best signal to noise ratio. A lens of 5 cm focal length was positioned in front of photomultiplier to focus the fringe beam reflected from cold mirror (M_2) on to the photomultiplier cathode.

3-3   Infra-red signal detector

To detect the infra-red signals, a sensitive detector must be used. The infra-red spectra lines are not sufficiently energetic to emit an electron right out of the surface in a photocathode, but they have enough energy to free an electron from the crystal lattice in a cooled lead sulphide semiconductor.

In previous measurement of infra-red spectrum of zirconium in 1976, The Kodak Ectron type O lead sulphide detector in the spectrometer was replaced by an Intermediate Temperature Operation (ITO) type lead sulphide detector number 4477 with element size 1 x 5mm made by Santa Barbara Research Centre (SBRC). The detail of replacement is given in the author's Thesis.[1] The second detector was more sensitive with less noise compared with the first one. The same detector is used to detect the infra-red spectrum of the materials under investigation in the present project. The detector was enclosed in an enclosure which could be evacuated to a pressure of nearly 2.5 x 10^{-2} Torr with a rotary pump. The cooling system consists of a brass dewar flask (Figure 3-3) which could be filled with a mixture of solid carbon dioxide and acetone. The above arrangement was not an ideal one for detecting signals. Previously, when the cell was cooled, there was a noticeable drop in pressure, i.e. water vapour was condensing on the cell and its supportings, leading to electrical leakage and noise, and possibly more pronounced

42

Lewar flask

Concave mirror

Lead sulphide cell

Cold mirror (M$_2$)

Photomultiplier

Exit slit
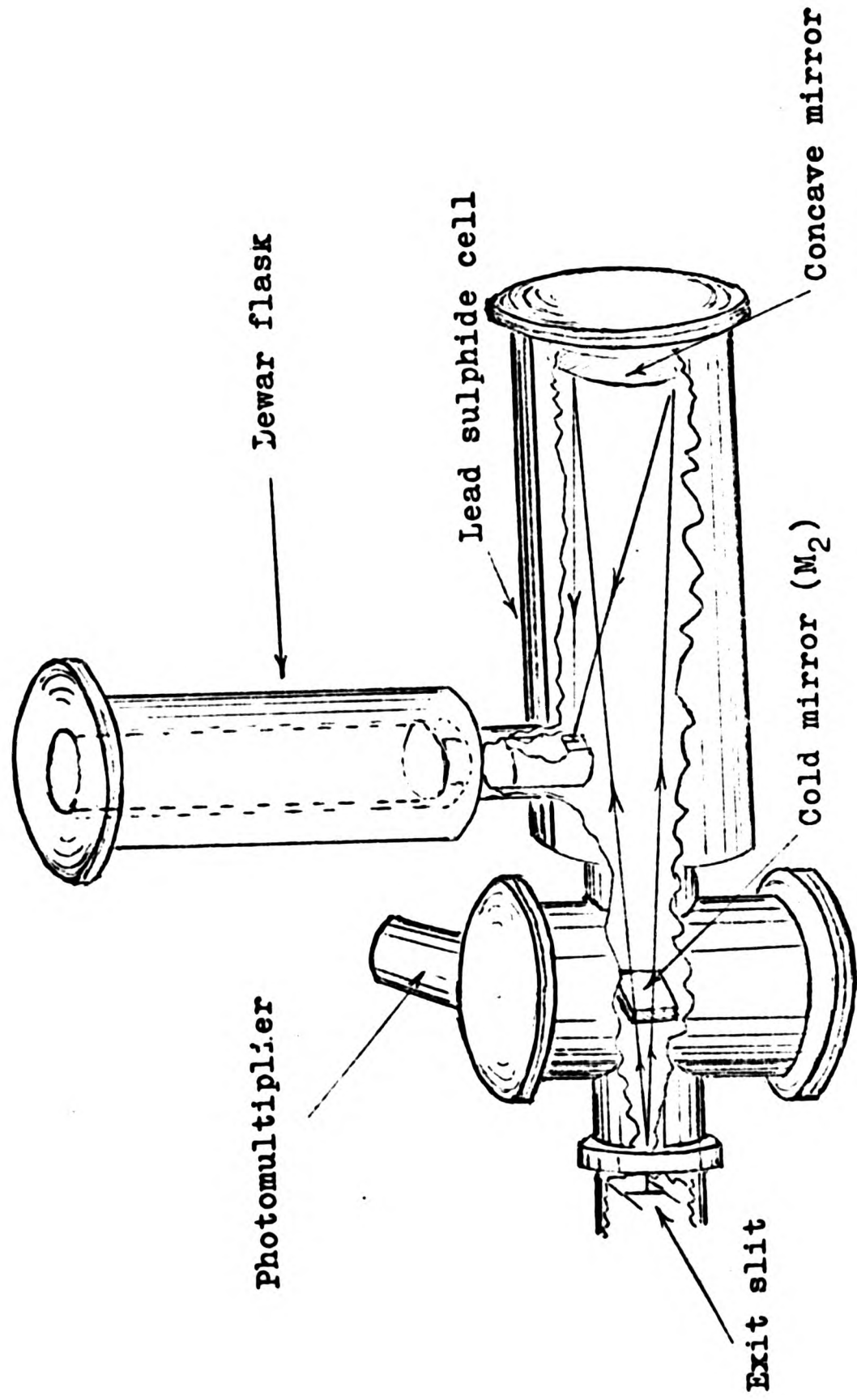
Fig. 3-3

43

absorption bands. To prevent this an auxiliary oil
diffusion pump was added to the system. Using this
pump the pressure dropped to nearly 3×10^{-3} Torr.
An auxiliary liquid nitrogen trap was also added to
condense the water vapour before filling the brass
dewar flask with carbon dioxide and acetone. This new
arrangement made a great improvement in the detecting
system. The appreciable water vapour bands previously
observed were no longer visible, and this apparently
means that the source of water vapour absorption is
close to the detector cell and the water vapour absorp-
tion between the entrance slit and the source was not
the main cause of the water vapour absorption bands
previously observed.

3-4 Signal recovery

The noise problem associated with infra-red
detector is a serious limitation in the signal recovery.
This noise is caused by Johnson noise, generation and
recombination noise, and noise due to surrounding
radiation. The usual solution to minimise the effect
of detector noise is to narrow the band width with
appropriate time constant on a phase sensitive amplifier
used for amplification of the a.c. signals introduced
to the detector by chopping the main beam. A coherent
a.c. voltage with the output signal from the detector
was introduced as reference voltage with the signals
to a phase-sensitive detector and reference amplifier

44

(Brookdeal lock-in-amplifier type 401A), to extract a signal buried in noise by multiplying the signal input voltage with the reference and filter the product with a low pass filter of variable time constant.

A time constant of one second was used with the phase-sensitive detector to reduce the band width.

In Figure 3-1, the main beam was chopped into square wave forms with frequency of 33.3 Hz, and alternatively introduced to the spectrometer. The coherent reference signal was obtained from a photocell by chopping the light of a small lamp illuminating the photocell. The photocell was mounted opposite the point where the chopper blade intercepted the spectral beam. The chopper blade used to chop the photocell light was mounted on the same shaft as the main chopper.

3-5 Light sources and Power generators

The preparation of the microwave excited discharge tubes have been given in full detail in Chapter 2. In this section only the significant points of the operational system will be dealt with. Three kinds of tube were used in this project.

Thorium tube was used as a light source of standard lines in the wavenumber calculation of manganese and zirconium infra-red spectrum. Manganese and zirconium tubes were used as the light source of the elements under investigation.

The power generator used to operate on the thorium tube was an Electro-Medical Suplies Microtron 200 (Mark II) Unit. This unit was not equipped with power stabilisation. The thorium tube was struck in a $\frac{3}{4}$ wavelength Broida Cavity with 2 inch diameter (E.M.S 210L).

A small cavity $\frac{3}{4}$ wavelength Broida Cavity (Figure 2-5) (1 inch diameter 215L) was used for manganese tube. The power generator used with this cavity was a magnetron used in conjunction with a constant current power supply (KSM,LTD, Brookmans Pk, HERTS, Type HVI 2200).

3.6 Wavenumber calculation

In section 3-2 the merits of Edser-Butler fringes in providing accurate scale for wavenumber calculation have been given, in Section 3-3 the accuracy and the factors in value in a Fabry-Perot interferometer was discussed. In this section the detail of actual measurement and use of equations involved in the calculation will be given and the coefficients will be mentioned.

Two Edser-Butler fringes have a constant wavenumber separation given by equation

$$A = \frac{1}{2\mu t \cos \theta} \qquad (3-5)$$

46

where μ is the refractive index of the medium
between the plates

t   is the etalon space (plate separation)

θ is the angle between the colimated
beam direction and the plate normal.

The Fabry-Perot interferometer equation representing
the wavenumber for the maximum intensity of the radiation
transmitted from the plates is given by:

$$\sigma = \frac{Ne}{2\mu t \cos \theta} = N_e A \qquad (3\text{-}6)$$

where σ is the wavenumber of the radiation
transmitted with maximum intensity

N_e is the order of interference

Equation (3-6) can be regarded as a dispersion
relation giving the wavenumber of any spectral line
whose position could be referred to the scale of the
fringe. The wavenumber σ_1 of a spectral observed in
grating order N_1 can be expressed as

$$\sigma_1/N_1 = \sigma_s/N_s + A/N_g \, (m+e_1+e_2) \qquad (3\text{-}7)$$

47

where σ_s is the standard wavenumber

N_s is the order of the standard line

A is the "fringe spacing" (wavenumber difference between two fringes)

m is the integral number of fringes between lines σ_1 and σ_s

e_1 & e_2 are the additional fractions of a fringe

N_g is the grating order of the band of continuous radiation used to produce fringes.

A, m, e, ... are shown in Figures 5-1 to 5-6 in practical measurement of the manganese spectra lines.

It was already mentioned in Section 3-1 that the grating instrument was enclosed in a cylindrical tank which could be evacuated to a pressure of 0.04 Torr, therefore in this system the vacuum wavenumber of Thorium lines can be used. Using vacuum standard wavenumbers in the measurement of the unknown wavelength of an element directly will avoid two possible sources of error:

48

1 - The error arising from conversion of wavenumbers
   to vacuum value.

2 - If the standard lines are observed in a different
   grating order from the measured lines in an air-
   filled instrument, the standard wavelengths should
   be converted to those at ambient conditions, and
   the measured values converted back to standard
   atmospheric condition.

   Therefore in this project, the spectrometer was
evacuated, and hence vacuum wavenumbers and wavelengths
were measured directly by using vacuum thorium standard
wavenumbers. Several thorium standard lines were
recorded on a chart during a run where no manganese
lines were observed. Two standards, one at each end of
the run were substituted for σ_1 and σ_s in equation
(3-7) to calculate 'A' and additional thorium standard
lines were used to check the accuracy of the wavenumber
calculation on the record.

   Referring to equation (3-5), the constant A
(separation of two fringes) is a function of the refract-
ive index of the medium between the etalon plates (μ).
Air is the medium between the plates in the measurement
of wavenumbers which can be warmed during the run and its
refractive index can be varied by variation of
temperature and pressure. A serious error can be
introduced if the wavenumber measurement was carried on

49

for a long run; and the charts were divided into short sections for measurement; and a number of calculations were made for an individual line using different standard wavenumbers to check the accuracy of A.

CHAPTER 4

EXPERIMENTAL PROCEDURE

4-1 Operation of Sources

To obtain the manganese spectrum one of the pre-
pared tubes (Chapter 2) containing manganese iodide was
used. The tube was struck in the small Broida cavity
while it was held along the axis of the cavity to
obtain the maximum intensity. The cavity was modified
by the author to hold the tube in the fixed position.
The tube was attached to a 5 mm diameter quartz rod,
and the rod was used to hold the tube in position in
the cavity. The tube could be turned and moved up and
down to achieve the proper position for maximum intensity
and minimum reflected power, and fixed by a locking
screw (Figure 4-1). This arrangement also prevented
the cold spot at the end of the tube which previously
rested on a cooled support. The tube was started at a
microwave power of seventy watts, reflected power
minimised to less than seven watts by adjusting the
tube and tuning the cavity, and then the power increased
to one hundred watts to obtain the optimum intensity.
The discharge was stable during the operation and had
a strong intensity with a diffuse glow filling the tube.

Thorium tube was struck in a 210 Broida cavity
and was used for standard lines.

4-2 Measurement of wavenumbers

The basic equations of a grating (e.g. Thorne[28]
1974) are:

In an auto-collimating grating spectrometer

$$n2\lambda = 2d \sin \theta$$

(4-1)

$$\text{or} \quad n = 2\sigma d \sin \theta$$

where λ is the wavelength of the incident light

σ is the wavenumber of the incident light

θ is the angle between the diffracted
light and the normal to the grating

d is the groove width of the grating

n is the order number of the wavelength

The angular dispersion of the grating is given by

$$d\theta/_{d\lambda} = \frac{n}{d\cos\theta} \qquad (4-2)$$

Rayleigks criterium condition for resolution in grating, leads to a slit limitation of the resolving power (Thorne[28] p.167) i.e. Two wavelengths $\delta\lambda$ apart can not be resolved unless they diverge at angle

$$\delta\theta \geqslant \frac{W}{f} \qquad (4-3)$$

where f is the focal length of the system

           W is the slit width of the grating spectro-meter

The resolving power achieved for $\theta = 30^{o}$, is given by

$$R = \frac{\lambda}{\delta\lambda} \sim \frac{f}{W} \qquad (4-4)$$

The optimum slit width (W) can be estimated from the expression (4-4)

$$W \sim \frac{f}{R}$$

where f is the focal length of the instrument, and R the resolving power of the grating. For the present

53

instrument R = 90000 and f = 150 cm, i.e. $W \sim 17 \mu$ m.

To record the majority of the manganese lines, with calibrating fringes of reasonable intensity, a slit width of 50 μ m, slightly greater than this optimum was used.

The recording procedure was started with locating the strong lines beforehand, suitable sensitivity of lock-in-amplifier was determined to record the peak of individual spectral lines during the run. Selected thorium standard lines to calibrate the fringes were recorded during the run by rotating at appropriate times a pivoted mirror Ma (Figure 4-2 and Figure 3-1).

Two standard thorium lines, one at each end of the run were used to calculate the fringe spacing A (equation 3-7). Additional thorium standard lines were recorded and used to check the accuracy of the measured wavenumbers.

Spectrum of manganese was also recorded with slit width of 75 and 100 μ for all section of spectrum to measure additional weak lines. The intensity of the calibrating fringes also increased whilst preserving the sharpness and symmetrical shape of the fringe profile.

The wavenumbers were calculated by substituting the number of calibrating fringes (m), the grating order (Ng) and the position of the line relative to the adjacent fringes (e_1, e_2) in equation (3-7).

Ma

Fig. 4-2

Water Jacket

Electrodeless discharge tube

Tube holder
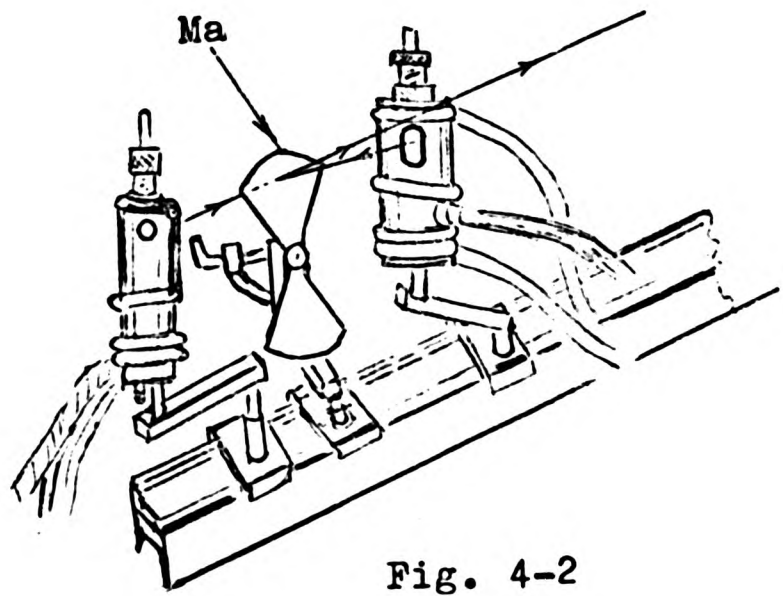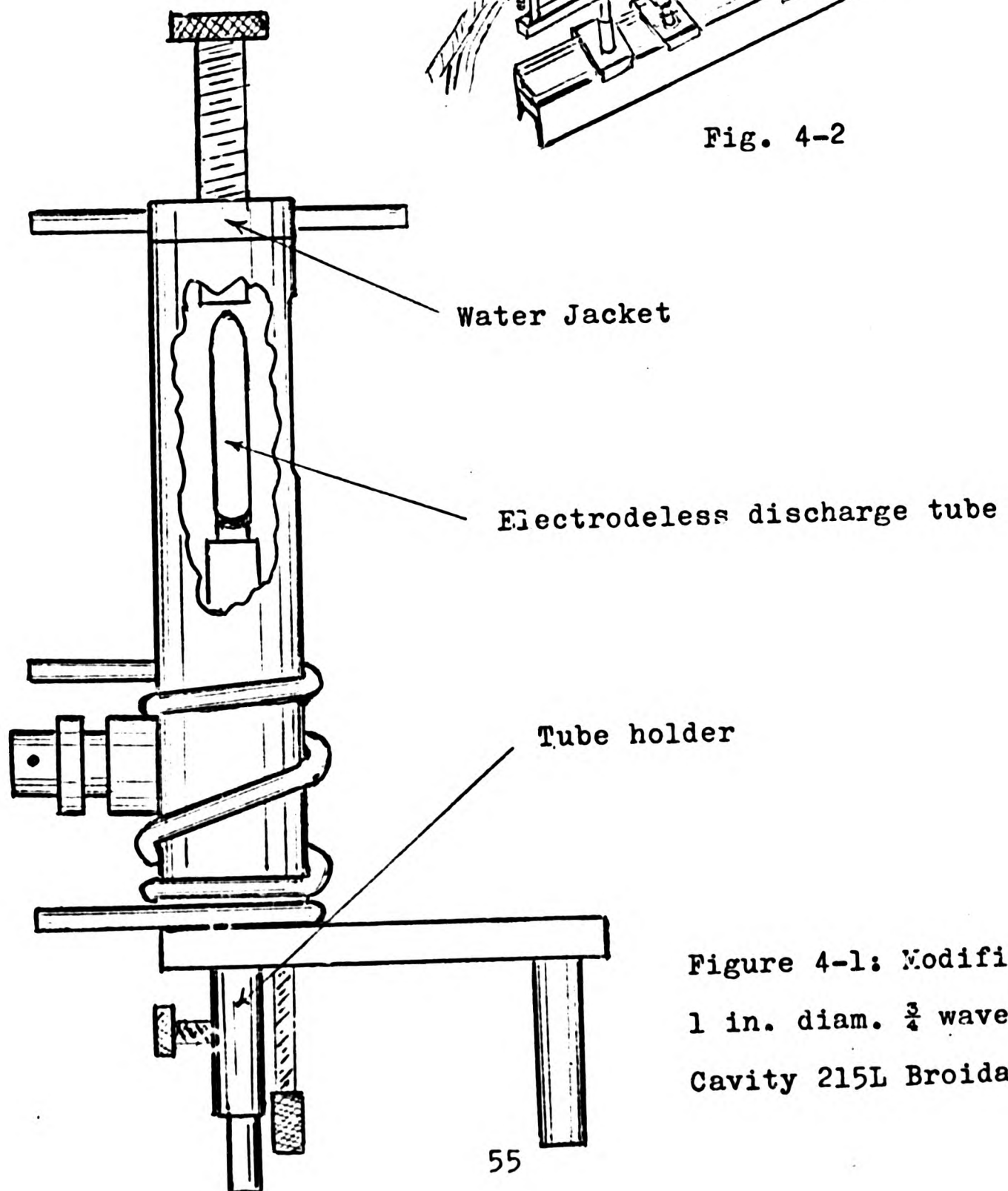
Figure 4-1: Modified
1 in. diam. ¾ wavelength
Cavity 215L Broida

55

The effect of strong water vapour absorption in the section of 1.3 - 1.4 μ and 1.8 - 1.95 μ of wavelength was reduced by pumping the main tank with a rotary pump to a pressure of 0.04 Torr during all measurements. The evacuation of the main tank also made possible the usage of vacuum standard wavenumbers of the thorium in calculation of the unknown wavenumbers.

The thorium and manganese visible light effect on the photomultiplier was avoided by using a "Chance" infra-red filter OX5 with 0.75 μ cut-off wavelength.

4-3 First and second order distinction

A spectrum was recorded without calibrating fringes using a Grubb-Parson silicon infra-red filter transmitting for $\lambda > 1.05$ in grating first order section 1.7 - 1.9 μ and 2.5 - 2.7 μ to eliminate the second order 0.89 - 0.98 μ and third order 0.83 - 0.9 μ , and a germanium infra-red filter transmitting $\lambda > 1.7 \mu$ in grating first order section 1.9 - 2.7 μ to eliminate the second order 0.95 - 1.35 μ . In the second setting silicon infra-red filter was used during the run to record the first order only.

4-4 Accuracy of wavenumbers

The accuracy of wavenumbers is affected by the errors such as:

56

a - dissimilar grating face illumination by
     manganese and thorium light.

b - variation of the fringe separation A due to
     variation of the wavelength while the two
     pens (pen recorder pens) have certain separ-
     ation during the run. Two traces slightly
     displaced due to the pen separation. This
     separation will correspond tc slightly differ-
     ing wavenumber interval at the two ends of the
     trace.

c - human error in measuring the relative position
     of the line from the fringe (e).

d - non-uniformity of drive at the end of lead
     screw in the spectrometer which affected the
     fringe spacing in this work.

a - Effort was made to arrange an optical system (Figure
     3-1) with the same path length for thorium and man-
     ganese lights. This was achieved by using a pivoted
     mirror Ma (Figure 4-2) (Section 4-2). In a later
     measurement of zirconium spectrum (Section 6-4)
     the tubes were changed place in the cavities to
     investigate the differences in callimation between
     zirconium light source and thorium caused by system-
     atic shifts in line position, but the result of the

57

calculation for the lines with precision A
(accuracy of ± 0.02 cm^{-1}) revealed a reasonable
agreement between the measurements.

b - The effect of fringe separation (A) variation on
the position measurement of the line relative to
the fringes (e) was reduced by dividing the trace
into relatively small sections.

c - The human error was reduced by repeating the
relative position measurement of the lines and
averaging the results, and also averaging the
calculated wavenumbers on at least three separate
charts for a line.

d - Non-uniformity of drive at the end of the lead
screw was reduced by ignoring the use of the end
part of the lead screw and record the same section
of spectrum in the other setting of the grating.

4-5 Error calculation

Considering equation (3-7) and the usual law of
errors in a fraction[37], the error in the wavenumber
is:

$$\Delta\sigma_1 = \left[(N_1 \Delta\sigma_s / Ng)^2 + (N_1 \, m^{\Delta A}/Ng)^2 + (A\Delta e_1/Ng)^2 \right.$$

$$\left. + (A\Delta e_2/Ng)^2 \right]^{\frac{1}{2}} \qquad\qquad (4-5)$$

58

(The symbols are as defined in Section 3-6)

where: $\Delta \sigma_s$ is the error in the thorium standard line, and is about 0.001 cm^{-1}.

N_i and N_s were in the order of 1 or 2.

Ng was in the order of 3.

m was in the average less than 500

A was in the order of 0.5 cm^{-1}.

Δe_1 or Δe_2 is the error on the relative position of a line measured by vernier, but since in re-measuring a maximum error of 0.02 cm was observed, this value is considered for Δe.

ΔA the fringe space A was calculated using a nine digit calculator. The calculator has an error of order of 10^{-9}, but, considering the temperature and pressure variation in the laboratory during the run, this will vary the air density surrounding the etalon and will affect the fringe space A. The other factor is the error in the standard line position

59

calculation. However, the error in
A calculated choosing different
standard lines in each run, and in the
same section of spectrum in different
charts, did not exceed 5×10^{-5} cm^{-1}.

Substituting the above errors and other factors
involved, in equation (4-5), the difference $\Delta\sigma_1$ in
second order will be:

$$\Delta\sigma_1 = \left[(2 \times \frac{10^{-3}}{3})^2 + (2 \times 500 \times 5 \times \frac{10^{-5}}{3})^2 \right.$$
$$\left. + 2(0.5 \times 0.02/3)^2 \right]^{\frac{1}{2}} \qquad (4-6)$$

$$\Delta\sigma_1 = 0.017 \text{ cm}^{-1}$$

In practice, the difference $\Delta\sigma_1$ calculated for
checking thorium standards had a majority of less than
half value of 0.017 cm^{-1}. 46 checking thorium spectra
lines were measured during a complete run ranging
$0.79 - 2.7 \mu$m. The errors of this measurement do not
include any collimation effects, since the same source
was used throughout the measurement for standard and
checking thorium lines. Table 4-1 shows the wavenumber
differences between the measured and standard wavenumber
of thorium lines as the checking thorium standard lines.
The histogram of the errors observed in the wavenumbers
(the wavenumber differences) of checking thorium standard

60

Table 4-1: Thorium standard lines used for checking

Vacuum standard wave No. in cm^{-1}	Vacuum measured wave No. in cm^{-1}	Wave No. Diff.	Vacuum standard wave No. in cm^{-1}	Vacuum measured wave No. in cm^{-1}	Wave No. Diff.
5052.698	5052.694	+0.004	7911.643	7911.641	−0.002
5055.690	5055.692	+0.002	8035.089	8035.080	−0.009
5172.059	5172.050	−0.009	8035.089	8035.095	+0.006
5314.339	5314.339	0.000	8035.089	8035.088	−0.001
5573.722	5573.713	−0.009	8052.465	8052.454	−0.011
5776.210	5776.202	−0.008	8176.934	8176.933	−0.001
5961.916	5961.925	+0.009	8244.201	8244.197	−0.004
6559.783	6559.782	−0.001	8489.233	8489.242	+0.009
6930.737	6930.748	+0.011	8605.376	8605.375	−0.001
7095.168	7095.151	−0.017	8700.925	8700.934	+0.009
7100.423	7100.419	−0.004	8719.781	8719.804	+0.029
7105.003	7105.010	+0.007	8879.362	8879.367	+0.005
7331.490	7331.509	+0.019	9041.561	9041.547	−0.014
7271.514	7271.497	−0.017	9179.980	9179.982	+0.002
7336.842	7336.856	+0.014	9296.035	9296.045	+0.010
7365.952	7365.949	−0.003	9525.879	9525.885	+0.006
7478.062	7478.064	+0.002	9525.885	9525.885	+0.006
7478.062	7478.060	−0.002	9783.554	9783.558	+0.004
7648.529	7648.518	−0.011	9958.060	9958.059	−0.001
7648.529	7648.533	+0.004	9958.060	9958.055	−0.005
7769.909	7769.905	−0.004	10654.337	10654.334	−0.003
7833.560	7833.561	+0.001	10702.890	10702.864	−0.026
7833.560	7833.556	−0.004	11048.779	11048.804	+0.005
7833.560	7833.561	+0.001			

61

lines is shown in figure 4-3.

Table 4-1 and the error histogram shown in figure
4-3 indicate that the average error on the wavenumbers
measured should not be more than 0.02 cm^{-1}, as the
calculated error from equation (4-6) confirms the
above indication.

However, the errors assigned to the wavenumbers
of the manganese spectra lines are based on the differ-
ence between the largest wavenumber value measured for
an individual line and the average wavenumber of that
line. This applies to the sharp and well defined peak
and symmetric line. But some manganese line profiles
are broad with undefined peak, errors estimated for
these lines based to some extent on accuracy of estimated
centre of the line. The minimum error $\pm$0.02 cm^{-1} with
code A is assigned to the lines with strong intensity
and defined peak. Error of 0.05 cm^{-1} with code B is
given to the asymmetric but strong and narrow lines.
The error of $\pm$ 0.10 cm^{-1} with code C is given to the weak
and asymmetric lines. An error of $\pm$ 0.2 cm^{-1} with
Code D is given to the weak and noisy lines. Finally
an error of $\pm$ 0.5 cm^{-1} is given to the very weak and
noisy lines and also to the broad lines with suspicion
of overlapping of the lines indicated with Code E. In
the event of poor line peak, the mean vertical through
the profile was taken for the reading and an error of
0.05 cm^{-1} to 0.1 cm^{-1} was assigned to these lines.

62
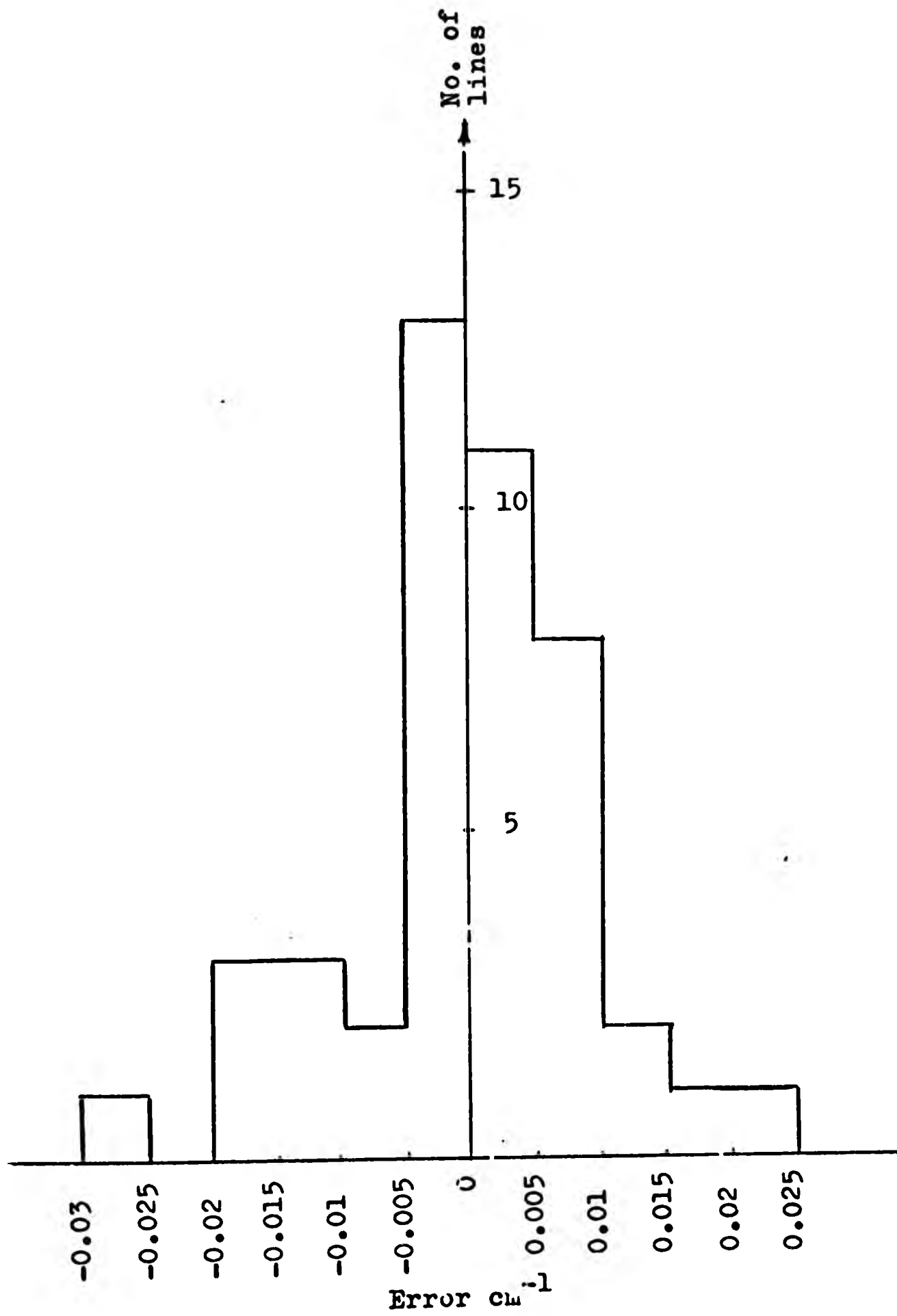
Fig. 4-3: Histogram of the errors observed in the Th checking lines.

63

4-6 Relative intensity

The relative intensity of the manganese lines are quoted by measuring the height of the lines above the average background levels on a chart.

The phase of the amplifier was adjusted for the maximum detection of the intensity and the phase accuracy by tuning the variable control and recording the increment of intensity to the maximum for a certain line.

The amplifier $30 \mu V$ sensitivity was used to record all the lines with intensity less than twenty (20 cm height on the chart). The amplifier sensitivity was reduced to the higher voltage appropriate to the strong line intensity to prevent the overloading of the penrecorder.

Relative intensity of the lines was reliable over a small wavelength range only as the efficiency of the blazed grating dropped for the wavelength longer than 2.4μ and the detector sensitivity reduced for the wavelength less than 1μ.

CHAPTER 5

MANGANESE RESULTS AND
INTERPRETATION

5-1 Introduction

Two manganese tubes were used to record the
wavenumbers of infra-red spectrum of manganese. The
tubes were stable with strong light intensity for an
incident power of 100 watts for the first 30 minutes
of operation after production, then the light intensity
reduced and the colour changed. To maintain the
optimum intensity the microwave power was increased
to 120 watts, the tube adjusted in the cavity, and the
cavity tuned to minimise the reflecting power. The
tube was intense and stable for the rest of the
recording but it was associated with background,
and the condition of the first 30 minutes was not
reproduceable. Both tubes behaved in the same way,
but one of them with less background compared with the
other and this was used in most of the wavenumber
measurements.

The recording and wavenumber calculation carried
on as explained in Chapter 4. Vacuum wavenumber of
218 manganese atom lines in the spectral range of
0.82 μ m to 1.97 μ m have been measured. These lines

have been compared with the strong iodine lines; two
iodine lines, 8897.113 cm^{-1} with intensity 6700 and
8803.262 cm^{-1} with intensity 2400 were found in the
measured wavenumber list of manganese as 8897.18 cm^{-1}
with relative intensity 4 and 8803.20 cm^{-1} with
intensity 1. These two lines were excluded from the
list, but they also confirmed the accuracy of the
present measurement, the present lines were also
checked with the calculated wavenumbers from the energy
levels of ionized manganese atom and no ionized lines
could be detected. The measured wavenumbers have been
compared with predicted lines from the known energy
levels and transitions assigned to 84 lines (TABLE
5-1, page 80), The majority of the strong lines
involve no change in spin, and confirm good L-S coup-
ling. The number of lines assigned with the trans-
itions involving a change in spin are very few and they
are weak lines. Eighty-four new lines were observed
in region 1.29 ~ 1.97 μ m in addition to 14 of the
sixteen strong lines recorded previously by Randal and
Barker[9] of these, 53 are assigned with the trans-
itions out of which 9 are overlapped close fine
structures which could not be resolved. The other two
lines observed by Randal and Barker (5767.0 cm^{-1} and
6262.1 cm^{-1}) may be buried in the wing of broad line
profile or overlapping fine structure of multiplet
$w^6F^o - e^6D$ and $z^8F^o - e^8D$ shown in Figures 5-1, 5-2 and

66
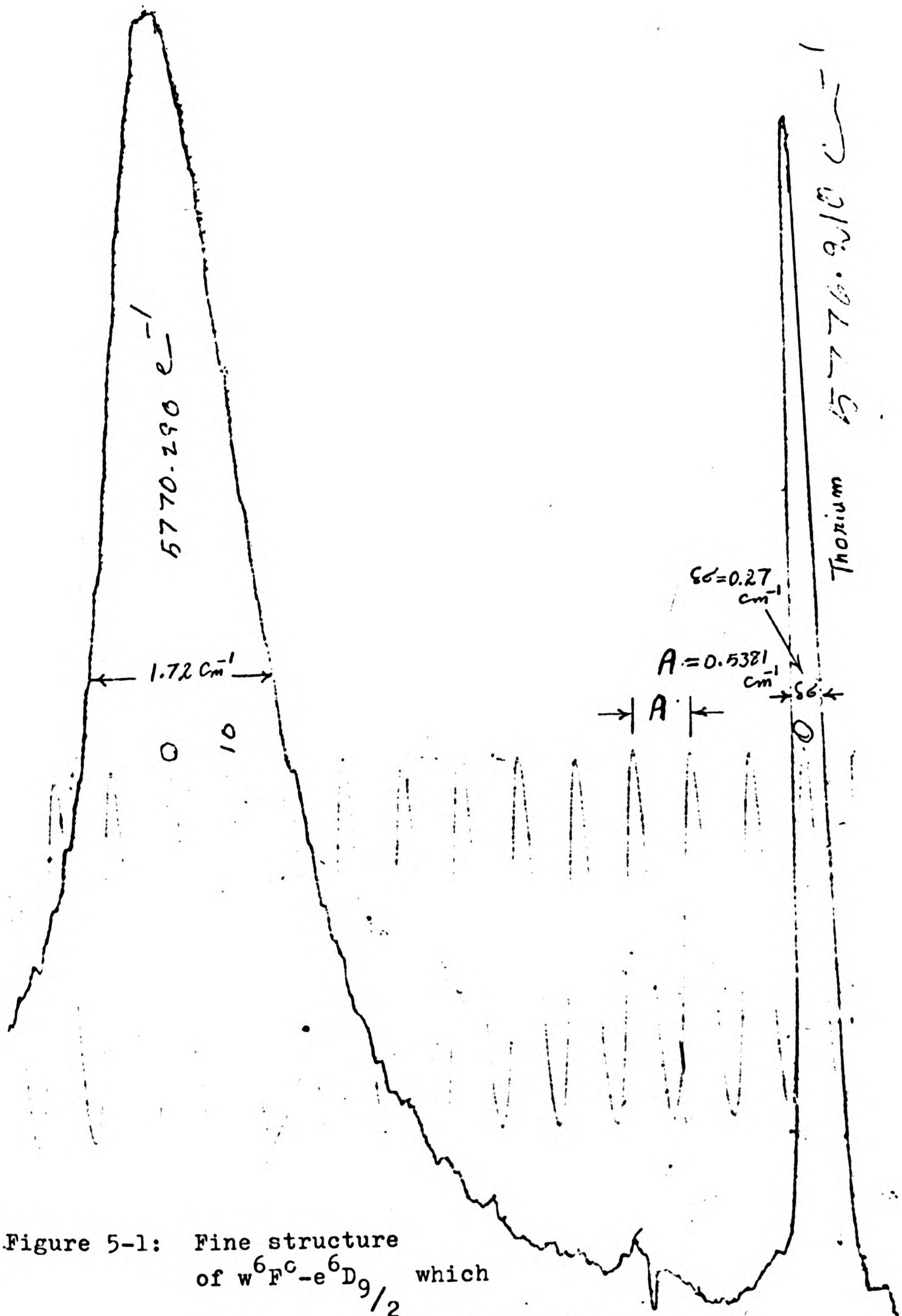
Figure 5-1: Fine structure
of $w^6F^c-e^6D_{9/2}$ which
gives a complicated structure
difficult to resolve.

67
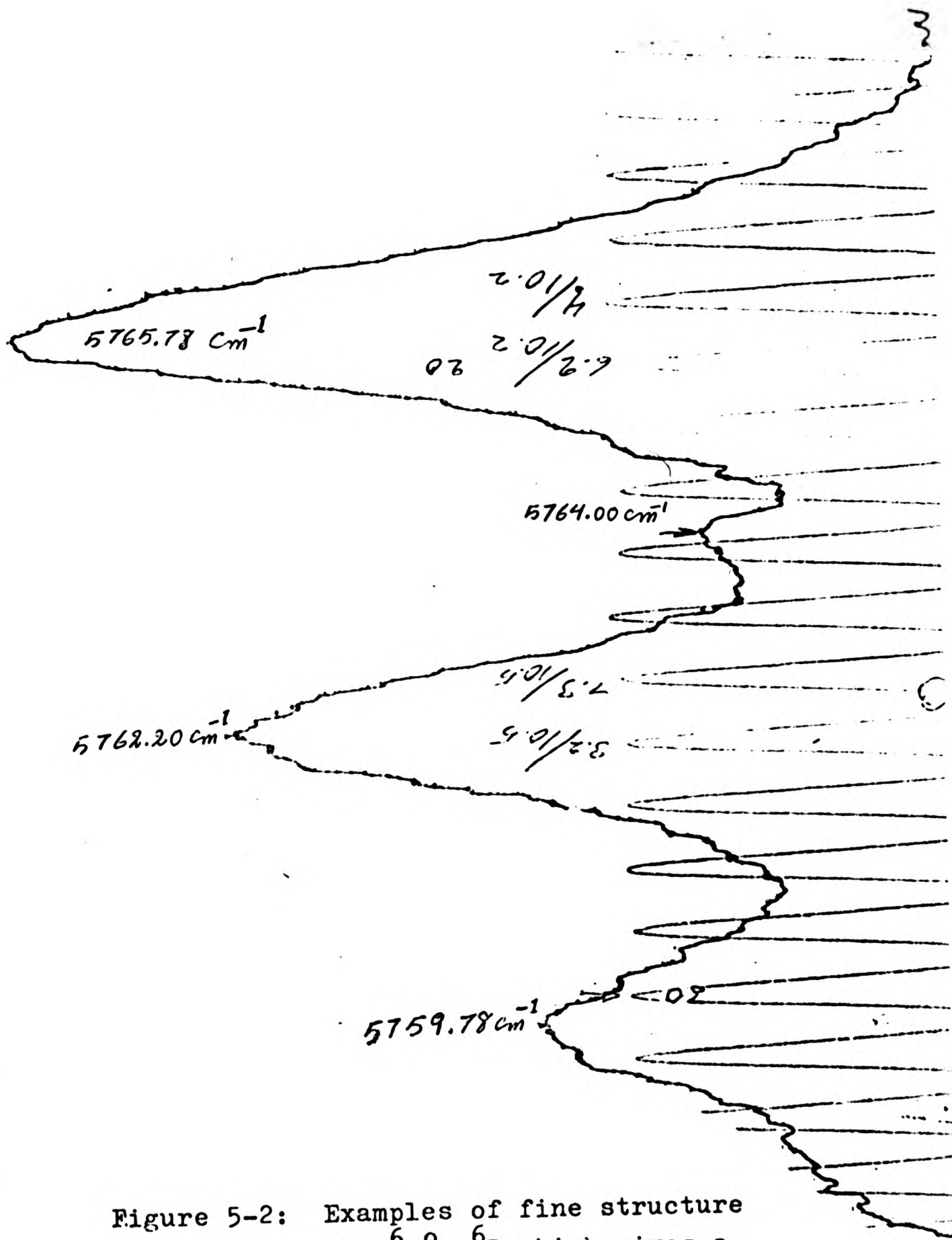
Figure 5-2: Examples of fine structure of w^6F^o-e^6D which gives a complicated structure.
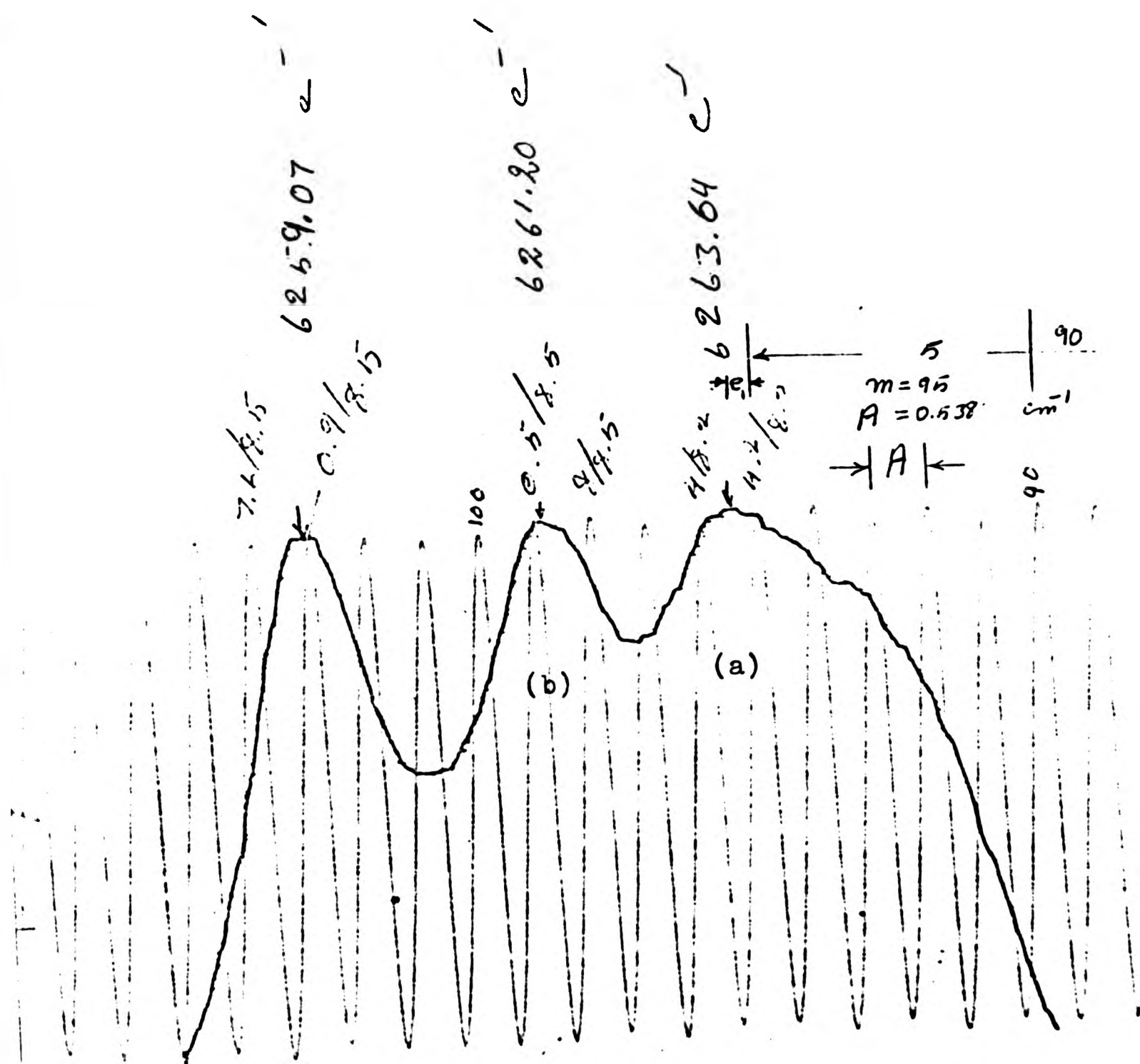
Figure 5-3:   Example of fine structure of $z^8F^o-e^8D$
which gives a complicated structure.

Figure 5-3.

18 transitions have been assigned to new lines in addition to other 15 lines given in Table of MnI – classified lines by Catolan, Meggers and Garcia[12] in spectral range of 0.826 to 1.239 μ m. There are nearly 20 strong lines, majority of them sharp and well defined in region 0.826 – 1.239 μ m (among the 120 observed lines in present) which could not be identified with the transitions involving manganese energy levels and they are listed in Table 5-2 (page 97). 82 lines in this wavelength region which have been previously observed and listed in MnI – classified lines could not be detected in present work but only seven lines are quoted strong and the rest quoted weak and hazy in the MnI – classified list.

Table 5-3 (page 98) compares previous and new measurements for the limited number of lines observed in both cases.

The wavelength measurement of manganese was extended to 2.8 μ m, but no line could be detected beyond 1.97 μ m in present observation of infra-red spectrum of manganese.

5-2 Shape of the line profile

The widths and shapes of the manganese lines recorded in this work varied very greatly. Many strong lines were well defined, reasonably narrow and

Figure 5-3.

18 transitions have been assigned to new lines in
addition to other 15 lines given in Table of MnI –
classified lines by Catolan, Meggers and Garcia[12] in
spectral range of 0.826 to 1.239 μ m. There are nearly
20 strong lines, majority of them sharp and well
defined in region 0.826 – 1.239 μ m (among the 120
observed lines in present) which could not be identi-
fied with the transitions involving manganese energy
levels and they are listed in Table 5-2 (page 97).
82 lines in this wavelength region which have been
previously observed and listed in MnI – classified
lines could not be detected in present work but only
seven lines are quoted strong and the rest quoted
weak and hazy in the MnI – classified list.

Table 5-3 (page 98) compares previous and new
measurements for the limited number of lines observed
in both cases.

The wavelength measurement of manganese was
extended to 2.8 μ m, but no line could be detected
beyond 1.97 μ m in present observation of infra-red
spectrum of manganese.

5-2 Shape of the line profile

The widths and shapes of the manganese lines
recorded in this work varied very greatly. Many strong
lines were well defined, reasonably narrow and

70

apparently symmetric, particularly the members of the
multiplet $z^6P^o - a^6D$ and $z^4P^o - a^4D$, although they are
still appreciably broader than the thorium standard
lines. Other lines are very much broader. The inter-
pretation of these variations in line profile is very
complex. In many terms, the fine structure interval
is small, often less than 1 cm^{-1}. The published data
on the hyperfine structure is restricted to a very
limited number of levels (H.E. White and R. Ritschl)[31, 32]
In some published cases, the interval factor A_F may
exceed 0.05 cm^{-1} and the total spread of components
exceeds 0.5 cm^{-1}. The interval factor can be positive
or negative. If it is positive for the terms
involved, the hyperfine splitting of the lines is less
marked (and the multiplet $z^6P^o - a^6D$ falls in this
category), but when the interval factors are of
opposite sign (e.g. e^6S, y^6P) very wide hyperfine
patterns must be expected. Lines in the multiplet
$e^6S - y^6P^o$ (Figures 5-4 and 5-5) thus show considerable
broadening; in agreement with hyperfine data. Other
even broader lines have been observed, (e.g. the
multiplet $w^6F^o - e^6D$ in Figures 5-1 and 5-2). No hfs
data is available for these levels, but the broadening
may well have the same origin. Broad lines are also
observed in the multiplet $z^8F^o - e^8D$ (Figure 5-3) -
in this case it appears to have been impossible to

71
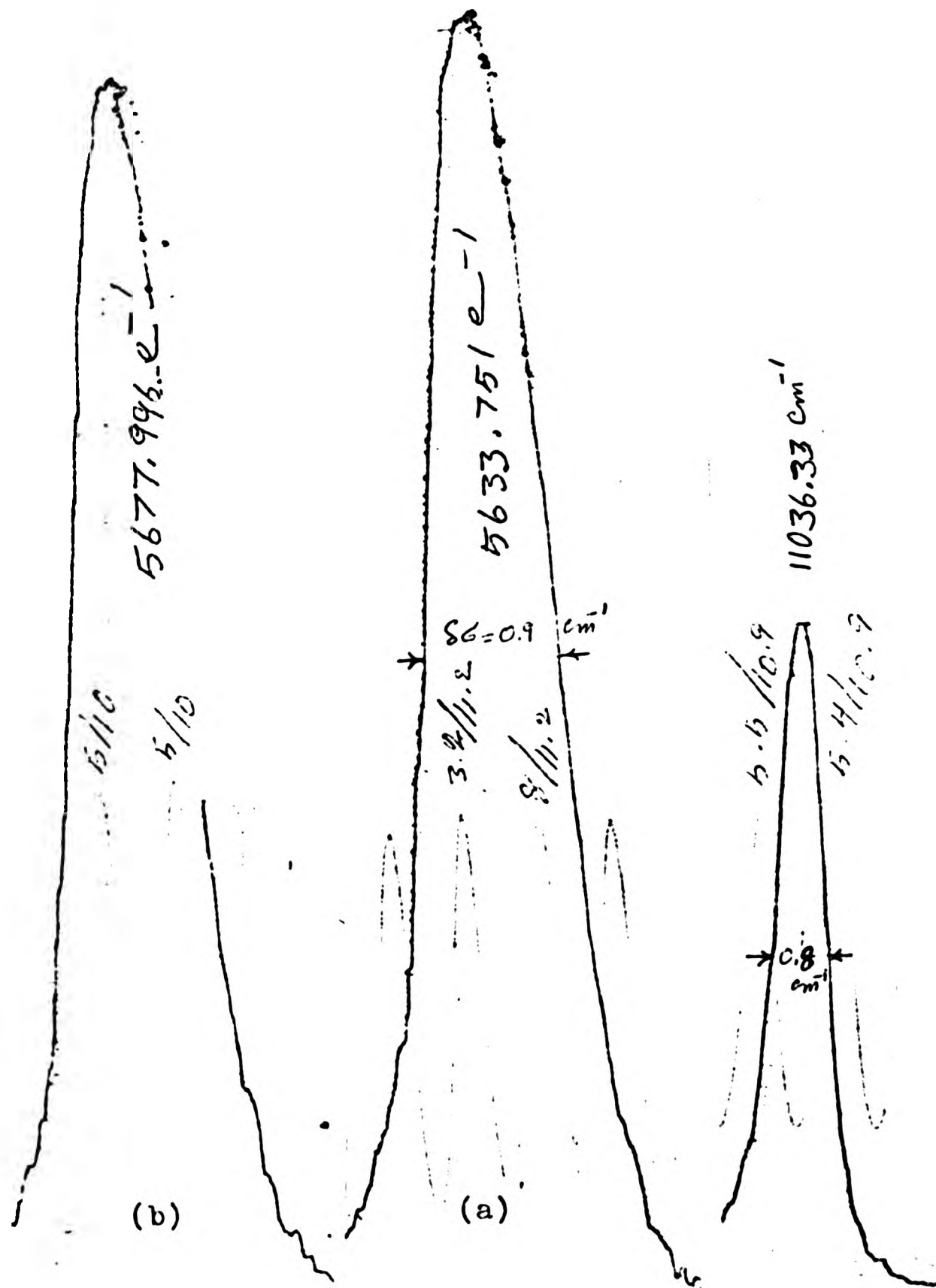
Figure 5-4: (a),(b) are the lines in
multiplet $e^6S - y^6P^o$
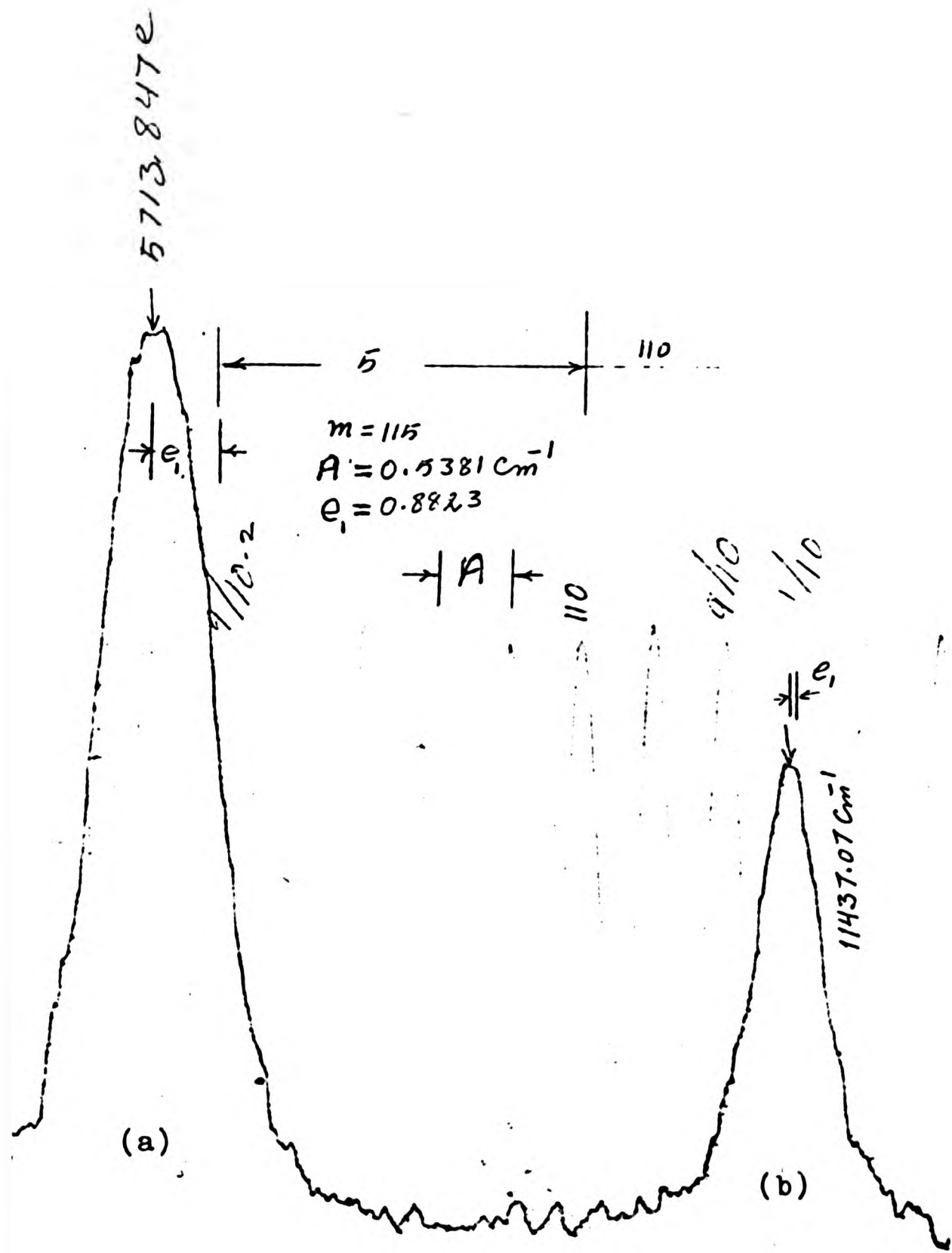
Figure 5-5: line (a) member of multiplet $e^6S - y^6P^o$

line (b) member of multiplet $e^6D - y^6P^o$

73
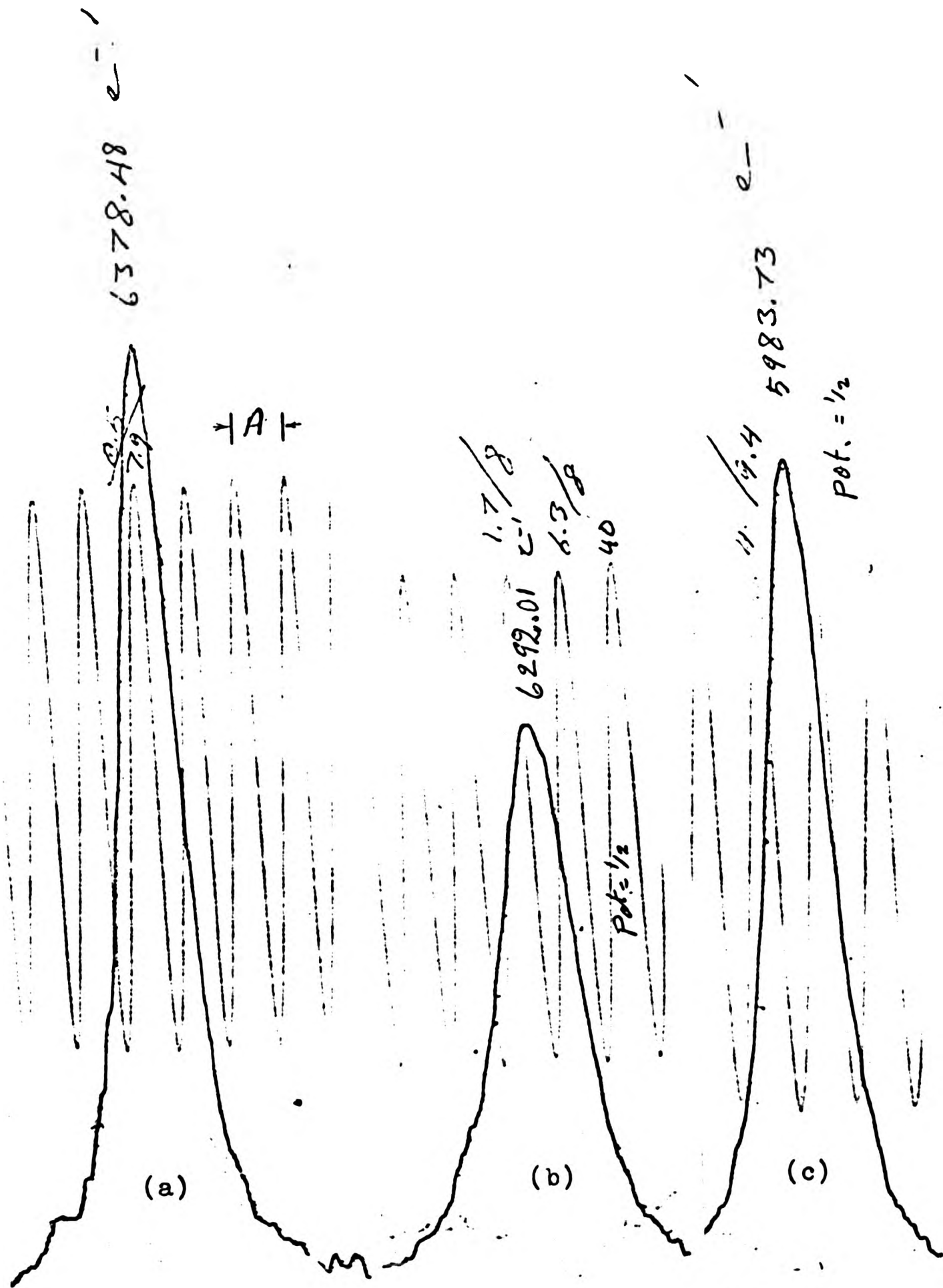
Figure 5-6: line (a) member of multiplet $y^6D^o - e^6S$
line (c) member of multiplet $w^6P^o - e^6S$

74

separate the fine structure components; since the
published data gives a common doubtful value of
52974.5? for the term z^8F^0.

5-3 Accuracy of present measurement

A comparison of present wavenumber measurement of
the manganese lines in multiplet $z^6P^0-a^6D$ and $z^4P^0-a^4D$
with the existing data and the predicted values from
energy levels are given as array multiplet in Table 5-4
and Table 5-5. These are multiplets involving strong
lines measured in present work and the lines fit
considerably well to the assigned transitions. The
complete multiplet array for $z^6P^0-a^6D$ and $z^4P^0-a^4D$,
with good agreement of multiplet intervals supports
the accuracy of the measurement.

Example of inaccuracy in energy levels have been
observed in present measurement, these are energy
levels involved in the transitions assigned to the
very weak lines in previous observation by other
investigators, and possibly the calculation of these
energy levels was made using a transition involved and
assigned to a weak line or a wrong assignment. An
example of this is the level $y^8P^0_{9/2}$ for which a
difference of 0.79 cm^{-1} have been observed in a
transition involving this level ($y^8P^0_{9/2} - e^8S_{7/2}$).

75

This is a strong line and the other two members of
this multiplet are present and fit the transition
assigned with a good agreement; the intensity of the
lines are as expected and confirm the assignement.

In the wavenumber list of manganese line[12], a
difference of 0.95 cm^{-1} is quoted for a transition
involving another level of the y^8P^o term, $y^8P^o_{7/2}$
($y^8P^o_{7/2} - a^6S_{5/2}$), this is a very weak line and could
well have been wrongly identified. The quoted value
for this level is in good agreement with the present
infra-red measurements.

In present work a repeated pattern of a group of
lines have been seen which are confined to a limited
spectrum band width of 23.2 nm in region 10260 Å to
10492.7 Å. These patterns are shown in Figure 5-7,
(recorded with fast scan speed of 40 Å/min. In slow
scan of 5 Å/min the repeated patterns are more
pronounced, and it appears likely to be a band struc-
ture. It is not expected to have a band structure
from the excited electrodeless tube containing halides,
since the procedure of tube preparation (Chapter 2)
should not permit a formation of manganese dioxide
and the halide is normally fully dissociated. But
a reaction may occur between manganese and the oxygen
released from the hot quartz wall of the tube when the
tube was sealed off using a gas torch. A black

76

9645.84 cm^{-1}

9639.27 cm^{-1}

9626.20 cm^{-1}

9615.37 cm^{-1}

9604.35 cm^{-1}

9593.27 cm^{-1}

9588.32 cm^{-1}

9582.16 cm^{-1}

9577.51 cm^{-1}

9570.31 cm^{-1}

9557.77 cm^{-1}

9551.66 cm^{-1}

9534.82 cm^{-1}

9531.29 cm^{-1}
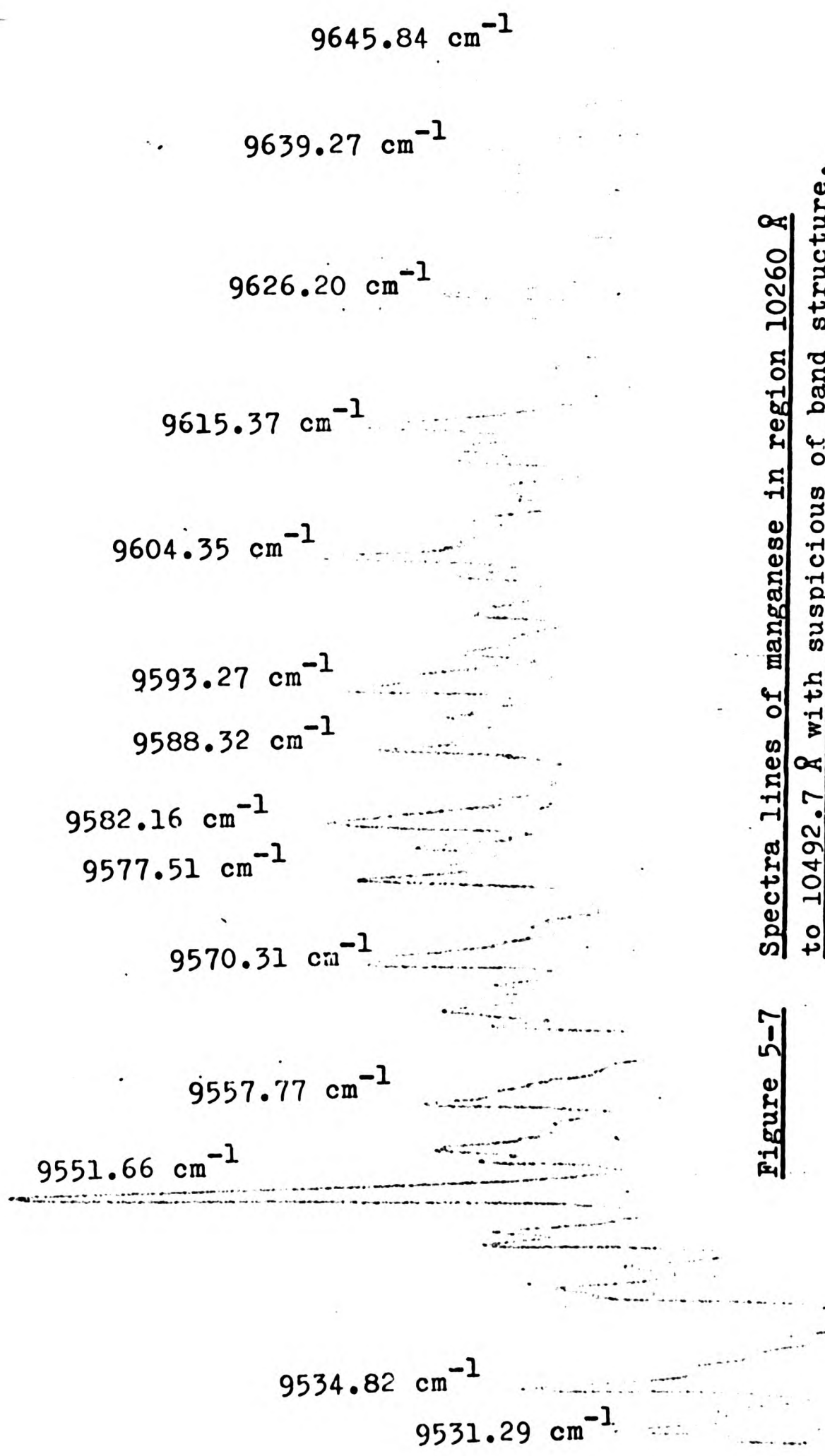
Figure 5-7   Spectra lines of manganese in region 10260 Å to 10492.7 Å with suspicious of band structure. This chart is taken with scan speed of 40 Å/min.

77

deposit was formed at the end of the tube when it
was sealed, and it was increased when the tube was
run for the first 30 minutes of recording. The
measured wavenumber of the manganese lines with
suspicious of band structure are rather weak and
these lines are marked in the Table 5-1 with an
asterisk.

5-4 Data presentation

In present measurement, vacuum wavenumber of 218
manganese lines in spectral range of $0.82\,\mu$ m $- 1.97\mu$ m
have been measured, normally from a minimum of three
charts for a line to be included.

The intensities quoted are measured as heights
above the average background level.

The wavelength quoted in Table 5-1 are simply
converted from vacuum wavenumbers to vacuum wavelentghs,
since the comparison made is only involving the vacuum
wavenumbers, and all the measurement was carried out
in vacuum condition using vacuum standard lines.

The Table 5-1 is arranged as follows:-

1. Observed vacuum wavelength ($\overset{o}{A}$). An asterisk
   denoted a suspected band structure (Sec.5-3)

2. Observed vacuum wavenumber (cm^{-1})

3. Relative intensity

78

4. Wavenumber precision:- A, $\pm$ 0.02 cm^{-1};
   B, $\pm$ 0.05 cm^{-1}; C, $\pm$ 0.10 cm^{-1}; D, $\pm$ 0.20 cm^{-1};
   E, $\pm$ 0.5- cm^{-1}.

5. Quality of lines:- The following letters
   stand for: B - broad; VB - very broad;
   h - hazy; AS - asymmetric; ASS - asymmetric
   with suspected line on short wavelength side;
   ASL - asymmetric with suspected line on long
   wavelength side.

6-12. Transition assigned:-
   6 - The upper level energy
   7 - The upper level J value
   8 - The upper level state
   9 - The lower level energy
   10 - The lower level J value
   11 - The lower level state
   12 - The calculated vacuum wavenumber from
        term values

13. The wavenumber difference between the observed
    and calculated wavenumbers from term values.

TABLE 5-1   THE INFRA-RED SPECTRUM OF MANGANESE

Vacuum wave length in Å	Vacuum wave No. in Cm⁻¹	Rela-tive inten-sity	Wave No of line pre-cision	Quality	Upper energy level		Lower energy level			Calcu-lated wave No in Cm⁻¹	Wave No diff. $\sigma_{obs} - \sigma_{calc}$
					energy	J value / state	energy	J value	state		
(1)	(2)	(3)	(4)	(5)	(6)	(7)(8)	(9)	(10)	(11)	(12)	(13)
19728.11	5068.91	8	D	B							
19514.25	5124.46	1	E	h							
19391.68	5156.85	2	D	h	56462.08	7/2 e⁴D	51305.41	5/2	x⁴P°	5156.67	0.18
18859.21	5302.45	2	D	AS							
18832.64	5309.93	2	D	h							
18729.12	5339.28	3	D								
18675.36	5354.65	3	D								
18049.96	5540.18	2	D	h							
17750.17	5633.75	20	D	B	41403.93	5/2 e⁶S	35769.97	7/2	y⁶P°	5633.96	0.21
17713.72	5645.34	2	E	Bh	50904.68	5/2 g⁶S	45259.17	3/2	x⁶P°	5645.51	-0.17

TABLE 5-1 (Continued)

(1)	(2)	(3)	(4)	(5)	(6)	(7)	(8)	(9)	(10)	(11)	(12)	(13)
17611.87	5677.99	18	D	B	41403.93	5/2	e^6S	35725.85	5/2	y^6P°	5678.08	-0.09
					55690.80	5/2	h^6D	50012.53	5/2	v^6P°	5678.27	-0.28
17560.96	5694.45	1	E	h								
17501.30	5713.86	12	B		41403.93	5/2	e^6S	35689.98	3/2	y^6P°	5713.95	-0.09
17396.42	5748.31	2	E	h	50904.68	5/2	g^6S	45156.11	5/2	x^6P°	5748.57	-0.26
17361.77	5759.78	10	E	B	52977.93	3/2	w^6F°	47218.15	3/2	e^6D	5759.78	0.00
					52978.03	5/2	w^6F°	47218.15	3/2	e^6D	5759.88	-0.10
17354.48	5762.20	15	E	B	52977.82	7/2	w^6F°	47215.61	5/2	e^6D	5762.21	-0.01
					52977.93	3/2	w^6F°	47215.61	5/2	e^6D	5762.32	-0.12
					52978.03	5/2	w^6F°	47215.61	5/2	e^6D	5762.42	-0.22
17343.71	5765.78	20	E	B	52977.75	9/2	w^6F°	47212.06	7/2	e^6D	5765.69	0.09
					52977.82	7/2	w^6F°	47212.06	7/2	e^6D	5765.76	0.02
					52978.03	5/2	w^6F°	47212.06	7/2	e^6D	5765.97	-0.19
17330.15	5770.29	25	E	B	52977.75	9/2	w^6F°	47207.28	9/2	e^6D	5770.47	-0.18
					52977.82	7/2	w^6F°	47207.28	9/2	e^6D	5770.54	-0.25
					52977.89	11/2	w^6F°	47207.28	9/2	e^6D	5770.61	-0.32

TABLE 5-1 (Continued)

(1)	(2)	(3)	(4)	(5)	(6)	(7)	(8)	(9)	(10)	(11)	(12)	(13)
17219.23	5807.46	6	C	h								
16995.70	5883.84	2	E	Bh	51638.17	5/2	e^4P	45754.27	7/2	z^4D^o	5883.90	−0.06
16918.84	5910.57	3	D	Bh	50904.68	5/2	g^6S	44993.92	7/2	x^6P^o	5910.76	−0.16
16874.96	5925.94	1	E	h								
16832.89	5940.75	1	E	h								
16797.43	5953.29	1	E	h	55368.66	3/2	w^4P^o	49415.35	5/2	f^6S	5953.31	−0.02
16765.90	5964.46	4	D	h								
16711.98	5983.73	25	B	AS	47387.62	7/2	w^6P^o	41403.93	5/2	e^6S	5983.69	0.04
16706.71	5985.62	1	E	h								
16685.52	5993.22	6	C	AS								
16659.36	6002.63	1	E	h								
16565.53	6036.63	1	E	h								
16559.83	6038.71	1	E	h								
16549.58	6042.45	1	E	h								
16543.83	6044.55	1	E	h								

TABLE 5-1 (Continued)

(1)	(2)	(3)	(4)	(5)	(6)	(7)	(8)	(9)	(10)	(11)	(12)	(13)
16526.74	6050.80	2	C	h								
16525.98	6051.08	1	C	h								
16517.79	6054.08	1	D	h	53261.42	7/2	t^6P^o	47207.28	9/2	e^6D	6054.14	-0.06
16500.02	6060.60	1	D	h								
16493.10	6063.14	10	C									
16490.09	6064.25	1	E	h								
16477.40	6068.92	2	C	h	57621.90	3/2	f^4D	51552.78	1/2	x^4P^o	6069.12	-0.20
16386.32	6102.65	4	C	h	56462.08	7/2	e^4D	50359.28	7/2	y^4F^o	6102.80	-0.15
16350.24	6116.12	1	D	h								
16246.37	6155.22	1	E									
16222.31	6164.35	1	E	h								
16220.15	6165.17	1	D	h								
16211.32	6168.53	1	E	h								
16205.51	6170.74	1	E	h								
16194.44	6174.96	1	E	h								

TABLE 5-1 (Continued)

(1)	(2)	(3)	(4)	(5)	(6)	(7)	(8)	(9)	(10)	(11)	(12)	(13)
16157.44	6189.10	1	E	h	56561.95	5/2	e^4D	50373.23	5/2	y^4F^o	6188.72	0.38
16099.95	6211.20	5	D	AS								
16064.98	6224.72	1	E	h								
16042.22	6233.55	3	D	h								
15976.81	6259.07	30	E	B								
15971.38	6261.20	30	E	VB	52974.50	9/2	z^8F^o	46712.58	11/2	e^8D	6261.92	−0.72
					52974.50	11/2	z^8F^o	46712.58	11/2	e^8D	6261.92	−0.72
					52974.50	13/2	z^8F^o	46712.58	11/2	e^8D	6261.92	−0.72
15965.16	6263.64	30	E	VBAS	52974.50	7/2	z^8F^o	46710.15	9/2	e^8D	6264.35	0.71
					52974.50	9/2	z^8F^o	46710.15	9/2	e^8D	6264.35	0.71
					52974.50	11/2	z^8F^o	46710.15	9/2	e^8D	6264.35	0.71
15893.17	6292.01	30	B	AS								
15793.05	6331.90	5	D	B								
15755.23	6347.10	2	E	Bh								
15747.73	6350.12	6	C	h	47753.99	5/2	y^6D^o	41403.93	5/2	e^6S	6350.06	0.06
15696.89	6370.69	8	C	C	47774.52	7/2	y^6D^o	.41403.93	5/2	e^6S	6370.59	0.10

TABLE 5-1 (Continued)

(1)	(2)	(3)	(4)	(5)	(6)	(7)	(8)	(9)	(10)	(11)	(12)	(13)
15693.41	6372.10	2	D									
15677.72	6378.48	15	C		47782.43	3/2	y^5D°	41403.93	5/2	e^6S	6378.50	0.02
15552.60	6425.66	1	E	B								
15267.11	5550.03	30	B	B	45981.44	5/2	y^8P°	39431.31	7/2	e^8S	6550.13	-0.10
15222.32	6569.30	50	B	B	46000.77	7/2	y^8P°	39431.31	7/2	e^8S	6569.46	-C.16
15163.81	6594.65	60	B	B	46026.75	9/2	y^8P°	39431.31	7/2	e^8S	6595.44	-0.79
15037.35	6650.11	1	E	h	54950.66	5/2	g^6D	48300.98	3/2	y^6F°	6649.68	0.43
14972.77	6678.79	5	E	Bh	52705.23	11/2	f^8D	46026.75	9/2	y^8P°	6678.48	0.31
14966.16	6681.74	5	E	B	54953.02	3/2	g^6D	48270.91	5/2	y^6F°	6682.11	-0.37
14922.17	6701.44	5	E	h	52702.48	5/2	f^8D	46000.77	7/2	y^8P°	6701.71	-0.27
					52702.48	7/2	f^8D	46000.77	7/2	y^8P°	6701.71	-0.27
14919.81	6702.50	3	E	h	56801.40	3/2	h^8D	50099.16	3/2	v^6P°	6702.24	0.26
					56801.40	5/2	h^6D	50099.16	3/2	v^6P°	6702.24	0.26
					52703.10	9/2	f^8D	46000.77	7/2	y^8P°	6702.33	0.17
14879.38	6720.71	2	E	h	54946.09	7/2	g^6D	48225.99	7/2	y^6F°	6720.10	0.61

TABLE 5-1 (Continued)

(1)	(2)	(3)	(4)	(5)	(6)	(7)	(8)	(9)	(10)	(11)	(12)	(13)
14878.49	6721.11	2	E	h	52702.48	3/2	f^8D	45981.44	5/2	y^8P^o	6721.04	0.07
					52702.48	5/2	f^8D	45981.44	5/2	y^8P^o	6721.04	0.07
					52702.48	7/2	f^8D	45981.44	5/2	y^8P^o	6721.04	0.07
14464.54	6913.46	2	E	Bh	56801.40	5/2	h^8D	49888.08	7/2	v^6P^o	6913.32	0.14
					56801.40	7/2	h^5D	49888.08	7/2	v^6P^o	6913.32	0.14
					56801.40	9/2	h^8D	49888.08	7/2	v^6P^o	6913.32	0.14
14228.48	7028.16	1	D	h	50081.31	11/2	z^4H^o	43053.30	13/2	b^2I	7028.01	0.15
14001.41	7142.14	200	A		24779.32	3/2	z^6P^o	17637.15	1/2	a^6D	7142.17	0.03
13867.99	7210.85	250	A		24779.32	3/2	z^6P^o	17568.48	3/2	a^6D	7210.84	0.01
13851.24	7219.57	80	A		24788.05	5/2	z^6P^o	17568.48	3/2	a^6D	7219.57	0.00
13778.66	7257.60	15	B		31076.42	3/2	z^4P^o	23818.87	1/2	a^4D	7257.55	0.05
13733.23	7281.61	10	C		31001.15	5/2	z^4P^o	23719.52	3/2	a^4D	7281.63	-0.02
13715.92	7290.80	1	E	h	54950.66	5/2	g^6D	47659.52	5/2	w^6P^o	7291.14	-0.34
13698.16	7300.25	1	E	h								
13687.12	7306.14	50	B		31124.95	1/2	z^4P^o	23818.87	1/2	a^4D	7306.08	0.06
13646.55	7327.86	70	A		24779.32	3/2	z^6P^o	17451.52	5/2	a^6D	7327.80	0.05

TABLE 5-1 (Continued)

(1)	(2)	(3)	(4)	(5)	(6)	(7)	(8)	(9)	(10)	(11)	(12)	(13)
13630.48	7336.50	300	A		24788.05	5/2	$z\,^6P^o$	17451.52	5/2	$a\,^6D$	7336.53	-0.03
13604.15	7350.70	60	A		24802.25	7/2	$z\,^6P^o$	17451.52	5/2	$a\,^6D$	7350.73	-0.03
13592.68	7356.90	60	A		31076.42	3/2	$z\,^4P^o$	23719.52	3/2	$a\,^4D$	7356.90	0.00
13503.59	7405.44	50	A		31124.95	1/2	$z\,^4P^o$	23719.52	3/2	$a\,^4D$	7405.43	0.01
13419.36	7451.92	30	A		31001.15	5/2	$z\,^4P^o$	23549.20	5/2	$a\,^4D$	7451.95	-0.03
13322.66	7506.01	400	A		24788.05	5/2	$z\,^6P^o$	17282.00	7/2	$a\,^6D$	7506.05	-0.04
13297.38	7520.28	600	A		24802.25	7/2	$z\,^6P^o$	17282.00	7/2	$a\,^6D$	7520.25	0.03
13285.10	7527.23	300	A		31076.42	3/2	$z\,^4P^o$	23549.20	5/2	$a\,^4D$	7527.22	0.01
13180.74	7586.83	3	E	Bh								
13153.29	7602.66	30	B									
13152.48	7603.13	50	A									
12979.44	7704.49	300	A		31001.15	5/2	$z\,^4P^o$	23296.67	7/2	$a\,^4D$	7704.48	0.01
12933.52	7731.85	1	E	h								
12903.29	7749.96	600	A		24802.25	7/2	$z\,^6P^o$	17052.29	9/2	$a\,^6D$	7749.96	0.00
12399.27	8064.99	1	E	h								

TABLE 5-1 (Continued)

(1)	(2)	(3)	(4)	(5)	(6)	(7)	(8)	(9)	(10)	(11)	(12)	(13)
12393.55	8068.71	1	E	h								
12274.14	8147.21	20	A									
12106.86	8259.78	20	B	B								
12034.82	8309.22	100	A									
11994.79	8336.95	30	B									
11987.48	8342.04	70	A		54460.30	5/2	h^6S	46083.89	3/2	z^4D^o	8376.41	0.21
11937.99	8376.62	2	E		43428.58	9/2	z^6F^o	35041.37	7/2	a^4F	8387.21	0.31
11922.46	8387.53	1	E		49888.08	7/2	v^6P^o	41403.93	5/2	e^6S	8484.15	−0.02
11786.71	8484.13	20	B	B								
11761.87	8502.05	1	E	h								
11732.32	8523.46	1	E	h	43524.08	7/2	z^6F^o	34938.70	9/2	a^4F	8585.38	−0.05
11647.78	8585.33	1	E	h								
11636.49	8593.66	1	E	h								
11622.64	8603.90	1	E	h	50012.53	5/2	v^6P^o	41403.93	5/2	e^6S	8608.60	−0.10
11616.43	8608.50	12	B	B								

TABLE 5-1 (Continued)

(1)	(2)	(3)	(4)	(5)	(6)	(7)	(8)	(9)	(10)	(11)	(12)	(13)
11500.77	8695.07	8	B	B	50099.16	3/2	v^6P^o	41403.93	5/2	e^6S	8695.23	−0.16
11447.91	8735.22	1	E	h								
11425.39	8752.44	1	E	h								
11249.78	8889.06	1	E	h								
11239.50	8897.14	3	D	h								
11190.84	8935.85	1	E	h								
11021.20	9073.42	6	D	h								
10982.49	9105.40	8	B									
10872.67	9197.37	40	B									
10847.03	9219.07	1	E	h								
10789.93	9267.90	10	B									
10752.46	9300.20	20	B									
10730.22	9319.47	3	E	B	55374.76	7/2	g^8D	46026.75	9/2	y^8P^o	9348.01	0.25
10697.18	9348.26	2	E	h	55375.70	9/2	g^8D	46026.75	9/2	y^8P^o	9348.95	−0.69

TABLE 5-1 (Continued)

(1)	(2)	(3)	(4)	(5)	(6)	(7)	(8)	(9)	(10)	(11)	(12)	(13)
10692.71	9352.17	1	E	h								
10664.07	9377.28	15	C									
10606.47	9428.21	12	C	AS								
10588.24	9444.44	20	A									
10558.77	9470.80	1	E	h								
10496.00	9527.44	1	E	h	50931.42	5/2	$x\,^6F^o$	41403.93	5/2	$e\,^6S$	9527.49	0.05
*10492.79	9530.35	1	E	h								
*10491.76	9531.29	2	D	AS	44696.29	5/2	$z\,^4F^o$	35165.05	3/2	$a\,^4F$	9531.24	0.05
*10490.08	9532.82	1	E	h								
*10487.87	9534.82	2	E	h								
*10486.02	9536.51	2	E	h								
*10479.71	9542.25	2	E	h								
*10478.65	9543.21	2	E	hAs								
*10476.81	9544.89	1	E	h								
*10474.64	9546.87	1	E	h								

TABLE 5-1 (Continued)

(1)	(2)	(3)	(4)	(5)	(6)	(7)	(8)	(9)	(10)	(11)	(12)	(13)
*10473.33	9548.06	1	E	h								
10469.38	9551.66	20	A		57305.62	7/2	f^4D	47753.99	5/2	y^6D^o	9551.63	0.03
*10465.83	9554.90	2	E	h								
*10463.79	9556.77	2	E	h								
*10461.71	9558.67	1	E	h	57218.15	7/2	e^8P	47659.52	5/2	w^6P^o	9558.63	0.04
*10460.72	9559.57	3	E	h								
*10454.66	9565.11	3	E	As								
*10453.25	9566.40	3	E	As								
*10450.98	9568.48	3	E	As	47154.51	3/2	y^4P^o	37586.03	3/2	a^2P	9568.48	0.00
*10448.98	9570.31	3	E	h								
*10448.18	9571.01	3	E	h								
*10441.13	9577.51	2	E	h								
*10439.60	9579.82	2	E	h								
*10438.33	9580.08	2	E	h								
*10436.06	9582.16	5	D	As								

TABLE 5-1 (Continued)

(1)	(2)	(3)	(4)	(5)	(6)	(7)	(8)	(9)	(10)	(11)	(12)	(13)
*10429.36	9588.32	2	D	h								
*10423.97	9593.27	1	E	h								
*10422.33	9594.78	2	E	h								
*10420.92	9596.08	1	E	h								
*10419.29	9597.58	1	E	h								
*10413.92	9602.53	1	E	h								
*10411.95	9604.35	3	E	h								
*10403.36	9612.28	2	E	AS.h								
*10401.96	9613.57	1	D	h								
*10400.02	9615.37	3	D	Asl								
*10394.17	9620.78	2	E	B.b	55374.76	7/2	g^8D	45754.27	7/2	z^4D°	9620.49	0.29
*10392.12	9622.68	1	E	h								
*10390.24	9624.42	1	E	h								
*10388.32	9626.20	2	E	ASL								
*10378.47	9635.33	1	E	h								

TABLE 5-1 (Continued)

(1)	(2)	(3)	(4)	(5)	(6)	(7)	(8)	(9)	(10)	(11)	(12)	(13)
10376.79	9536.89	1	E	h								
10374.23	9639.27	5	D									
10369.12	9644.02	2	D	h	51787.92	1/2	e⁴P	42143.57	3/2	z⁶D°	9644.35	−0.33
10368.42	9644.67	2	D	h								
10367.16	9645.84	1	E	h	57305.62	7/2	f⁴D	47659.52	5/2	w⁶P°	9646.10	−0.36
10365.48	9647.41	2	E	h	56871.10	1/2	u⁶F°	47218.15	3/2	e⁶D	9652.95	−0.26
10359.81	9652.69	2	E	h	56871.10	3/2	u⁶F°	47218.15	3/2	e⁶D	9652.95	−0.26
					56871.10	5/2	u⁶F°	47218.15	3/2	e⁶D	9652.95	−0.26
10357.67	9654.68	2	E	h	44696.29	5/2	z⁴F°	35041.37	7/2	a⁴F	9654.92	−0.24
10356.13	9656.12	2	E	h	56561.95	5/2	e⁴D	46901.13	5/2	y⁴P°	9660.82	0.22
10354.34	9657.79	1	E	h								
10350.85	9661.04	1	E	h								
10343.99	9667.45	1	E	h								
10342.76	9668.60	2	E	h								

TABLE 5-1 (Continued)

(1)	(2)	(3)	(4)	(5)	(6)	(7)	(8)	(9)	(10)	(11)	(12)	(13)
10331.33	9679.30	1	E	h								
10322.05	9688.00	1	E	h								
10320.54	9689.42	1	E	h								
10311.30	9698.10	2	E	h								
10309.54	9699.75	2	D	h	44814.73	3/2	z^4F^o	35114.98	5/2	a^4F	9699.75	0.00
10298.55	9710.10	2	E	h								
10292.12	9716.17	2	E	h								
10287.43	9720.21	2	E	h								
10269.63	9737.45	2	E	h								
10267.65	9739.33	2	D	h								
10266.87	9740.07	8	B	B								
10241.64	9764.06	10	B	h								
10167.87	9874.90	2	D	h								
10147.67	9854.48	2	D	h								
10086.25	9914.49	2	D	h								

TABLE 5-1 (Continued)

(1)	(2)	(3)	(4)	(5)	(6)	(7)	(8)	(9)	(10)	(11)	(12)	(13)
10005.75	9994.25	5		B								
9734.43	10272.82	40		B								
9719.25	10288.86	10		C								
9655.92	10356.34	30		C								
9611.47	10404.24	10		D	57305.62	7/2	f^4D	46901.13	5/2	y^4P^o	10404.49	−0.25
9245.90	10815.6?	15		D	45754.27	7/2	z^4D^o	34938.70	9/2	a^4F	10815.57	0.04
9174.75	10899.48	5		D	45940.93	5/2	z^4D^o	35041.37	7/2	a^4F	10899.56	0.08
9116.50	10969.12	5		D	46083.89	3/2	z^4D^o	35114.98	5/2	a^4F	10968.91	0.21
9060.98	11036.33	30		A								
8743.50	11437.07	10		C	47207.28	9/2	e^6D	35769.97	7/2	y^6P^o	11437.31	−0.24
8739.82	11441.88	5		D	47212.06	7/2	e^6D	35769.97	7/2	y^6P^o	11442.02	−0.14
8706.33	11485.89	5		D	47212.06	7/2	e^6D	35725.85	5/2	y^6P^o	11486.21	−0.32
8703.58	11489.52	10		D	47215.61	5/2	e^6D	35725.85	5/2	y^6P^o	11489.76	−0.24
8701.76	11491.93	2		E	47218.15	3/2	e^6D	35725.85	5/2	y^6P^o	11492.30	−0.37
8674.51	11528.03	5		C	47218.15	3/2	e^6D	35689.98	3/2	y^6P^o	11528.17	−0.14

TABLE 5-1 (Continued)

(1)	(2)	(3)	(4)	(5)	(6)	(7)	(8)	(9)	(10)	(11)	(12)	(13)
8383.02	11928.87	15	B		45754.27	7/2	z^4D^o	33825.49	5/2	b^4P	11928.78	0.09
8269.53	12092.59	5	B		55688.10	7/2	h^6D	43595.50	5/2	z^6F^o	12092.60	-0.01

96

TABLE 5-2: The rather strong manganese lines
observed in photographic region
0.826 μ m to 1.239 μ m which could
not be identified by transitions
involving energy levels.

Vacuum Wave-length in Å	Vacuum Wave No. in cm^{-1}	Relative intensity	Wave No Preci-sion	Quality of line
12274.14	8147.21	20	A	
12106.86	8259.78	20	B	B
12034.82	8309.22	100	A	
11994.79	8336.95	30	B	
11987.48	8342.04	70	A	
10872.67	9197.37	40	B	
10789.93	9267.90	10	B	
10752.46	9300.20	20	B	
10664.07	9377.28	15	C	
10606.47	9428.21	12	C	ASS
10588.24	9444.44	20	A	
10266.87	9740.07	8	B	
10241.64	9764.06	10	B	
9734.43	10272.82	40	B	
9719.25	10288.86	10	C	
9655.92	10356.34	30	A	
9060.98	11036.33	30	A	

TABLE 5-3 : Comparison of present manganese wavenumbers measured with the existing data for a limited number of the lines.

Present obs. σ (cm^{-1})	Relative intensity	Existing data σ (cm^{-1})	Intensity	Transition	Predicted wave No. (cm^{-1})	Wave No. difference between observed & calculated wave No. Present obs.	Existing data
(1)	(2)	(3)	(4)	(5)	(6)	(7)	(8)
5677.99	18 DB	5677.9	20	$e^6S_{5/2} - y^6P_{5/2}$	5678.08	-0.09	-0.18
6550.03	30 BB	6550.0	200	$y^8P_{3/2} - e^8S_{7/2}$	6550.13	-0.10	-0.13
6569.30	50 BB	6569.4	80	$y^8P_{7/2} - e^8S_{7/2}$	6569.46	-0.16	-0.06
6678.79	5 E.Bh	6678.2	30	$f^8D_{11/2} - y^8P_{9/2}$	6678.48	0.31	-0.28
7142.14	200 A	7142.4	120	$z^6P_{3/2} - a^6D_{1/2}$	7142.17	-0.03	0.23

98

TABLE 5-3 (Continued)

(1)	(2)	(3)	(4)	(5)	(6)	(7)	(8)
7210.85	250 A	7211.1	100	$z\,^6P^o_{3/2} - a\,^6D_{3/2}$	7210.84	0.01	0.26
7306.14	50 B	7305.5	80	$z\,^4P^o_{1/2} - a\,^4D_{1/2}$	7306.08	0.06	-0.58
7336.50	300 A	7337.1	200	$z\,^6P^o_{5/2} - a\,^6D_{5/2}$	7336.53	-0.03	0.57
7405.44	50 A	7405.4	100	$z\,^4P^o_{1/2} - a\,^4D_{3/2}$	7405.43	0.01	-0.03
7451.92	30 A	7451.8	80	$z\,^4P^o_{5/2} - a\,^4D_{5/2}$	7451.95	-0.03	-0.15
7506.01	400 A	7506.7	30	$z\,^6P^o_{5/2} - a\,^6D_{7/2}$	7506.05	-0.04	-0.65
7520.28	600 A	7520.1	50	$z\,^6P^o_{7/2} - a\,^6D_{7/2}$	7520.25	0.03	-0.15
7704.49	300 A	7704.5	40	$z\,^4P^o_{5/2} - a\,^4D_{7/2}$	7704.48	0.01	0.02
7749.96	600 A	7750.0	80	$z\,^6P^o_{7/2} - a\,^6D_{9/2}$	7749.96	0.00	0.04

TABLE 5-3 (Continued)

(1)	(2)	(3)	(4)	(5)	(6)	(7)	(8)
8484.13	20 BB	8484.07	60	$v^6P^o_{7/2} - e^6S_{5/2}$	8484.15	-0.02	-0.08
8585.33	1 Eh	8585.14	3	$z^6F^o_{7/2} - a^4F_{9/2}$	8585.38	-0.05	-0.24
8608.50	12 BB	8608.50	50	$v^6P^o_{5/2} - e^6S_{5/2}$	8608.60	-0.10	-0.10
8695.07	8 BB	8695.08	40	$v^6P^o_{3/2} - e^6S_{3/2}$	8695.23	-0.16	-0.15
10404.24	10 D	10404.54	100 h	$f^4D^o_{7/2} - y^4P^o_{5/2}$	10404.49	-0.25	0.05
10815.61	15 D	10815.69	150	$z^4D^o_{7/2} - a^4F_{9/2}$	10815.57	0.04	0.12
10899.48	5 D	10899.66	100	$z^4D^o_{5/2} - a^4F_{7/2}$	10899.56	-0.08	0.10
10969.12	5 D	10969.10	50	$z^4D^o_{3/2} - a^4F_{5/2}$	10968.91	0.21	0.19
11437.07	10 C	11437.29	1000 CW	$e^6D_{9/2} - y^6P^o_{7/2}$	11437.31	-0.24	-0.02

100

TABLE 5-3 (Continued)

(1)	(2)	(3)	(4)	(5)	(6)	(7)	(8)
11441.88	5 D	11442.02	300 C	$e^6D_{7/2} - y^6P^o_{7/2}$	11442.09	-0.21	0.00
11485.89	5 D	11486.14	500 CW	$e^6D_{7/2} - y^6P^o_{5/2}$	11485.21	-0.31	0.07
11489.52	10 D	11489.71	300 C	$e^6D_{5/2} - y^6P^o_{5/2}$	11489.76	0.24	0.05
11491.93	2 E	11492.25	100 C	$e^6D_{3/2} - y^6P^o_{5/2}$	11492.30	-0.37	-0.05
11528.03	5 C	11528.12	300 C	$e^6D_{3/2} - y^6P^o_{3/2}$	11528.17	-0.14	0.05
11928.87	15 B	11928.80	40	$z^4D^o - b^4P_{5/2}$	11928.78	0.09	0.02

TABLE 5-4 : Multiplet array for $z^6P^o - a^6D$

z^6P^o \ a^6D	1/2		3/2		5/2		7/2		9/2
3/2	7142.17	68.67	7210.84	116.96	7327.80				
	7142.14	68.71	7210.85	117.01	7327.86				
	7142.4		7211.1						
			8.73		*8.73*				
			8.72		*8.62*				
5/2			7219.57	116.96	7336.53	169.52	7506.05		
			7219.57	116.93	7336.50	169.51	7506.01		
					7337.1		7506.7		
					14.20		*14.20*		
					14.20		*14.27*		
7/2					7350.73	169.52	7520.25	229.71	7749.96
					7350.70	169.58	7520.28	229.68	7749.96
							7520.1		7750.0

Key for wavenumbers: Calculated
Experimental (author)
Experimental (Randall)

Key for differences: Calculated
Experimental (author)

102

TABLE 5-5 : Multiplet array for z^4P^o - a^4D

z^4P^o \ a^4D	1/2	3/2	5/2	7/2
1/2	7306.08 / 7306.14 / 7305.5 (99.35 / 99.30)	7405.43 / 7405.44 / 7405.4		
(diff)	48.53 / 48.54	48.53 / 48.54		
3/2	7257.55 / 7257.60 (99.35 / 99.30)	7356.90 / 7356.90 (170.32 / 170.33)	7527.22 / 7527.23	
(diff)		75.27 / 75.29	75.27 / 75.31	
5/2		7281.63 / 7281.61 (170.32 / 170.31)	7451.95 / 7451.92 / 7451.8 (252.53 / 252.57)	7704.48 / 7704.49 / 7704.5

Key for wavenumbers: Calculated
                      Experimental (author)
                      Experimental (Randall)

Key for differences: *Calculated*
                     Experimental (author)

CHAPTER 6

ADDITIONAL MEASUREMENTS OF
ZIRCONIUM INFRA-RED SPECTRUM

6-1 Introduction

It was already mentioned in the first chapter that
the further observation on the zirconium spectrum in the
infra-red region are to check the accuracy of the previous
measurements made in 1976, and also to determine the
wavenumbers of the additional weak lines which were
excluded from the previous results because the accuracy
of these lines could not be guaranteed. But now the
availability of new prepared zirconium tubes (chapter 2),
the modification of detecting vacuum system (chapter 3
Section 3-4) which certainly will improve the signal
recovery, the optical system of the spectrometer which
have been modified (chapter 3 Section 3-1), and the small
Broida Cavity is equipped with a tube holder (chapter 4
Section 4-1) which will give more stability to the light
source in present measurement, all these improvements made
the calculation of the weak lines possible with appreciable
accuracy.

6-2 Operation of sources

In re-measurement of zirconium spectrum a prepared tube
containing zirconium iodide was used. The tube struck in

a small Broida Cavity under the operation of seventy watts, reflecting power minimised to less than three watts by adjusting the tube and tuning the cavity. The reflected power remained less than three watts during six hours of operation, and also reduced by increasing the incident power to one hundred watts. The discharge was stable during the operation with strong intensity and diffuse glow filled the zirconium tube.

Thorium tube was used for standard lines and struck in 210 Broida cavity.

In a later attempt the zirconium tube was struck in 210 Broida cavity and Thorium tube in small Broida cavity. This was to investigate the effect of systematic change in the optical path. Differences in collimation between zirconium and thorium sources could give a slight systematic shift to the results.

6-3 Measurement of wavenumbers

The recording procedure was carried on as was explained in Chapter 4 Section 4-2. The majority of the weak lines appeared to be concentrated in the wavelength region 0.79 - 1.37 μ m (observed in record order) and 1.75 - 2.7 μ m, and scan were taken in these regions with a slit width of 75 μ m. This slit width was used for all the spectra recorded with the calibration fringes and the thorium standard lines. The recording in the grating first order in the range 1.75 - 2.7 μ m are taken in one setting of the grating which was

scanned along the whole length of the driving lead screw.

The first order and second order distinction was performed as it is given in Section 4-3 for manganese spectrum.

6-4 Accuracy of the measurement

A record was taken running the zirconium tube in the 1 inch diameter $\frac{3}{4}$ wavelength Broida cavity 215L (Figure 4-1) and thorium tube in the 2 inch diameter Broida cavity 210L. The recording was repeated and wavenumbers calculated and listed with the procedure explained in Chapter 4. As discussed in Section 4-4 a systematic error may arise due to collimation, to investigate the magnitude of any such effect in a further attempt the tubes were changed place in the cavities. Zirconium tube was struck in 2 inch diameter Broida cavity and thorium tube in 1 inch diameter Broida cavity. To have the optimum light intensity in zirconium tube, the tube was run in a higher microwave power in 2 inch diameter Broida cavity (120W) compared with the 1 inch diameter Broida cavity (100W). The result of the calculation is given in line list in Appendix 1, for the lines with precision A (i.e. estimated error $\pm$ 0.02 cm^{-1}). The comparison of the results reveals a reasonable agreement between the measurements. Figure 6-1 shows the histogram of the difference between the wavenumbers measured with this accuracy in present time and measurements made in 1976.
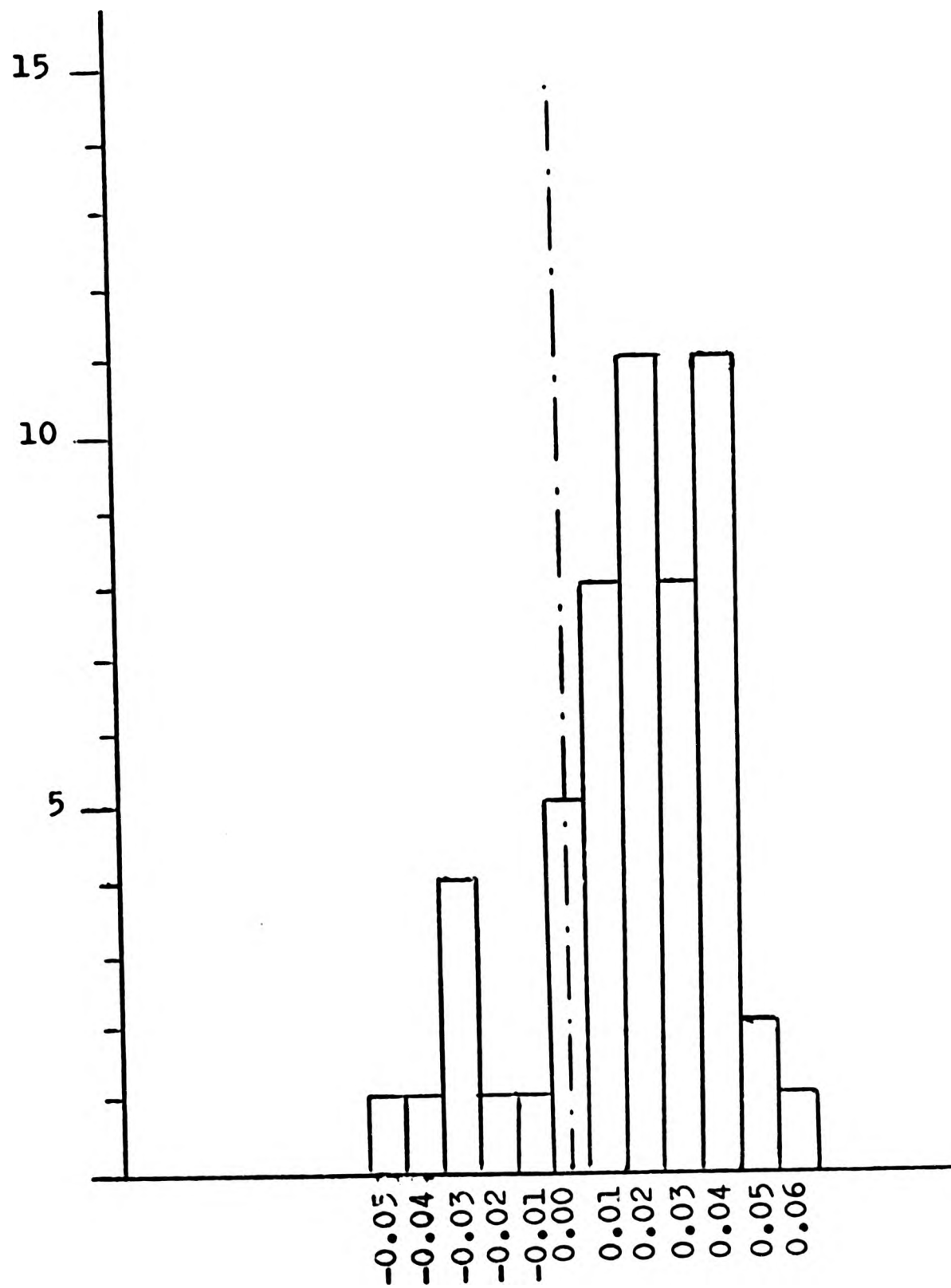
Figure 6-1 Histogram of the difference between the wavenumbers measured with precision A in present time and measurements made in 1976.

Considering all the lines observed, the magnitude of the difference in the wavenumber of the lines measured in this work and in 1976 is less than 0.05 cm^{-1} for 80% of the lines; and in the range $0.05 - 0.10$ for a further 18%.

6-5 Data presentation

In present measurement, vacuum wavenumber of 181 new zirconium lines in the spectral range of $0.78 - 1.36 \mu$ m and $1.77 - 2.7 \mu$ m have been measured. These lines have been compared with the strong iodine lines, and the result showed that the spectrum is free from iodine lines. The intensities quoted are measured as heights above the average background level. In general, these intensities are about twice those observed in the previous (1976) work, but there are enough discrepancies to make reduction to a common scale difficult, and the quoted intensities should be used as a guide within the new results. These new lines are weak and the errors assigned to the wavenumbers are based on the considerations discussed in Chapter 4 Section 4-5.

The present zirconium lines are compared with the predicted spectral lines from neutral zirconium energy levels[30]. In this comparison seventy-nine spectral lines have been assigned to the known energy levels of neutral zirconium atom. These wavenumbers were also checked with the calculated wavenumbers from the energy levels of ionized zirconium atom and no ionized lines could be detected. In 28 cases the transitions completed or partially

completed the multiplet assigned in 1976.

Table 6-1 gives a consolidated list of zirconium lines measured in 1976 and the present work; the latter are indicated by an asterisk. The vacuum wavelengths quoted were obtained by direct conversion from the measured vacuum wavenumbers. The arrangement of the table follows that adapted for the manganese lines in Table 5-1 (Chapter 5).

The study of the observed zeeman patterns discussed in Section 7-8 in Chapter 7 has led to some revision to the classification of levels and the lines affected are indicated thus +; (full details of the changes are given in Section 7-8).

TABLE 6-1　　　THE INFRA-RED SPECTRUM OF ZIRCONIUM

Vacuum wave length in Å	Vacuum wave No. in Cm⁻¹	Relative intensity	Wave precision	Quality of line	No. of pre-line cision	energy	Upper energy level J value	state energy	Lower energy level J value	state energy	Calculated wave No in Cm⁻¹	Wave No diff $6_{obs} - 6_{Calc}$
(1)	(2)	(3)	(4)	(5)	(6)	(7)	(8)	(9)	(10)	(11)	(12)	(13)
*27141.68	3684.37	2	D	h								
27134.54	3685.34	4	B	AS								
26362.55	3793.26	43	A									
*26181.78	3819.45	2	B	h								
*26175.89	3820.31	2	D	h								
*26173.83	3820.61	5	B									
*25939.40	3855.14	2	B	h								
*25928.23	3856.80	2	C	h								
25716.73	3888.52	3	D	h								
*25708.33	3889.79	2	C	h								

110

(1)	(2)	(3)	(4)	(5)	(6)	(7)	(8)	(9)	(10)	(11)	(12)	(13)
25675.72	3894.73	3	D	h								
25350.21	3944.79	15	A									
25125.12	3980.08	38	B									
*25022.65	3996.38	4	B									
*24909.21	4014.58	4	A		37459.60	2	e^3F	33444.87	1	w^5D°	4014.73	−0.15
*24625.20	4060.88	4	D	h								
*24588.39	4066.96	2	C									
*24577.81	4068.71	2	B		37701.08	3	e^3F	33632.48	2	w^5D°	4068.60	0.11
24489.52	4083.38	42	A		16843.93	3	z^3F°	12760.66	4	a^3G	4083.27	0.11
24265.72	4121.04	32	A		22398.00	4	a^5D	18276.92	5	z^5F°	4121.08	−0.04
*23974.95	4171.02	4	B									
*23970.01	4171.88	4	B									
*23823.25	4197.58	2	D	h								
*23749.75	4210.57	4	B		26154.13	1	x^3D°	21943.74	2	a^5D	4210.39	0.18
*23656.10	4227.24	2	B		41068.00	5	f^5F	36840.59	6	x^3H°	4227.41	−0.17

111

(1)	(2)	(3)	(4)	(5)	(6)	(7)	(8)	(9)	(10)	(11)	(12)	(13)
*23577.57	4241.32	4		A	40849.70	4	f^5F	36608.41	4	x^3H^o	4241.29	0.03
*23464.21	4261.81	8		A	38101.09	4	e^3F	33839.20	5	z^1H^o	4261.89	-0.08
*23439.57	4266.29	4		B								
22313.99	4289.27	2		B	21801.21	1	a^5D	17511.78	2	z^1D^o	4289.43	-0.16
*23276.06	4295.26	6		B	21726.28	0	a^5D	17429.86	1	z^3D^o	4296.42	-0.16
23245.38	4301.93	6		B								
23190.40	4312.13	3		C								
23188.30	4312.52	25		A	22145.31	3	a^5D	17832.73	4	z^5F^o	4312.58	-0.06
*23108.62	4327.39	4		B								
*23050.03	4338.39	4		B								
23039.67	4340.34	14		B	16843.93	3	z^3F^o	12503.44	3	a^3G	4340.49	-0.15
*23037.44	4340.76	4		B								
*23036.17	4341.00	2		B								
*22917.44	4363.49	2		B								
*22407.15	4365.45	2		B	h							

(1)	(2)	(3)	(4)	(5)	(6)	(7)	(8)	(9)	(10)	(11)	(12)	(13)
*22883.35	4369.99	2	B									
*22768.72	4391.99	4	A									
*22686.49	4407.91	2	B									
*22683.35	4408.52	2	D	h								
22218.77	4500.70	22	A									
22213.93	4501.68	4	B		16843.93	3	z^3P^o	12342.37	4	b^3F	4501.56	0.12
22184.11	4507.73	10	A		21943.74	2	a^5D	17422.17	3	z^5P^o	4521.57	-0.05
22116.46	4521.52	25	A		20466.83	2	z^3P^o	15932.10	2	b^3P	4534.73	0.21
22051.01	4534.94	19	A									
21981.65	4549.25	5	B									
21907.39	4564.67	4	B		22398.00	4	a^5D	17832.73	4	z^5P^o	4565.27	-0.06
21904.80	4565.21	10	A		20519.20	1	z^3P^o	15932.10	2	b^3P	4587.10	0.07
21799.93	4587.17	15	A									
*21660.12	4616.78	5	C									
21502.69	4650.58	2	C	h								

(1)	(2)	(3)	(4)	(5)	(6)	(7)	(8)	(9)	(10)	(11)	(12)	(13)
21477.80	4655.97	170	A		16296.51	2	z^3P^o	11640.72	2	b^3F	4655.79	0.18
*21491.88	4652.92	4	D	h	21974.18	1	z^3S^o	17321.52	0	c^3P	4652.66	0.26
*21190.75	4719.04	4	D	h								
21172.53	4723.10	20	A		22145.31	3	a^5D	17422.17	3	z^5F^o	4723.14	-0.04
21091.04	4741.35	17	A		21801.21	1	a^5D	17059.61	2	z^5F^o	4741.60	-0.25
*21082.15	4743.35	15	A									
*21065.14	4747.18	4	B									
*20939.21	4775.73	12	B									
20905.76	4783.37	9	A		17556.26	4	z^3F^o	12772.78	5	a^3G	4783.48	-0.11
20852.27	4795.64	100	A		17556.26	4	z^3F^o	12760.66	4	a^3G	4795.60	0.04
20847.93	4796.64	2	C									
20716.76	4827.01	3	C									
20696.95	4831.63	28	A		21974.18	1	z^3S^o	17142.72	2	c^3P	4831.46	0.17
20675.00	4836.76	2	C									
20654.93	4841.46	2	C		22398.00	4	a^5D	17556.26	4	z^3F^o	4841.74	-0.28

(1)	(2)	(3)	(4)	(5)	(6)	(7)	(8)	(9)	(10)	(11)	(12)	(13)
20474.85	4884.04	18	A		21943.74	2	a^5D	17059.61	2	z^5F^o	4884.13	−0.09
20459.35	4887.74	200	A		16843.93	3	z^3F^o	11956.33	3	b^3F	4887.60	0.14
+20429.84	4894.80	80	A		41068.00	5	f^5F	36173.03	6	z^3I^o	4894.97	−0.17
20347.95	4914.50	28	B		21974.18	1	z^3S^o	17059.82	1	c^3P	4914.36	0.14
20329.87	4918.87	6	B		17422.17	3	z^5F^o	12503.44	3	a^3G	4918.73	0.14
20289.37	4928.69	4	B		19625.58	3	z^5D^o	14697.03	3	a^3D	4928.55	0.14
20216.11	4946.55	20	A									
20074.44	4981.46	6	C									
20025.07	4995.74	3	C		42706.00	2	q^3F^o	37701.08	3	e^3F	5004.92	−0.17
19981.02	5004.75	2	C									
19966.54	5008.38	8	B	B	17511.78	2	z^1D^o	12503.44	3	a^3G	5008.34	0.04
*19962.87	5009.30	4	B	h	20466.83	2	z^3P^o	15457.40	3	c^3F	5009.43	−0.13
19943.92	5014.06	14	A		21801.21	1	a^5D	16786.93	1	z^5F^o	5014.28	−0.22
19935.13	5016.27	12	A	?S								
19857.58	5035.86	5	C									

(1)	(2)	(3)	(4)	(5)	(6)	(7)	(8)	(9)	(10)	(11)	(12)	(13)
19790.62	5052.90	3	B		17556.26	4	z^3F^o	12503.44	3	a^3G	5052.82	0.08
*19775.16	5056.85	6	A		45710.29	3	p^3D^o	40653.41	3	f^5F	5056.88	−0.03
19723.98	5069.97	4	C									
19715.66	5072.11	2	B	B	17832.73	4	z^5F^o	12760.66	4	a^3G	5072.07	0.04
19685.47	5079.89	20	A		17422.17	3	z^5F^o	12342.37	4	b^3F	5079.80	0.09
*19663.17	5085.65	2	B		22145.31	3	^5D	17059.61	2	z^5F^o	5085.70	−0.05
19615.65	5097.97	5	C		42799.20	3	q^3D^o	37701.08	3	e^3F	5098.12	−0.15
19594.70	5103.42	40	B		17059.61	2	z^5F^o	11956.33	3	b^3F	5103.28	0.14
19585.38	5105.85	3	B									
*19468.85	5136.41	2	D	h	19833.78	4	z^5D^o	14697.03	3	a^3D	5136.75	−0.34
19431.36	5146.32	75	A		16786.93	1	z^5F^o	11640.72	2	b^3F	5146.21	0.11
19408.85	5152.29	3	C									
19392.28	5156.69	3	C		21943.74	2	a^5D	16786.93	1	z^5F^o	5156.81	−0.12
19326.40	5174.27	5	C									
19218.46	5203.33	40	A		16843.93	3	z^3F^o	11640.72	2	b^3F	5203.21	0.12

(1)	(2)	(3)	(4)	(5)	(6)	(7)	(8)	(9)	(10)	(11)	(12)	(13)
19179.28	5213.96	240		A	17556.26	4	z^3F^o	12342.37	4	b^3F	5213.89	0.07
19154.63	5220.67	4		B								
19140.73	5224.46	4		D								
18984.95	5267.33	5		A	24006.30	4	y^3F^o	18738.94	5	a^1H	5267.36	−0.03
18831.29	5310.31	24		B	17813.64	2	z^3D^o	12503.44	3	a^3G	5310.20	0.11
18809.54	5316.45	8		A								
18755.81	5331.68	3		D								
18726.91	5339.91	4		C								
18574.97	5383.59	4		A								
18453.56	5419.01	70		A								
18348.19	5450.13	75		A	45798.48	2	f^5G	40346.35	3	r^3D^o	5452.13	−0.10
18341.79	5452.03	120		A								
18309.25	5461.72	5		B								
18295.22	5465.91	9		B								
18256.07	5477.63	3		B								

(1)	(2)	(3)	(4)	(5)	(6)	(7)	(8)	(9)	(10)	(11)	(12)	(13)
18238.56	5482.89	75	A		18243.56	3	z^3D^o	12760.66	4	a^3G	5482.90	−0.01
18213.51	5490.43	4	B		17832.73	4	z^5F^o	12342.37	4	b^3F	5490.36	0.07
18118.37	5519.26	15	C									
18094.24	5526.62	4	B									
18052.92	5539.27	6	A									
18022.47	5548.63	18	A		17511.78	2	z^1D^o	11956.33	3	b^3F	5555.45	0.04
18000.21	5555.49	7	A									
17981.57	5561.25	50	A		40653.41	3	f^5F	35090.90	3	y^5P^o	5562.51	0.28
17976.59	5562.79	20	A									
17951.03	5570.71	23	A									
17903.15	5585.61	3	B		16843.93	3	z^3F^o	11258.38	3	a^5P	5585.55	0.06
17876.36	5593.08	6	A		17556.26	4	z^3F^o	11956.33	3	b^3F	5599.93	0.07
17857.14	5600.00	50	A		22750.53	2	y^1D^o	17142.72	2	c^3P	5607.81	0.08
17832.02	5607.89	28	A		37459.60	2	e^3F	31850.77	1	y^3S^o	5608.83	−0.10
17829.35	5608.73	9	B									

(1)	(2)	(3)	(4)	(5)	(6)	(7)	(8)	(9)	(10)	(11)	(12)	(13)
17802.94	5617.05	10	A									
17791.88	5620.54	6	C									
*17765.97	5628.74	4	A	B	27572.52	1	y^3P^o	21943.74	2	a^5D	5628.78	-0.04
17718.78	5643.73	23	A									
17677.15	5657.02	5	A	B								
17635.16	5670.49	15	B	ASL								
17592.07	5684.38	3	B									
17586.07	5686.32	11	A									
17580.69	5688.06	14	B	ASL								
17538.29	5701.81	12	A									
17521.94	5707.13	8	A	B								
17481.54	5720.32	7	A									
17438.59	5734.41	4	B	B								
17421.18	5740.14	11	A		18243.56	3	z^3D^o	12503.44	3	a^3G	5740.12	0.02
17276.98	5788.05	2	B		41940.86	6	e^5G	36152.85	7	z^3I^o	5788.01	0.04

(1)	(2)	(3)	(4)	(5)	(6)	(7)	(8)	(9)	(10)	(11)	(12)	(13)
17273.57	5789.19	120	.	A	17429.86	1	z^3D^o	11640.72	2	b^3F	5789.14	0.05
17232.35	5803.04	13		A								
17198.62	5814.42	90		A	23567.12	3	y^3F^o	17752.73	4	b^1G	5814.39	0.03
17160.55	5827.32	14		A	16843.93	3	z^3F^o	11016.65	2	a^5P	5827.28	0.04
17152.07	5830.20	9		A								
17072.42	5857.40	160		A	17813.64	2	z^3D^o	11956.33	3	b^3F	5857.31	0.09
17032.70	5871.06	150		A	17511.78	2	z^1D^o	11640.72	2	b^3F	5871.06	0.00
17017.02	5876.47	9		A	17832.73	4	z^5F^o	11956.33	3	b^3F	5876.40	0.07
16990.36	5885.69	15		A								
16977.21	5890.25	66		A								
16969.20	5893.03	35		A								
16962.29	5895.43	12		A								
16945.71	5901.20	190		A	18243.56	3	z^3D^o	12342.37	4	b^3F	5901.19	0.01
16932.51	5905.80	4		B	ASL							
16925.57	5908.22	33		A	23660.97	3	y^3D^o	17752.73	4	b^1G	5908.24	-0.02

120

(1)	(2)	(3)	(4)	(5)	(6)	(7)	(8)	(9)	(10)	(11)	(12)	(13)
16921.99	5909.47	12	A									
16850.31	5934.61	8	A		18276.92	5	z^5F°	12342.37	4	b^3F	5934.55	0.06
16845.85	5936.18	12	A									
16833.68	5940.47	5	A									
16828.05	5942.49	3	B		23085.06	2	z^5S°	17142.72	2	c^3P	5942.34	0.12
16785.96	5957.36	7	A	AS								
16671.86	5998.13	3	B	AS								
16659.78	6002.48	3	B									
16616.84	6017.99	2	B		23246.33	1	y^5D°	17228.42	2	b^1D	6017.91	0.08
16550.13	6042.25	60	A		21974.18	1	z^3S°	15932.10	2	b^3P	6042.08	0.17
16506.39	6058.26	9	A									
16461.75	6074.59	3	B		27876.16	2	w^3F°	21801.21	1	a^5D	6074.95	-0.26
16422.19	6089.32	2	B									
16344.84	6118.14	31	A		20466.83	2	z^3P°	14348.78	2	a^3D	6118.05	0.09
16296.60	6136.25	15	A		23889.03	3	y^5D°	17752.73	4	b^1G	6136.30	-0.05

(1)	(2)	(3)	(4)	(5)	(6)	(7)	(8)	(9)	(10)	(11)	(12)	(13)
16223.73	6163.81	8	A		17422.17	3	z^5F^o	11258.38	3	a^5P	6163.79	0.02
16199.63	6172.98	31	A		17813.64	2	z^3D^o	11640.72	2	b^3F	6172.92	0.06
16073.76	6221.32	17	A									
15974.62	6259.93	3	B		23319.86	2	y^3D^o	17059.82	1	c^3P	6260.04	-0.11
15936.00	6275.10	5	B									
15905.15	6287.27	125	A		18243.56	3	z^3D^o	11956.33	3	b^3F	6287.23	0.04
15878.38	6297.87	30	A		17556.26	4	z^3F^o	11258.38	3	a^5P	6297.88	-0.01
15816.30	6322.59	40	A									
15763.07	6343.94	3	A		20466.83	2	z^3P^o	14123.01	1	a^3D	6343.82	0.12
15748.28	6349.90	15	A									
15727.33	6358.36	95	A									
15702.31	6368.49	2	B									
15653.10	6388.51	5	B									
15634.36	6396.17	7	A		20519.20	1	z^3P^o	14123.01	1	a^3D	6396.19	-0.02
15611.54	6405.52	5	A		17422.17	3	z^5F^o	11016.65	2	a^5P	6405.52	0.00

(1)	(2)	(3)	(4)	(5)	(6)	(7)	(8)	(9)	(10)	(11)	(12)	(13)
15504.65	6449.68	3	B		28595.03	2	y^5F^o	22145.31	3	a^5D	6449.72	−0.04
15481.71	6458.40	2	B									
15396.25	6495.09	6	B		17511.78	2	z^1D^o	11016.65	2	a^5P	6495.13	−0.04
15392.41	6496.71	4	B	B								
15384.57	6500.02	5	A									
15377.07	6503.19	3	B		28446.92	1	y^5F^o	21943.74	2	a^5D	6503.18	0.01
15341.45	6518.29	7	B	AS	23660.97	3	y^3D^o	17142.72	2	c^3P	6518.25	0.04
15314.19	6529.89	7	A									
15279.91	6544.54	8	C	AS$	17429.86	1	z^3D^o	10885.36	1	a^5P	6544.50	0.04
15210.65	6574.34	8	A	AS	17832.73	4	z^5F^o	11258.38	3	a^5P	6574.35	0.01
15184.58	6585.63	2	B									
15151.29	6600.10	2	B		40887.61	3	e^5G	34287.49	4	w^5D^o	6600.12	−0.02
15144.91	6602.88	13	A		18243.56	3	z^3D^o	11640.72	2	b^3F	6602.84	0.04
15143.58	6603.46	7	B		29001.65	5	x^3G^o	22398.00	4	a^5D	6603.65	−0.19
15141.40	6604.41	1	B		28749.80	4	x^3G^o	22145.31	3	a^5D	6604.49	−0.08

(1)	(2)	(3)	(4)	(5)	(6)	(7)	(8)	(9)	(10)	(11)	(12)	(13)
15072.00	6634.82	140		A	24387.52	3	y^1F^o	17752.73	4	b^1G	6634.79	0.03
15046.94	6645.87	20		A	28446.92	1	y^5F^o	21301.21	1	a^5D	6645.71	0.16
15034.70	6651.28	30		A	28595.03	2	y^5F^o	21943.74	2	a^5D	6651.29	-0.01
15019.21	6658.14	3		B	35476.07	3	e^5F	28818.02	3	y^5F^o	6658.05	0.09
14996.69	6668.14	4		B								
14986.46	6672.69	30		A	28818.02	3	y^5F^o	22145.31	3	a^5D	6672.71	-0.02
14946.90	6690.35	23		A								
14879.45	6720.68	23		A	28446.92	1	y^5F^o	21726.28	0	a^5D	6720.64	0.04
14870.71	6724.63	20		A	29122.71	4	y^5F^o	22398.00	4	a^5D	6724.71	-0.08
14860.89	6729.07	5		B								
14857.80	6730.47	1		B								
14840.41	6738.36	5		B								
14738.13	6785.12	7		A								
14718.98	6793.95	47		A	28595.03	2	y^5F^o	21801.21	1	a^5D	6793.82	0.13
14711.46	6797.42	40	C	ASI								

(1)	(2)	(3)	(4)	(5)	(6)	(7)	(8)	(9)	(10)	(11)	(12)	(13)
14684.09	6810.09	3		A								
14668.89	6817.15	7		A								
14652.53	6824.76	5		A	36360.20	5	e^5F	29535.48	5	y^5F^o	6824.72	0.04
14588.87	6854.54	13		A								
14585.72	6856.02	28		A								
14570.80	6863.04	33		A	19625.58	3	z^5D^o	12760.66	4	a^3G	6864.92	0.08
14566.64	6865.00	15		A	28818.02	3	y^5F^o	21943.74	2	a^5D	6874.28	−0.01
14547.00	6874.27	65		A	17813.64	2	z^3D^o	10885.36	1	a^5P	6928.28	0.02
14433.56	6928.30	18		A								
14389.11	6949.70	4		B								
14332.21	6977.29	92		A	29122.71	4	y^5F^o	22145.31	3	a^5D	6977.40	−0.11
14316.13	6985.13	30		A	18243.56	3	z^3D^o	11258.38	3	a^5P	6985.18	−0.05
14225.46	7029.65	5		A								
14194.67	7044.90	8		A	21849.33	3	z^3G^o	14791.28	4	a^3H	7058.05	0.03
14168.16	7058.08	270		A								

(1)	(2)	(3)	(4)	(5)	(6)	(7)	(8)	(9)	(10)	(11)	(12)	(13)
14133.84	7075.22	20	B									
14124.77	7079.76	5	B									
+14110.50	7086.92	55	A		23018.92	1	y^3D^o	15932.10	2	b^3P	7086.82	0.10
14031.27	7126.94	7	A	B								
14010.51	7137.50	82	A		29535.48	5	y^5F^o	22398.00	4	a^5D	7137.48	0.02
14008.23	7138.66	80	A									
13975.13	7155.57	275	A		22144.08	4	z^3G^o	14988.51	5	a^3H	7155.57	0.00
13837.31	7226.84	58	A		18243.56	3	z^3D^o	11016.65	2	a^5P	7226.91	-0.07
13750.37	7272.53	15	A		26011.55	4	y^3G^o	18738.94	5	a^1H	7272.61	-0.08
13748.24	7273.66	2	B									
13730.02	7283.31	16	A		19625.58	3	z^5D^o	12342.37	4	b^3F	7283.21	0.10
*13671.66	7314.40	2	C	ASL	23246.33	1	y^5D^o	15932.10	2	b^3P	7314.23	0.17
13600.28	7352.79	32	A		22144.08	4	z^3G^o	14791.28	4	a^3H	7352.80	-0.01
*13582.05	7362.66	2	B	h	45798.48	2	f^5G	38435.88	3	s^3D^o	7362.60	0.06
*13580.74	7363.37	2	D	n								

(1)	(2)	(3)	(4)	(5)	(6)	(7)	(8)	(9)	(10)	(11)	(12)	(13)
*13576.48	7365.68	4	A									
13574.53	7366.74	25	B									
13572.87	7367.64	9	B		19323.84	2	z^5D^o	11956.33	3	b^3F	7367.51	0.13
*13556.62	7376.47	6	A									
+13535.94	7387.74	75	B		23319.86	2	y^3D^o	15932.10	2	b^3P	7387.76	−0.02
+13523.36	7394.61	75	A									
*13505.03	7404.65	4	A		22862.02	3	z^1F^o	15457.40	3	c^3F	7404.62	0.03
13500.83	7406.95	10	A									
*13500.12	7407.34	4	A		43268.24	3	q^3F^o	35860.83	4	e^5F	7407.41	−0.07
13433.20	7444.24	310	A		22563.89	5	z^3G^o	15119.66	6	a^3H	7444.23	0.01
13413.04	7455.99	5	C	AS	19096.53	1	z^5D^o	11640.72	2	b^3F	7455.81	0.18
13411.06	7456.53	30	B		35860.83	4	e^5F	28404.26	3	x^3G^o	7456.57	−0.04
*13383.85	7471.69	4	B		45798.48	2	f^5G	38326.72	2	s^3D^o	7471.76	−0.07
*13379.82	7473.94	4	D	h								
*13332.52	7500.46	4	B		21849.33	3	z^3G^o	14348.78	2	a^3D	7500.55	−0.09

(1)	(2)	(3)	(4)	(5)	(6)	(7)	(8)	(9)	(10)	(11)	(12)	(13)
*13279.95	7530.15	2	D									
13200.59	7575.36	50	A		22563.89	5	z^3G^o	14988.51	5	a^3H	7575.36	−0.02
13182.32	7585.92	12	A									
13180.54	7586.94	15	A									
13153.29	7602.66	8?	A									
13152.48	7603.13	125	B	AS								
*13139.84	7610.44	4	B		36360.20	5	e^5F	28749.80	4	x^3G^o	7610.40	0.04
13125.98	7618.48	5	B	ASL								
*13111.19	7627.07	4	B	h								
*13108.12	7628.86	2	D									
13045.62	7665.41	54	A		23597.47	2	y^3F^o	15932.10	2	b^3P	7665.37	0.04
13038.91	7669.35	10	B	AS	19625.58	3	z^5D^o	11956.33	3	b^3F	7669.25	0.10
*13022.31	7679.13	4	B									
*13019.51	7680.78	4	D									
13015.38	7683.22	10	B	B	19323.84	2	z^5D^o	11640.72	2	b^3F	7683.12	0.10

(1)	(2)	(3)	(4)	(5)	(6)	(7)	(8)	(9)	(10)	(11)	(12)	(13)
13005.05	7689.32	38	A		30087.33	3	x^5D^o	22398.00	4	a^5D	7689.33	-0.01
*12996.53	7694.36	2	C									
12983.30	7702.20	46	A		29847.49	2	x^5D^o	22145.31	3	a^5D	7702.18	0.02
12974.73	7707.29	15	B									
*12961.19	7715.34	4	B		22862.02	3	z^1F^o	15146.48	2	c^3F	7715.54	-0.20
12960.40	7715.81	15	A		22862.02	3	z^1F^o	15146.48	2	c^3F	7715.54	0.27
12930.86	7733.44	70	B		29677.14	1	x^5D^o	21943.74	2	a^5D	7733.40	0.04
12927.23	7735.61	4	D	B								
*12901.36	7751.12	4	B									
12895.85	7754.43	6	C	AS								
12895.31	7754.76	5	C									
*12850.78	7781.63	2	C									
12841.90	7787.01	42	A		29588.07	0	x^5D^o	21801.21	1	a^5D	7786.86	0.15
12808.00	7807.62	9	C									
12776.19	7827.06	3	B	B								

(1)	(2)	(3)	(4) (5)	(6)	(7)	(8)	(9)	(10)	(11)	(12)	(13)
12774.28	7828.23	il	A								
*12770.43	7830.59	4	B								
*12719.65	7861.85	4	B	29588.07	0	x^5D^o	21726.28	0	a^5D	7861.79	-0.06
12714.12	7865.27	100	B								
12696.64	7876.10	8	A	29677.14	1	x^5D^o	21801.21	1	a^5D	7875.93	0.17
*12694.35	7877.52	4	B	19833.78	4	z^5D^o	11956.33	3	b^3F	7877.45	0.07
12652.19	7903.77	55	B	29847.49	2	x^5D^o	21943.74	2	a^5D	7903.75	0.02
12617.47	7925.52	5	B								
+12591.29	7942.00	77	A	30087.33	3	x^5D^o	22145.31	3	a^5D	7942.02	-0.02
12577.15	7950.93	34	A	29677.14	1	x^5D^o	21726.28	0	a^5D	7950.86	0.07
12540.49	7974.17	5	A								
12535.62	7977.27	8	A	25729.96	3	y^3G^o	17752.73	4	b^1G	7977.23	0.04
*12528.53	7981.78	6	C								
+12521.10	7986.52	185	A	30384.50	4	x^5D^o	22398.00	4	a^5D	7986.50	0.02
12517.78	7988.64	17	A								

130

(1)	(2)	(3)	(4)	(5)	(6)	(7)	(8)	(9)	(10)	(11)	(12)	(13)
*12509.38	7994.00	4	B									
*12507.54	7995.18	2	C									
*12480.62	8012.42	6	B									
12443.82	8036.12	8	B									
+12427.81	8046.47	54	A		29847.49	2	x^5D^o	21801.21	1	a^5D	8046.28	0.19
12398.49	8065.50	70	A		19323.84	2	z^5D^o	11258.38	3	a^5P	8065.46	0.04
12391.65	8069.95	6	B									
*12386.65	8073.21	2	C	h								
+12376.28	8079.97	200	B		19096.53	1	z^5D^o	11016.65	2	a^5P	8079.88	0.09
12373.17	8082.00	2	C	h								
12369.35	8084.50	4	B									
+12359.41	8091.00	290	A		18976.36	0	z^5D^o	10885.36	1	a^5P	8091.00	0.00
*12309.72	8123.66	4	B	h								
*12302.53	8128.41	2	C	h								
12299.22	8130.60	5	B	h								

(1)	(2)	(3)	(4)	(5)	(6)	(7)	(8)	(9)	(10)	(11)	(12)	(13)
*12296.90	8132.13	4	C	B	43182.96	1	w^3S^o	35046.95	1	e^5F	8136.01	−0.25
.12291.41	8135.76	5	B	B								
12286.64	8138.92	5	B									
*12284.56	8140.30	2	B									
12279.64	8143.56	60	A		30087.33	3	x^5D^o	21943.74	2	a^5D	8143.59	−0.03
12276.67	8145.53	6	B		25898.16	3	z^5P^o	17752.73	4	b^1G	8145.43	0.10
12272.72	8148.15	6	B		36360.20	5	e^5F	28211.82	5	z^3H^o	8148.38	−0.23
12212.19	8188.54	6	A									
12210.16	8189.90	6	B									
12206.32	8192.48	310	A		26931.35	4	z^1D^o	18738.94	5	a^1H	8192.41	0.07
12195.85	8199.51	77	A		26938.42	4	x^3F^o	18738.94	5	a^1H	8199.48	0.03
*12186.56	8205.76	4	B									
+12178.37	8211.28	540	B		19096.53	1	z^5D^o	10885.36	1	a^5P	8211.17	0.11
12145.05	8233.81	23	B									
12142.61	8235.46	20	A									

(1)	(2)	(3)	(4)	(5)	(6)	(7)	(8)	(9)	(10)	(11)	(12)	(13)
12137.12	8239.19	35	A		30384.50	4	x^5D°	22145.31	3	a^5D	8239.19	0.00
12072.99	8282.95	12	C	AS								
*12047.66	8300.37	6	A									
+12037.66	8307.26	770	B		19323.84	2	z^5D°	11016.65	2	a^5P	8307.19	0.07
12034.78	8309.25	5	C									
*12006.66	8328.71	6	B									
11975.99	8350.04	20	A									
11973.90	8351.50	5	B									
1?960.42	8360.91	9	B									
+11951.36	8367.25	580	B		19625.58	3	z^5D°	11258.38	3	a^5P	8367.2	0.05
11948.18	8373.68	26	A									
11940.13	8375.12	5	C									
*11921.37	8388.30	6	C	AS								
11919.32	8389.74	5	B	B								
*11917.56	8390.98	2	D									

133

(1)	(2)	(3)	(4)	(5)	(6)	(7)	(8)	(9)	(10)	(11)	(12)	(13)
11908.79	8397.16	8	B									
11894.84	8407.01	30	A									
*11883.03	8415.36	4	D									
11861.85	8430.39	11	A									
11853.05	8436.65	11	B	B								
+11850.36	8438.56	460	B		19323.84	2	z^5D^o	10885.36	1	a^5P	8438.48	0.08
11830.22	8452.93	12	B									
*11825.45	8455.62	4	B	ASL								
11800.38	8474.30	140	B		26226.97	3	x^1F^o	17752.73	4	b^1G	8474.24	0.06
11757.79	8505.00	5	C									
11755.43	8506.71	3	C									
*11751.99	8509.20	4	B									
*11746.60	8513.10	4	B		22862.02	3	z^1F^o	14348.78	2	a^3D	8513.24	-0.14
11723.05	8530.20	5	C									
11710.01	8539.70	3	D									

(1)	(2)	(3)	(4)	(5)	(6)	(7)	(8)	(9)	(10)	(11)	(12)	(13)
11686.24	8557.07	12	B									
*11674.41	8565.74	6	A		38101.09	4	e^3F	29535.48	5	y^5F^o	8565.61	0.13
*11668.20	8570.30	2	B									
*11666.65	8571.44	6	A									
11661.26	8575.40	1500	A		19833.78	4	z^5D^o	11258.38	3	a^5P	8575.40	0.00
11653.46	8581.14	7	D									
*11646.50	8586.27	2	D		25645.97	2	z^5P^o	17059.82	1	c^3P	8586.15	0.12
+11615.86	8608.92	900	A		19625.58	3	z^5D^o	11016.65	2	a^5P	8608.93	-0.01
11590.90	8627.46	28	B		22750.53	2	y^1D^o	14123.01	1	a^3D	8627.52	-0.06
11589.59	8628.43	11	D									
11585.28	8631.64	43	A		37701.08	3	e^3F	29057.84	2	v^3D^o	8643.24	0.08
*11569.63	8643.32	4	D		35210.30	2	e^5F	26557.21	2	x^3D^o	8653.09	0.20
*11556.30	8653.29	4	C									
*11540.61	8665.05	4	B	AS								
11528.25	8674.34	28	B									

(1)	(2)	(3)	(4)	(5)	(6)	(7)	(8)	(9)	(10)	(11)	(12)	(13)
*11507.55	8689.95	2	D									
11506.09	8691.05	3	D		26443.88	3	x^3F^o	17752.73	4	b^1G	8691.15	−0.10
*11484.48	8707.40	4	D									
*11475.72	8714.05	2	B									
*11474.36	8715.08	6	A									
*11470.56	8717.97	6	D									
11451.26	8732.66	6	C									
11421.30	8755.57	6	D	AS	25898.16	3	z^5P^o	17142.72	2	e^3P	8755.44	0.13
11395.02	8775.76	23	B		23567.12	3	y^3F^o	14791.28	4	a^3H	8775.84	−0.08
11380.82	8786.71	51	A		16843.93	3	z^3F^o	8057.30	4	a^1G	8786.63	0.08
11345.99	8813.69	5	B									
*11339.27	8818.91	4	D	h								
11328.65	8827.18	5	B									
11324.16	8830.68	12	B									
*11318.29	8835.26	4	D									

(1)	(2)	(3)	(4) (5)	(6)	(7)	(8)	(9)	(10)	(11)	(12)	(13)
11273.79	8870.13	29	A	23567.12	3	y^3F^o	14697.03	3	a^3D	8870.09	0.04
11249.81	8889.04	8	A	23597.47	2	y^3F^o	14697.03	3	a^3D	8900.44	0.21
*11235.13	8900.65	4	C								
*11227.88	8906.40	6	D h								
11217.74	8914.45	11	B								
11206.77	8923.18	9	B								
*11192.63	8934.45	6	A								
11190.08	8936.49	70	B	37701.08	3	e^3F	28749.80	4	x^3G^o	8951.28	0.05
11171.52	8951.33	9	B								
11166.35	8955.48	20	B								
*11155.86	8953.90	4	A	23660.97	3	y^3D^o	14697.03	3	a^3D	8963.94	−0.04
11151.16	8967.68	5	B								
11147.13	8970.92	17	A	23319.86	2	y^3D^o	14348.78	2	a^3D	8971.08	−0.16
11133.29	8982.07	14	B								
11132.13	8983.01	3	D								

(1)	(2)	(3)	(4)	(5)	(6)	(7)	(8)	(9)	(10)	(11)	(12)	(13)
*11089.20	9017.78	4	A		24006.30	4	y^3F^o	14988.51	5	a^3H	9017.79	-0.01
11081.54	9024.02	3	B									
11203.08	9026.12	28	B									
*11008.09	9084.23	4	A		26226.97	3	x^1F^o	17142.72	2	c^3P	9084.25	-0.02
11043.09	9055.44	9	B		37459.60	2	e^3F	28404.26	3	x^3G^o	9055.34	0.10
11002.63	9088.74	70	A		21849.33	3	z^3G^o	12760.66	4	a^3G	9088.67	0.07
10995.91	9094.29	3	B		26154.13	1	x^3D^o	17059.82	1	c^3P	9094.31	-0.02
10991.93	9097.58	2	D	h	23889.03	3	y^5D^o	14791.28	4	a^3H	9097.75	-0.17
10989.42	9099.66	20	A		38101.09	4	c^3F	29001.65	5	x^3G^o	9099.44	0.22
10960.30	9123.84	3	B									
10940.14	9140.65	3	A		23489.43	2	y^5D^o	14348.78	2	a^3D	9140.65	0.00
*10928.56	9150.34	4	D									
10924.90	9153.40	6	B									
10905.83	9169.41	8	A		27908.28	4	z^3H^o	18738.94	5	a^1H	9169.34	0.07
10901.76	9172.83	11	B		37701.08	3	e^3F	28528.36	4	w^3F^o	9172.72	0.11

(1)	(2)	(3)	(4)	(5)	(6)	(7)	(8)	(9)	(10)	(11)	(12)	(13)
10894.84	9178.66	25		A	26931.35	4	z^1D^o	17752.73	4	b^1G	9178.62	0.04
10886.49	9185.70	32		A	26938.42	4	x^3P^o	17752.73	4	b^1G	9185.69	0.01
*10881.97	9189.51	6		D								
*10878.95	9192.06	8		A	23889.03	3	y^5D^o	14697.03	3	3^3D	9192.00	0.06
+10873.47	9196.70	115		A	23319.86	2	y^3D^o	14123.01	1	a^3D	9196.85	−0.15
10870.38	9199.31	98		A								
*10866.84	9202.31	6		D								
10859.50	9208.53	62		A	20466.83	2	z^3P^o	11258.38	3	a^5T	9208.45	0.08
10847.99	9218.30	380		A	23567.12	3	y^3F^o	14348.78	2	a^3D	9218.34	−0.04
*10824.13	9238.62	4		A	35210.30	2	e^5F	25971.71	3	y^5G^o	9238.59	0.03
10812.39	9248.65	51		A	23597.47	2	y^3F^o	14348.78	2	a^3D	9248.69	−0.04
10750.04	9302.29	3		C	37459.60	2	e^3F	28157.42	3	w^3F^o	9302.18	0.11
+10742.00	9309.25	460		A	24006.30	4	y^3F^o	14697.03	3	a^3D	9309.27	−0.02
10735.11	9315.23	3		C								
10709.32	9337.66	3		C								

(1)	(2)	(3)	(4)	(5)	(6)	(7)	(8)	(9)	(10)	(11)	(12)	(13)
10699.76	9346.00	550	A		21849.33	3	z^3G^o	12503.44	3	a^3G	9345.89	0.11
10696.80	9348.59	14	A		20233.97	0	z^3P^o	10885.36	1	a^5P	9348.61	-0.02
10685.52	9358.46	12	B		27111.16	3	x^3D^o	17752.73	4	b^1G	9358.43	0.03
10676.41	9366.44	123	A		23489.43	2	y^5D^o	14123.01	1	a^3D	9366.42	0.02
10670.87	9371.31	140	A		22144.08	4	z^3G^o	12772.78	5	a^3G	9371.30	0.01
*10668.42	9373.46	4	B	h	41068.00	5	f^5F	31694.52	4	w^3G^o	9373.48	-0.02
10665.52	9376.01	21	B									
10557.07	9383.44	570	A	h	22144.08	4	z^3G^o	12760.66	4	a^3G	9383.42	0.02
10621.78	9414.62	5	B		26557.21	2	x^3D^o	17142.72	2	c^3P	9414.49	0.13
*10565.68	9464.61	6	B		35476.07	3	e^5F	26011.55	4	y^3G^o	9464.52	0.09
+10554.71	9474.44	170	A		23597.47	2	y^3F^o	14123.01	1	a^3D	9474.46	-0.02
*10548.31	9480.19	10	B		35210.30	2	e^5F	25729.96	3	y^3G^o	9480.34	-0.15
*10534.29	9492.81	4	D									
10529.11	9497.48	8	B		26557.21	2	x^3D^o	17059.82	1	c^3P	9497.39	0.09
*10527.40	9499.02	2	C		17556.26	4	z^3F^o	8057.30	4	a^1G	9498.95	0.06
10523.55	9502.49	5	B		20519.20	1	z^3P^o	11016.65	2	a^5P	9502.55	-0.06

(1)	(2)	(3)	(4)	(5)	(6)	(7)	(8)	(9)	(10)	(11)	(12)	(13)
10518.49	9507.07	33	A		21849.33	3	$z\,^3G^\circ$	12342.37	4	$b\,^3F$	9506.96	0.11
*10488.51	9534.24	2	C		14783.54	2	$z\,^5G^\circ$	5249.07	3	$a\,^5P$	9534.47	-0.23
10482.05	9540.12	38	B		23889.03	3	$y\,^5D^\circ$	14348.78	2	$a\,^3D$	9540.25	-0.13
*10473.86	9547.58	8	B									
*10450.48	9568.94	4	C	h	38101.09	4	$e\,^3F$	28528.36	4	$w\,^3F^\circ$	9572.73	0.31
*10446.00	9573.04	4	C									
10436.69	9581.58	54	A		20466.83	2	$z\,^3P^\circ$	10985.36	1	$a\,^5P$	9581.47	0.11
10420.85	9596.15	31	B		24387.52	3	$y\,^1F^\circ$	14791.28	4	$a\,^3H$	9596.24	-0.09
10389.88	9624.75	6	A									
10380.13	9633.79	21	A		20519.20	1	$z\,^3P^\circ$	10885.36	1	$a\,^5P$	9633.84	-0.05
10372.77	9640.63	3	B		22144.08	4	$z\,^3G^\circ$	12503.44	3	$a\,^3G$	9640.64	-0.01
10370.83	9642.43	5	C									
10356.66	9655.62	3	C									
10331.37	9679.26	38	B		24376.37	4	$y\,^5D^\circ$	14697.03	3	$a\,^3D$	9679.34	-0.08

(1)	(2)	(3)	(4)	(5)	(6)	(7)	(8)	(9)	(10)	(11)	(12)	(13)
10325.84	9684.44	3	B									
10319.35	9690.53	23	A		24387.52	3	y^1F^o	14637.03	3	a^3D	9690.49	0.04
*10295.95	9712.56	4	C	h								
*10294.43	9713.09	8	B		25645.97	2	z^5P^o	15932.10	2	b^3P	9713.87	0.12
*10250.61	9755.52	4	C									
+10245.64	9760.25	110	B		14783.54	2	z^5G^o	5023.41	2	a^5F	9760.13	0.12
10219.21	9785.49	4	C									
+10213.37	9791.09	510	A		22563.89	5	z^3G^o	12772.78	5	a^3G	9791.11	-0.02
10202.31	9801.70	120	A		22144.08	4	z^3G^o	12342.37	4	b^3F	9801.71	-0.01
10200.74	9803.21	30	A		22563.89	5	z^3G^o	12760.66	4	a^3G	9803.23	-0.02
10159.71	9842.80	8	C		26902.45	1	w^3D^o	17059.82	1	c^3P	9842.63	0.17
*10152.39	9840.90	4	D	h								
*10124.82	9876.72	2	D	h								
10123.04	9878.46	10	A									
*10118.79	9882.60	6	B		27111.16	3	x^3D^o	17228.42	2	b^1D	9882.74	-0.14

(1)	(2)	(3)	(4)	(5)	(6)	(7)	(8)	(9)	(10)	(11)	(12)	(13)
10096.67	9904.26	5	C									
*10096.62	9904.30	4	D	ASL								
+10087.61	9913.15	380	A		14783.54	2	z^5G^o	4870.53	1	a^5F	9913.01	0.14
10079.05	9921.57	3	B									
10047.98	9952.25	150	B		15201.26	3	z^5G^o	5249.07	3	a^5F	9952.19	0.06
10031.54	9968.56	38	C	W	27111.16	3	x^3D^o	17142.72	2	c^3P	9968.44	0.12
10020.03	9979.99	30	B	B								
10001.54	9998.46	2	D									
9993.56	10006.44	3	D									
9970.19	10029.90	8	A									
9965.15	10034.97	23	B	AS	24387.52	3	y^1F^o	14348.78	2	a^3D	10038.74	-0.04
9961.45	10038.70	31	A									
9931.19	10069.29	9	B									
9920.37	10080.27	5	B									
9912.64	10088.13	30	B									

(1)	(2)	(3)	(4)	(5)	(6)	(7)	(8)	(9)	(10)	(11)	(12)	(13)
9903.38	10097.56	2	B									
9901.15	10099.84	2	B									
9879.40	10122.07	6	B									
9872.02	10129.64	5	B		16061.70	2	x^3P^o	15932.10	2	b^3P	10129.60	0.04
9862.67	10139.24	8	B									
9846.78	10155.60	11	B	AS	27908.28	4	z^3H^o	17752.73	4	b^1G	10155.55	0.05
9825.15	10177.96	380	B		15201.26	3	z^5G^o	5023.41	2	a^5F	10177.85	0.11
9823.35	10179.83	150	A		15720.36	4	z^5G^o	5540.54	4	a^5F	10179.82	0.01
9815.70	10187.76	230	A		22144.08	4	z^3G^o	11956.33	3	b^3F	10187.75	0.01
9795.59	10208.68	150	B		21849.33	3	z^3G^o	11640.72	2	b^3F	10208.61	0.07
9783.29	10221.51	280	A		22563.89	5	z^3G^o	12342.37	4	b^3F	10221.52	-0.01
9776.18	10228.94	15	B									
9773.44	10231.81	5	C	B								
9758.85	10247.11	5	B		22750.53	2	y^1D^o	12503.44	3	a^3G	10247.09	0.02
9731.08	10276.35	3	C									

144

(1)	(2)	(3)	(4)	(5)	(6)	(7)	(8)	(9)	(10)	(11)	(12)	(13)
9708.40	10300.36	2		D								
9678.21	10332.49	5		D								
9669.56	10341.73	9		B								
9652.33	10360.19	3		D								
9640.99	10372.38	7		B	27515.38	2	x^1D^o	17142.72	2	c^3P	10372.66	−0.28
9587.79	10429.93	14		D	27572.52	1	y^3P^o	17142.72	2	c^3P	10429.80	0.13
9549.97	10471.24	770		B	15720.36	4	z^5G^o	5249.07	3	a^5F	10471.29	−0.05
9522.31	10501.65	2		C								
9520.03	10504.17	12		B								
9512.22	10512.79	11		A	27572.52	1	y^3P^o	17059.82	1	c^3P	10512.70	0.09
9507.70	10517.79	2	h	B								
9496.89	10525.76	23		B								
9496.13	10530.61	60		A	27673.35	2	y^3P^o	17142.72	2	c^3P	10530.63	−0.02
9487.31	10540.40	15		B	27600.24	0	y^3P^o	17059.82	1	c^3P	10540.42	−0.02
9486.25	10541.57	52		A								

(1)	(2)	(3)	(4)	(5)	(6)	(7)	(8)	(9)	(10)	(11)	(12)	(13)
9455.27	10576.11	6	B									
*9452.47	10579.25	2	B	h	37701.08	3	e^3F	27121.96	2	w^3D^o	10579.12	0.13
9443.83	10588.92	57	A									
9421.99	10613.47	15	A		27673.35	2	y^3P^o	17059.82	1	c^3P	10613.53	−0.06
9411.61	10625.17	28	A		26557.21	2	x^3D^o	15932.10	2	b^3P	10625.11	0.06
9316.78	10733.32	6	C		27876.16	2	w^3F^o	17142.72	2	c^3P	10733.44	−0.12
9292.76	10761.06	8	D									
9279.51	10776.43	380	A		16316.96	5	z^5G^o	5540.54	4	a^5F	10776.42	0.01
9253.72	10806.47	115	A		23567.12	3	y^3P^o	12760.66	4	a^3G	10806.46	0.01
9251.02	10809.62	5	B									
9245.27	10816.34	100	A		27876.16	2	w^3P^o	17059.82	1	c^3P	10816.34	0.00
9231.97	10831.92	38	A									
9183.10	10889.57	6	B									
9141.95	10938.65	150	B		25729.96	3	y^3G^o	14791.28	4	a^3H	10938.68	−0.03
9136.73	10944.86	8	C									

(1)	(2)	(3)	(4)	(5)	(6)	(7)	(8)	(9)	(10)	(11)	(12)	(13)
*9120.53	10964.28	2	B									
9115.50	10970.33	5	C									
9102.39	10986.12	50	A		23489.43	2	y^5D^o	12503.44	3	a^3G	10985.99	0.13
9099.52	10989.59	3	C		38101.09	4	e^3F	27111.16	3	x^3D^o	10989.93	0.01
*9099.23	10989.94	4	A									
9071.88	11023.07	150	B		26011.55	4	y^3G^o	14988.51	5	a^3H	11023.04	0.03
*9060.74	11036.63	6	A									
9051.84	11047.48	3	C		16296.51	2	z^3F^o	5249.07	3	a^5F	11047.44	0.04
9038.57	11063.70	3	B		23567.12	3	y^3F^o	12503.44	3	a^3G	11063.68	0.02
9017.64	11089.38	120	A	h	16978.29	6	z^5G^o	5888.93	5	a^5F	11089.36	0.02
9013.81	11094.09	58	B		23697.47	2	y^3F^o	12503.44	3	a^3G	11094.03	0.06
9001.11	11109.74	2	C		22750.53	2	y^1D^o	11640.72	2	b^3F	11109.81	-0.07
*9001.08	11109.78	2	B		22750.53	2	y^1D^o	11640.72	2	b^3F	11109.81	-0.03
8986.09	11128.31	20	B		23889.03	3	y^5D^o	12760.66	4	a^3G	11128.37	-0.06
8978.55	11137.65	8	B									

117

(1)	(2)	(3)	(4)	(5)	(6)	(7)	(8)	(9)	(10)	(11)	(12)	(13)
*8967.45	11151.44	6	B		38101.09	4	e^3F	26938.42	4	x^3F^o	11162.67	0.07
*8958.37	11162.74	4	B		25971.71	3	y^5G^o	14791.28	4	a^3H	11180.43	0.03
8944.18	11180.46	40	A		16296.51	2	z^3F^o	5101.68	2	a^1D	11194.83	0.14
8932.58	11194.97	54	B		25898.16	3	z^5P^o	14697.03	3	a^3D	11201.13	0.14
8927.56	11201.27	30	B									
8912.52	11220.17	12	A		26011.55	4	y^3G^o	14791.28	4	a^3H	11220.27	-0.1
8908.86	11224.75	26	A		23567.12	3	y^3F^o	12342.37	4	b^3F	11224.75	0.00
8901.94	11233.51	170	A		24006.30	4	y^3F^o	12772.78	5	a^3G	11233.52	-0.01
*8890.58	11247.86	4	A									
*8869.26	11274.90	4	B	ASL								
8851.71	11297.25	3	C		25645.97	2	z^5P^o	14348.78	2	a^3D	11297.19	0.06
8846.84	11303.47	20	C	ASL	16843.93	3	z^3F^o	5540.54	4	e^5F	11303.39	0.08
8838.57	11314.05	130	B		40849.70	4	f^5F	29535.48	5	y^5F^o	11314.22	-0.17
8835.05	11318.55	8	B		23660.97	3	y^3D^o	12342.37	4	b^3F	11318.60	-0.05
8807.42	11354.06	30	B		26342.53	4	y^5G^o	14988.51	5	a^3H	11354.02	0.04

(1)	(2)	(3)	(4)	(5)	(6)	(7)	(8)	(9)	(10)	(11)	(12)	(13)
8788.74	11378.20	21	A		23018.92	1	y^3D^o	11640.72	2	b^3F	11378.20	0.00
*8780.86	11388.40	2	C	h	28709.88	1	x^3P^o	17321.52	0	c^3P	11388.36	0.04
*8773.56	11397.88	2	B	h	37459.60	2	e^3F	26061.70	2	x^3F^o	11397.90	-0.02
8751.88	11426.11	60	A		16296.51	2	z^3F^o	4870.53	1	a^5F	11425.98	0.13
8746.70	11432.88	4	C									
8744.61	11435.61	5	C	h	26226.97	3	x^1F^o	14791.28	4	a^3H	11435.69	-0.08
8737.33	11445.15	16	B									
*8723.59	11463.26	2	D	h								
*8723.04	11463.89	2	D	h								
*8711.62	11478.92	4	B		28800.51	1	v^3D^o	17321.52	0	c^3P	11478.99	-0.07
*8710.17	11480.83	8	A	h	26938.42	4	x^3F^o	15457.40	3	c^3F	11481.02	-0.19
*8688.01	11510.11	6	B									
*8667.56	11537.27	4	B									
*8666.59	11533.56	4	D	h	25898.16	3	z^5P^o	14348.78	2	a^3D	11549.38	0.07
*8658.42	11549.45	2	B									

(1)	(2)	(3)	(4)	(5)	(6)	(7)	(8)	(9)	(10)	(11)	(12)	(13)
*8657.00	11551.34	4	B	AS	26342.53	4	$y\,^5G^o$	14791.28	4	$a\,^3H$	11551.25	0.09
*8545.14	11567.19	6	B		28709.88	1	$x\,^3P^o$	17142.72	2	$c\,^3P$	11567.16	0.03
8643.45	11569.45	6	D									
*8630.32	11587.05	4	B		35476.07	3	$e\,^5F$	23889.03	3	$y\,^5D^o$	11587.04	0.01
*8616.64	11605.45	2	B		23246.33	1	$y\,^5D^o$	11640.72	2	$b\,^3F$	11605.61	-0.16
*8615.76	11606.64	4	B									
8612.70	11610.76	10	B		23567.12	3	$y\,^3F^o$	11956.33	3	$b\,^3F$	11610.79	-0.03
*8611.40	11612.52	2	B									
8590.25	11641.11	14	B		23597.47	2	$y\,^3F^o$	11956.33	3	$b\,^3F$	11641.14	-0.03
*8588.28	11643.77	2	B	h	33444.87	1	$w\,^5D^o$	21801.21	1	$a\,^5D$	11643.66	0.11
8586.65	11645.98	27	A		26765.66	5	$y\,^5G^o$	15119.66	6	$a\,^3H$	11646.00	-0.02
*8585.23	11647.91	2	D									
*8581.87	11652.47	4	D		26443.88	3	$x\,^3F^o$	14791.28	4	$a\,^3H$	11652.60	-0.13
8573.53	11663.81	17	B		24006.30	4	$y\,^3F^o$	12342.37	4	$b\,^3F$	11663.93	-0.12
8570.95	11667.32	30	A		17556.26	4	$z\,^3F^o$	5888.93	5	$a\,^5F$	11667.33	-0.01

(1)	(2)	(3)	(4)	(5)	(6)	(7)	(8)	(9)	(10)	(11)	(12)	(13)
*8556.76	11686.66	2	B	h								
*8537.51	11713.02	2	D		26061.70	2	x^3F^o	14348.78	2	a^3D	11712.92	0.10
8517.47	11740.58	6	C		28800.51	1	v^3D^o	17059.82	1	c^3P	11740.69	-0.11
8516.19	11742.34	21	B		16843.93	3	z^3F^o	5101.68	2	a^1D	11742.25	0.09
*8513.00	11746.74	2	B	h	26443.88	3	x^3F^o	14697.03	3	a^3D	11746.85	-0.11
*8505.15	11757.58	8	A									
8500.81	11763.58	78	B		16786.93	1	z^5F^o	5023.41	2	a^5F	11763.52	0.06
8498.32	11767.03	9	B		28909.57	2	x^3P^o	17142.72	2	c^3P	11766.85	0.18
*8491.14	11776.98	4	C		26765.66	5	y^5G^o	14988.51	5	a^3H	11777.15	-0.17
8466.98	11810.59	770	A	h	17059.61	2	z^5F^o	5249.07	3	a^5F	11810.54	0.05
8459.84	11820.56	17	A		16843.93	3	z^3F^o	5023.41	2	a^5F	11820.52	0.04
8455.47	11826.56	65	B		23085.06	2	z^5S^o	11258.38	3	a^5P	11826.68	-0.02
8416.33	11881.67	77	B		17422.17	3	z^5F^o	5540.54	4	a^5F	11881.63	0.04
+8391.75	11916.47	86	C		16786.93	1	z^5F^o	4870.53	1	a^5F	11916.40	0.07
8389.04	11920.31	9	B		16296.51	2	z^3F^o	4376.28	1	a^3P	11920.23	0.08

(1)	(2)	(3)	(4)	(5)	(6)	(7)	(8)	(9)	(10)	(11)	(12)	(13)
8372.53	11943.82	51	A		17832.73	4	z^5F°	5888.93	5	a^5F	11943.80	0.02
*8368.39	11949.73	6	C	ASL	26938.42	4	x^3F°	14988.51	5	a^3H	11949.91	-0.18
*8363.50	11956.71	6	B		23597.47	2	y^3F°	11640.72	2	b^3F	11956.75	-0.04
*8342.87	11985.29	2	C	h								
8334.74	11997.98	17	A		29057.84	2	v^3D°	17059.82	1	c^3P	11998.02	-0.04
8322.43	12015.72	13	A		17556.26	4	z^3F°	5540.54	4	a^5F	12015.72	0.00
*8319.29	12020.26	2	C	h	23660.97	3	y^3D°	11640.72	2	b^3F	12020.25	0.01
*8311.87	12031.05	2	C		26154.13	1	x^3D°	14123.01	1	a^3D	12031.12	-0.07
8308.22	12036.27	58	B		17059.61	2	z^5F°	5023.41	2	a^5F	12036.20	0.07
8302.07	12045.19	4	B		24387.52	3	y^1F°	12342.37	4	b^3F	12045.15	0.04
*8298.93	12049.74	2	C	h	24006.30	4	y^3F°	11956.33	3	b^3F	12049.97	-0.23
*8294.01	12056.89	2	D	h								
*8287.65	12066.15	4	B									
8286.11	12068.35	32	A		23085.06	2	z^5S°	11016.65	2	a^5P	12068.41	-0.02
8242.68	12131.98	9	C		29274.82	3	v^3D°	17142.72	2	c^3P	12132.10	-0.12

(1)	(2)	(3)	(4)	(5)	(6)	(7)	(8)	(9)	(10)	(11)	(12)	(13)
8214.84	12173.09	58	A		17422.17	3	z^5F^o	5249.07	3	a^5F	12173.10	-0.01
*8212.18	12177.04	4	B									
8204.03	12189.13	39	B		17059.61	2	z^5F^o	4870.53	1	a^5P	12189.08	0.05
+8196.95	12199.66	19	B		23085.06	2	z^5S^o	10885.36	1	a^5P	12199.70	-0.04
*8171.96	12236.96	4	3		23122.29	0	y^5D^o	10885.36	1	a^5P	12236.93	0.03
*8168.86	12241.61	2	D	h	26938.42	4	x^3F^o	14697.03	3	a^3D	12241.39	0.22
*8158.50	12257.16	4	B									
8154.86	12262.63	17	C		17511.78	2	z^1D^o	5249.07	3	a^5F	12262.71	-0.09
8135.23	12292.22	20	B	ASL	17832.73	4	z^5F^o	5540.54	4	a^5F	12292.19	0.03
*8125.40	12307.09	4	B		17556.26	4	z^3F^o	5249.07	3	a^5F	12307.19	-0.10
*8124.33	12308.70	4	B		23567.12	3	y^3F^o	11258.38	3	a^5P	12308.74	-0.04
*8122.42	12311.60	12	A		31050.48	4	y^1G^o	18738.94	5	a^1H	12311.54	0.06
8116.53	12320.54	4	C	h	17422.17	3	z^5F^o	5101.68	2	a^1D	12320.49	0.05
*8111.42	12328.30	4	B	ASL	17429.86	1	z^3D^o	5101.68	2	a^1D	12328.18	0.12
8072.32	12388.01	30	B	B	18276.92	5	z^5F^o	5888.93	5	a^5F	12387.99	-0.02

(1)	(2)	(3)	(4)	(5)	(6)	(7)	(8)	(9)	(10)	(11)	(12)	(13)
8065.32	12398.77	23	B		17422.17	3	z^5F^o	5023.41	2	a^5F	12398.76	0.01
8060.32	12406.46	16	B		17429.86	1	z^3D^o	5023.41	2	a^5F	12406.45	0.01
8057.98	12410.06	8	B		17511.78	2	z^1D^o	5101.68	2	a^1D	12410.10	−0.04
8057.55	12410.72	4	B		16786.93	1	z^5F^o	4376.28	1	a^3P	12410.65	0.07
*8055.28	12414.22	6	B		27111.16	3	x^3D^o	14697.03	3	a^3D	12414.13	0.09
*8052.41	12418.64	2	B	h	27876.16	2	w^3F^o	15457.40	3	c^3F	12418.76	−0.12
*8051.41	12420.18	2	B	h	24376.37	4	y^5D^o	11956.33	3	b^3F	12420.04	0.14
*8017.42	12472.84	2	D		23489.43	2	y^5D^o	11016.65	2	a^5P	12472.78	0.06
*8007.48	12488.32	8	A		17511.78	2	z^1D^o	5023.41	2	a^5F	12488.37	−0.05
7962.18	12559.38	8	B		17429.86	1	z^3D^o	4870.53	1	a^5F	12559.33	0.05
7958.88	12564.58	6	B		17813.64	2	z^3D^o	5249.07	3	a^5F	12564.57	0.01
7946.83	12583.64	8	B		17832.73	4	z^5F^o	5249.07	3	a^5F	12583.66	−0.02
*7942.67	12590.23	8	B		16786.93	1	z^5F^o	4196.85	0	a^3P	12590.08	0.15
*7910.58	12641.30	6	A		17511.78	2	z^1D^o	4870.53	1	a^5F	12641.25	0.05
*7884.35	12683.35	6	A		17059.61	2	z^5F^o	4376.28	1	a^3P	12683.33	0.02
*7872.13	12703.04	6	A		18243.56	3	z^3D^o	5540.54	4	a^5F	12703.02	0.02

CHAPTER 7

ZEEMAN PATTERN OF ZIRCONIUM

INFRA-RED SPECTRA LINES

7-1 Introduction

It has already been mentioned in Chapter 1 that
interferometric techniques in infra-red spectroscopy
will provide an instrumental ability to observe the
zeeman pattern of the spectra lines. Using a pressure
scanning Fabry-Perot interferometer (F.P.I) to scan
the zeeman components, the zeeman structure of select-
ed lines could be investigated to obtain data either to
assist in identifying the transition or in determining
the quantum state of the levels involved.

49 lines were examined by pressure scanning Fabry-
Perot interferometer in zeeman effect investigation.
But the number of lines is limited by the available
intensity in the measured region, and the infra-red
region was limited by the lack of Fabry-Perot plates
of suitable high reflectivity coating. The lines
studied are involved in transitions in the following
multiplets:

$$z^5D^o - a^5P \qquad z^5G^o - a^5F$$

$$z^5S^o - a^5P \qquad z^3G^o - a^3G$$

$$z^5F^o - a^5F \qquad y^3F^o - a^3D$$

$$y^3D^o - a^3D \qquad x^5D^o - a^5D$$

$$y^3D^o - b^3P \qquad f^5G - v^3P^o$$

$$z^3P^o - b^3P$$

The above line profiles resolved by varying the magnetic field across the line source and the g values of the terms involved was re-measured. Four lines proved to be wrongly assigned to the transitions, from these one was assigned to the right transition, two others suggested an involvement of b^3P_1 term which its value is not quoted in the available energy level list of zirconium. A new energy value for b^3P_0 (there is no value for b^3P_0 in energy level list of zirconium) was found and confirmed by the lines fitted to the transitions involving this energy level and the transitions also confirmed by zeeman effect observation.

Seven new Landé g factor are also calculated and are given in Section 7-7.

7-2 Fabry-Perot Interferometer

The Fabry-Perot interferometer has multiple pass-
bands according to the basic equation

$$\Delta = n \lambda = 2 \mu t \, \cos \theta$$

<div align="right">(7-1)</div>

$$n = \sigma \cdot \Delta = 2 \mu t \, \sigma \cos \theta$$

where Δ is the optical retardation.

         λ is the wavelength of the spectral line

         σ is the wavenumber of the spectral line

         μ is the refractive index of the gas between
            the plates

         n   is the order of interference

         t   is the distance between the plates

         θ is the angle between the normal to the
            plates and the emergent light.

To isolate one of these pass bands and use the
Fabry-Perot interferometer as a spectrometer a mono-
chromator must be used in conjunction with the Fabry-Perot.

In this part of the project the Ebert mounting
spectrometer discussed in Chapter 3 was employed as a
monochromator.

If the plates of a Fabry-Perot were perfectly
plane and parallel and the diaphragm had very narrow
width and the reflectivity was considered to be equal
to unity, then under these conditions the instrumental
function would be presented by a series of infinitely
sharp peaks called Dirac peaks.

$$W(\sigma) = \sum_0^\infty \delta(\sigma - \sigma_n) \qquad (7\text{-}2)$$

separated by interval

$$\Delta\sigma = \frac{1}{\Delta} \qquad (7\text{-}3)$$

But with a reflectivity R less than unity the instrumen-
tal function is represented by the Airy function

$$A(\sigma) = \left(\frac{T}{1-R}\right)^2 \frac{1}{1 + (4R\,\mathrm{Sin}^2\,\delta/2)\,/(1-R)^2} \qquad (7\text{-}4)$$

and shown in Figure 7-2. The transmitted light intensity
then, is given by

$$I = \frac{I_0}{(1+\frac{A}{T})^2} \times \frac{1}{1 + \left[\frac{4R}{(1-R)^2}\right]\mathrm{Sin}^2\,\delta/2} \qquad (7\text{-}5)$$
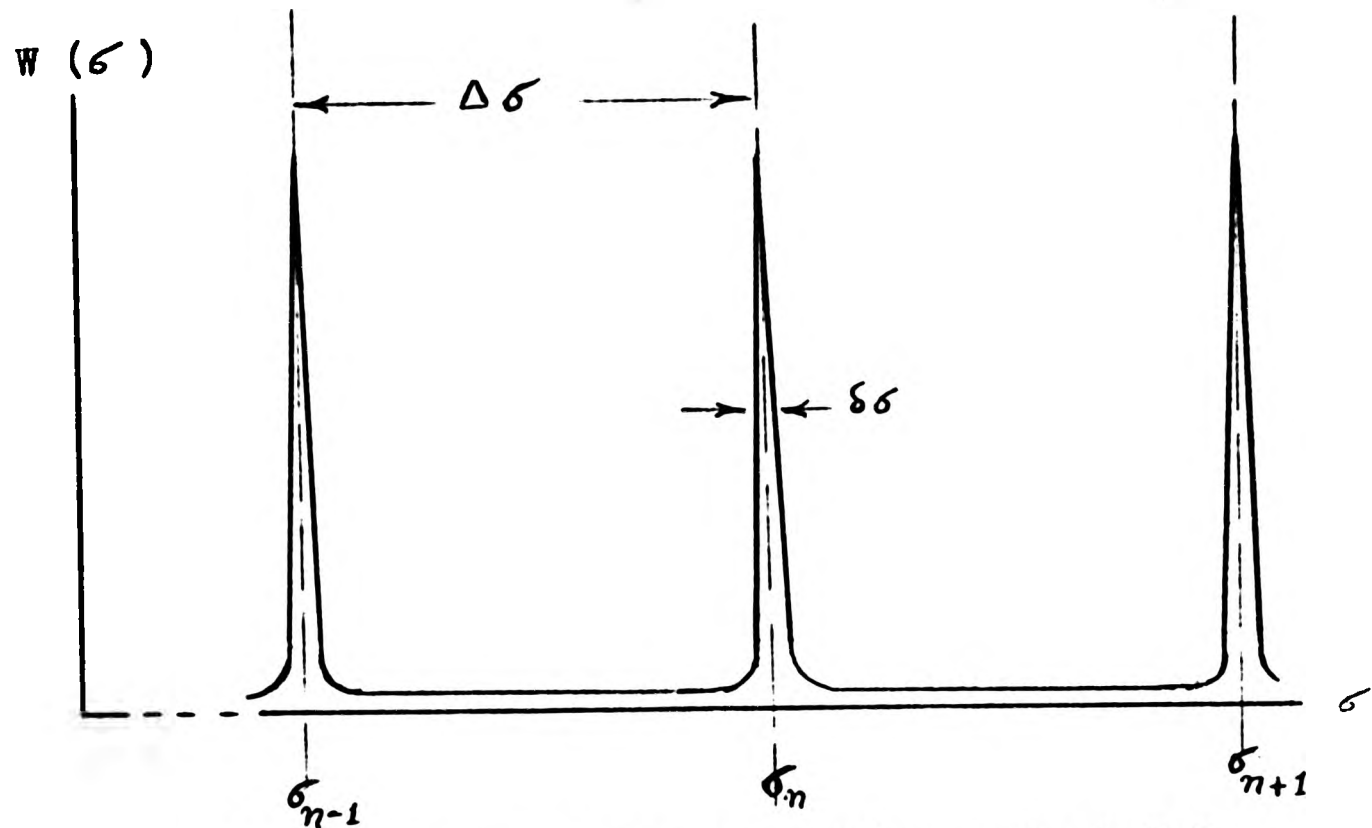
Fig. 7-2: Instrumental function of an actual F.P.
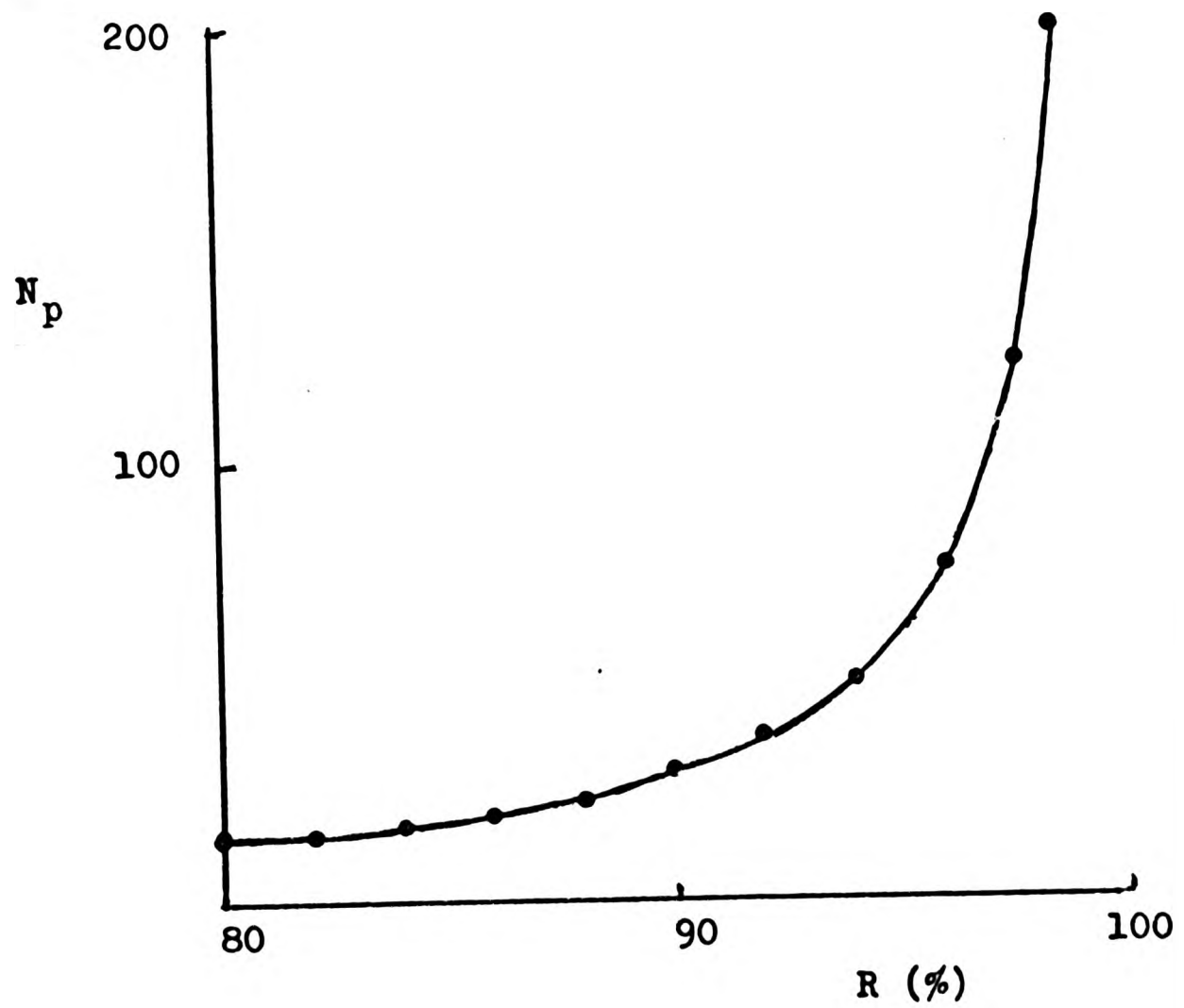
Fig. 7-1: Reflectivity finesse vs reflectivity

where: 1   is the transmitted light intensity

I_o is the incident light intensity

A   is the absorptivity of the plates

T   is the transmissivity of the plates

R   is the reflectivity of the plates

δ is the phase difference between successive reflected rays

The plot of the Airy function (7-4) produces a successive peak (Figure 7-2) with half width of:

$$\delta\sigma = \frac{\Delta\sigma}{N_R} \qquad (7\text{-}6)$$

where:

$$N_R = \frac{\pi\sqrt{R}}{1-R} \qquad (7\text{-}7)$$

N_R is called reflecting finesse and is a constant for a given of Fabry-Perot plates in proper adjustment and at a given wavelength. A graph of N_R versus R is given in Figure 7-1.

The Airy function approximates to a Lorentzian distribution for high values of reflectivity and gives the maximum light intensity when $\sin \delta/2 = 0$

$$I_{max} = \frac{I_o}{(1+\frac{A}{T})^2} \qquad (7\text{-}8)$$

where I_o is the incident light intensity.

In Chapter 3 Section 3-2, it was mentioned how the maximum intensity transmitted is dependent on $A/_T$ of the plate coatings, and the maximum intensity was calculated for a typical glass and quartz metallic coated plates for a wavelength between 500 - 700 nm. A relatively high absorptivity will reduce the light throughput when the reflectivity is high. Values for reflectivity R, absorptivity A and transmissivity T in visible region for two pairs of glass and quartz metallic coated plates are given in Table A_2 - 1 and Table A_2 - 2 in Appendix 2.

As was mentioned in Chapter 3 Section 3-2, the effective finesse is a function of roughness of the optical plates, and angular diameter of the fringe pattern isolated as well as reflectivity R (Chabbal 1958). [27] The roughness component of finesse is given by

$$N_D = m/_2 \qquad (7\text{-}9)$$

N_D is also called the limiting finesse for the plates with a roughness of λ/m. The aperture finesse N_A is given by

$$N_A = \frac{2\pi}{n\Omega} \qquad (7\text{-}10)$$

161

where Ω is the solid angle subtended by the limiting
diaphragm at camera lens (section 3-2) and n is the order
of interference.

7-3 Optical Components

The monochromator used to separate the line being
studied from the next nearest zirconium line, was the
1.5m Ebert mounting grating used to measure the infra-
red spectrum of manganese and zirconium. A maximum
slit width of 0.5 mm was used to record the line profile,
and this was sufficient to isolate the line under
investigation from the closest line by 0.3 nm away.

One inch diameter Fabry-Perot metallic coated
quartz plates were first used to record all given lines
in Section 7-1. Only a few lines with high g value
differences between the levels involving the transitions
could be resolved, but not sufficient enough to calculate
the separation of the components (π components or σ
components) accurately under the operation of high
magnetic field. The metallic coated plates had a low
reflectivity in infra-red, and a high absorptivity
which led to a low light throughput.

The weakness of the signals on the infra-red detec-
tor cell, was not only related to the characteristic
of the Fabry-Perot plates, but also was affected by
decrease of the light intensity of the source by the
presence of the magnetic field (due to the Lorentz
force on electrons and confinement of the electrons

162

in the centre of discharge channel). To maintain the
light source intensity in the field, the microwave
power on the tube must be increased, and this will
enhance the movement of the gas inside the tube and
spinning and fluctuation of the light. The spinning
and fluctuation of the light caused by localized
effect in the tube may cease after a few minutes, but
the intensity will also reduce, and the source weakness
will only provide weak signals associated with noise.

One of the major difficulties which hampered the
measurement and decreased the accuracy of the calcula-
tion was the presence of the noise in the infra-red
detector cell, specially for the weak signals. To
overcome the problem, it was decided to use an infra-
red multi-layer dielectric coated plate with higher
reflectivity, lower absorptivity and bigger diameter
to increase the resolving power and luminosity
(Chapter 1 Section 1-5) and record the line profiles
in lower magnetic field. Two pairs of 2 inch diameter
Fabry-Perot plates were bought from IC Optical System
Limited (ICOS). The plates were multi-layer dielectric
coated and had a wedge of 0.25° so that reflections
from their back surface were sent off the optical axis
and cut out by the entrance slit of the monochromator.
These plates have a high reflectivity over a band
width of 0.48μ from 0.97μ to 1.45μ :

Plates A:-	R = 90%	98%	90%
	$0.97\,\mu$	$1.1\,\mu$	$1.25\,\mu$
Plates B:-	R = 90%	98%	90%
	$1.25\,\mu$	$1.35\,\mu$	$1.45\,\mu$

7-4 Pressure scanning

The most efficient method of wavelength scanning in a Fabry-Perot instrument is by the variation of refractive index of the gas between the plates by changing the pressure P of the gas between the plates inside the pressure chamber where the Fabry-Perot is mounted. Alternatively the distance between the plates (t) can be varied by using piezo-electric discs as spacers between the plates, and changing the voltage across discs, but it is more difficult to ensure the parallelism of the plates during the measurement.

The change of the pressure in pressure chamber will change the refractive index of the gas (nitrogen or argon) between the plates, provided that the gas obey Boyle's law the related equation will be: (e.g. R. Beer and J. Ring)[23]

$$\mu - 1 = aP \qquad (7-8)$$

where 'a' is a constant over a limited pressure range.

Differentiating equation (7-1) on axis ($\theta \approx 0$)

$$\Delta \lambda = \lambda \frac{\Delta \mu}{\mu} \qquad\qquad (7-9)$$

for standard atmospheric P = 1, $\mu = \mu_1$, then a = $\mu_1 - 1$.
from equation (7-8)

$$\Delta \mu = (\mu_1 - 1) \Delta P$$

therefore $\qquad \frac{\Delta \lambda}{\lambda} = \frac{(\mu_1 - 1)}{\mu} \cdot \Delta P \qquad\qquad (7-10)$

Once the plates were made parallel by applying a force to the pressure pads (Figure 7-3) of quartz spacer, the plates stayed parallel for days of measurement. The parallelism of the plates was carried out by applying a force directly on the pads of the quartz spacer via a leaf spring and ball 1 of the T piece. The force on the pads was controlled by a screw in block 1 at a. This arrangement was repeated at 120° intervals for the three pads on the quartz spacer.

The pressure chamber is fitted with a pressure transducer giving an output voltage proportional to the pressure. The pressure transducer used was a C.E.L Transducer Ltd. type RV24 (Range 0-35 P.S.i.) with a non-linearity of 0.5% over the full range. The output of the transducer went via a d.c. amplifier to the X axis of a X - Y pen recorder. The recommended voltage input to the transducer was 10Vd.c. which was
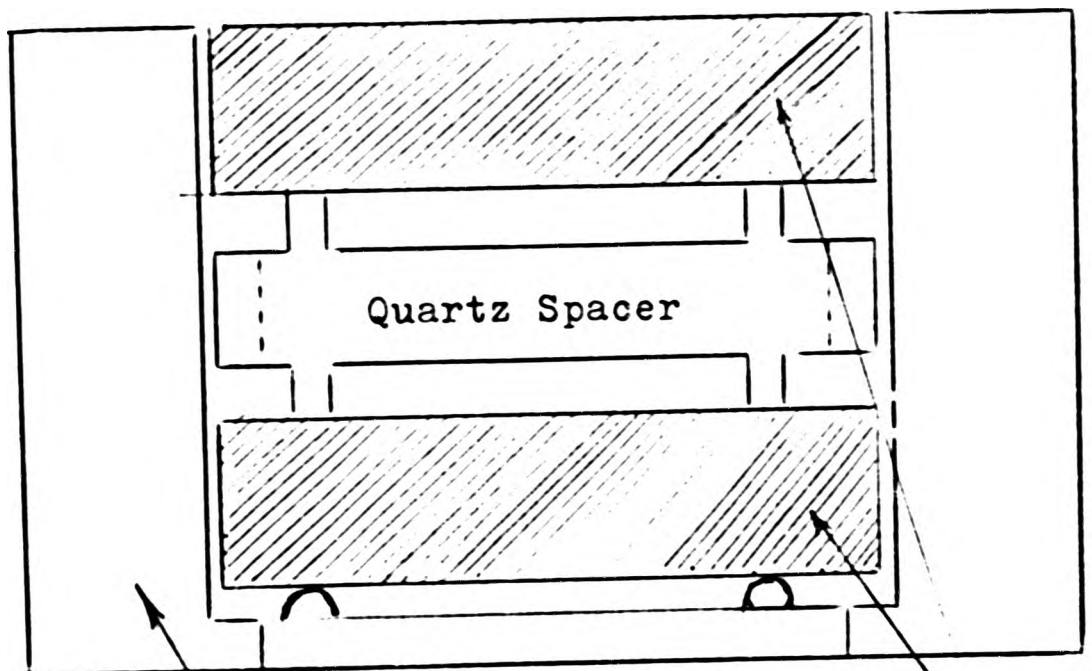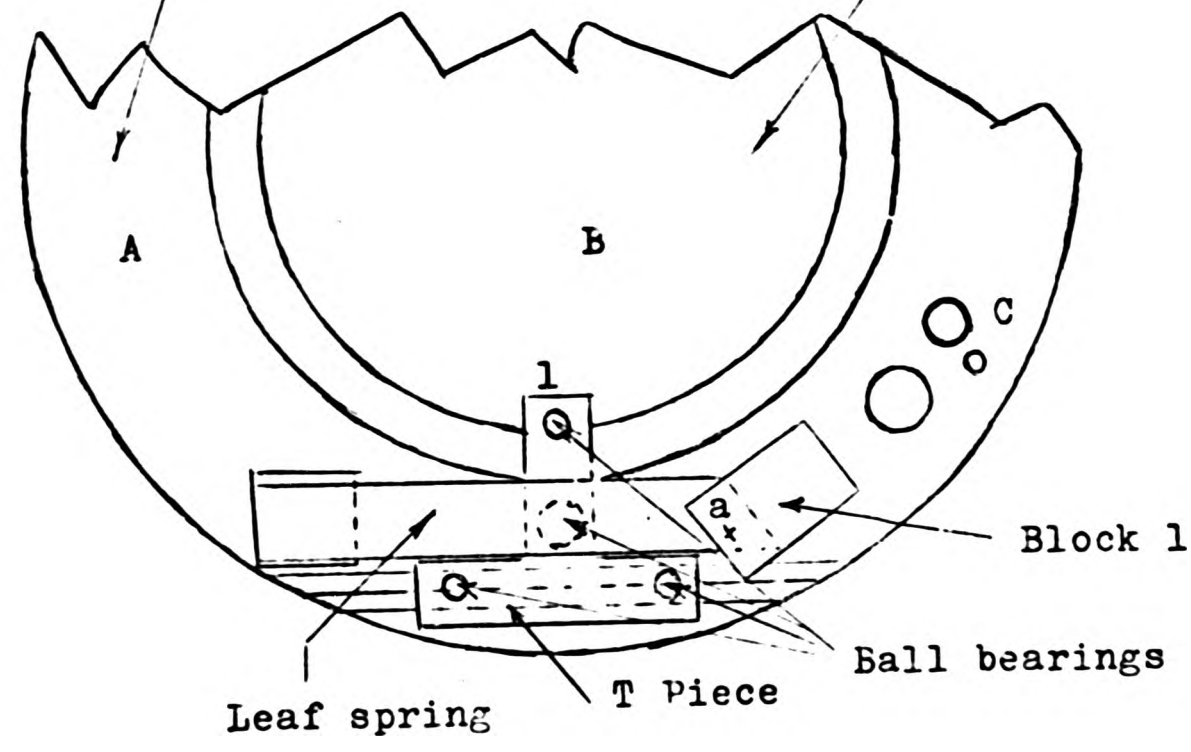
Fig. 7-3: Controls for plate parallelism

provided by a stabilised supply.

The output signal from infra-red detector went via the Brookdeal 401A phase sensitive detector to the Y axis of the X - Y penrecorder.

The penrecorder used was a BW-133 Model (RIKADENKI KOGYO CO. LTD.) X - Y Recorder.

7-5 Optical arrangement

The optical arrangement for pressure scanning is shown in Figure 7-4. The space problem made the experimental arrangement for the recording of zirconium line profile to take the present shape.

A water cooled Newport Instrument 7 inch electro-magnet type E with iron-cord, capable of giving a maximum magnetic field of 18 KG for a gap-distance of 1 inch to accomodate a small Broida Cavity was used in this work. The electromagnet was placed below and in right angle with the optical bench. The light of the source was focused on the diaphragm D by lens L_1 ($f = 17$ cm) after the reflection in a pivoted mirror PM, designed and built by the author. Aperture D was the limiting diaphragm which isolated the central region of the concentric fringe patterns produced by the interferometer. A camera lens L_3 of focal length 30^{cm} was used to fill the aperture of the monochromator. Polarised components of light were selected by an infra-red polaroid placed behind diaphragm D. The polarised light was then introduced to fill the usable area of
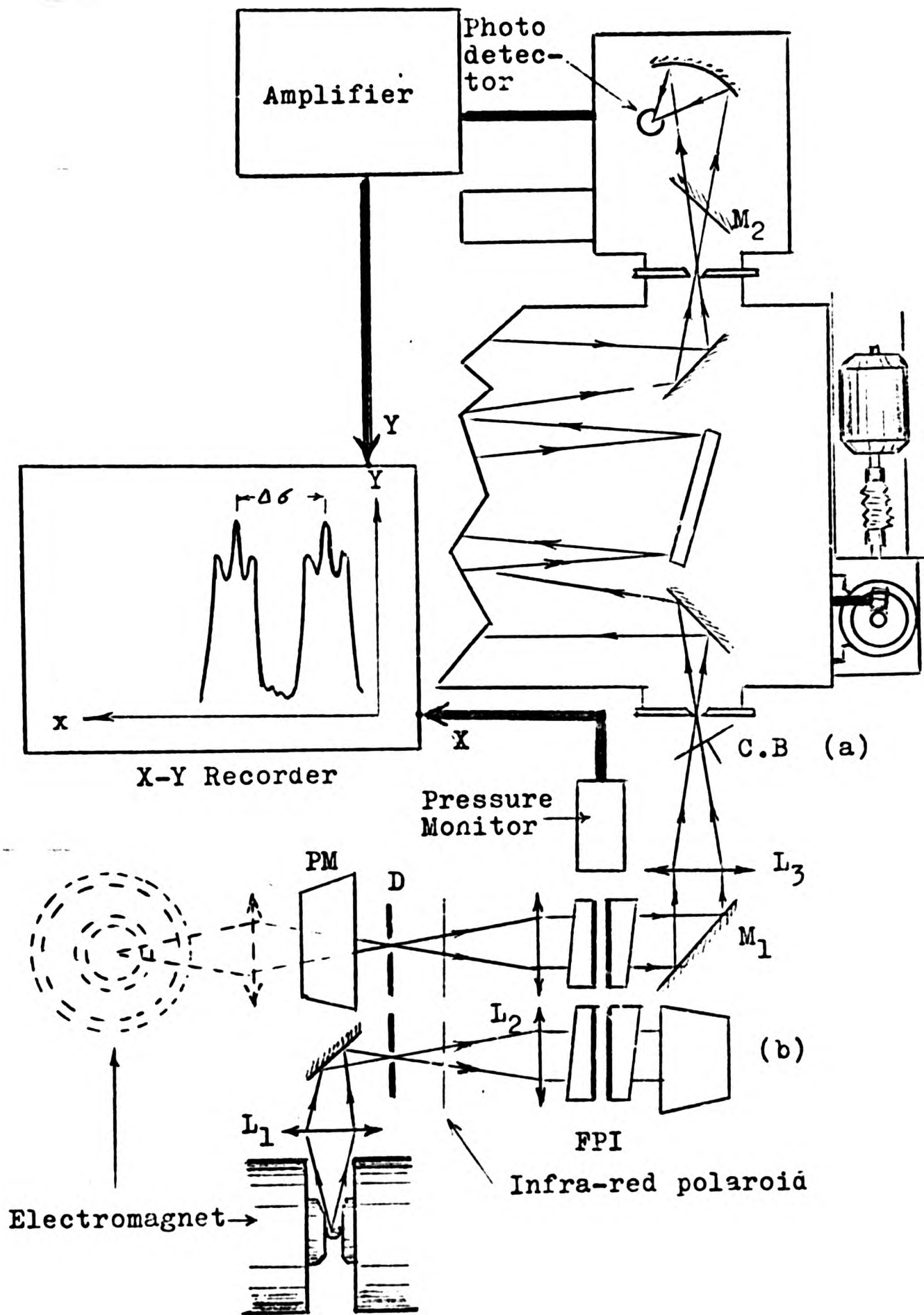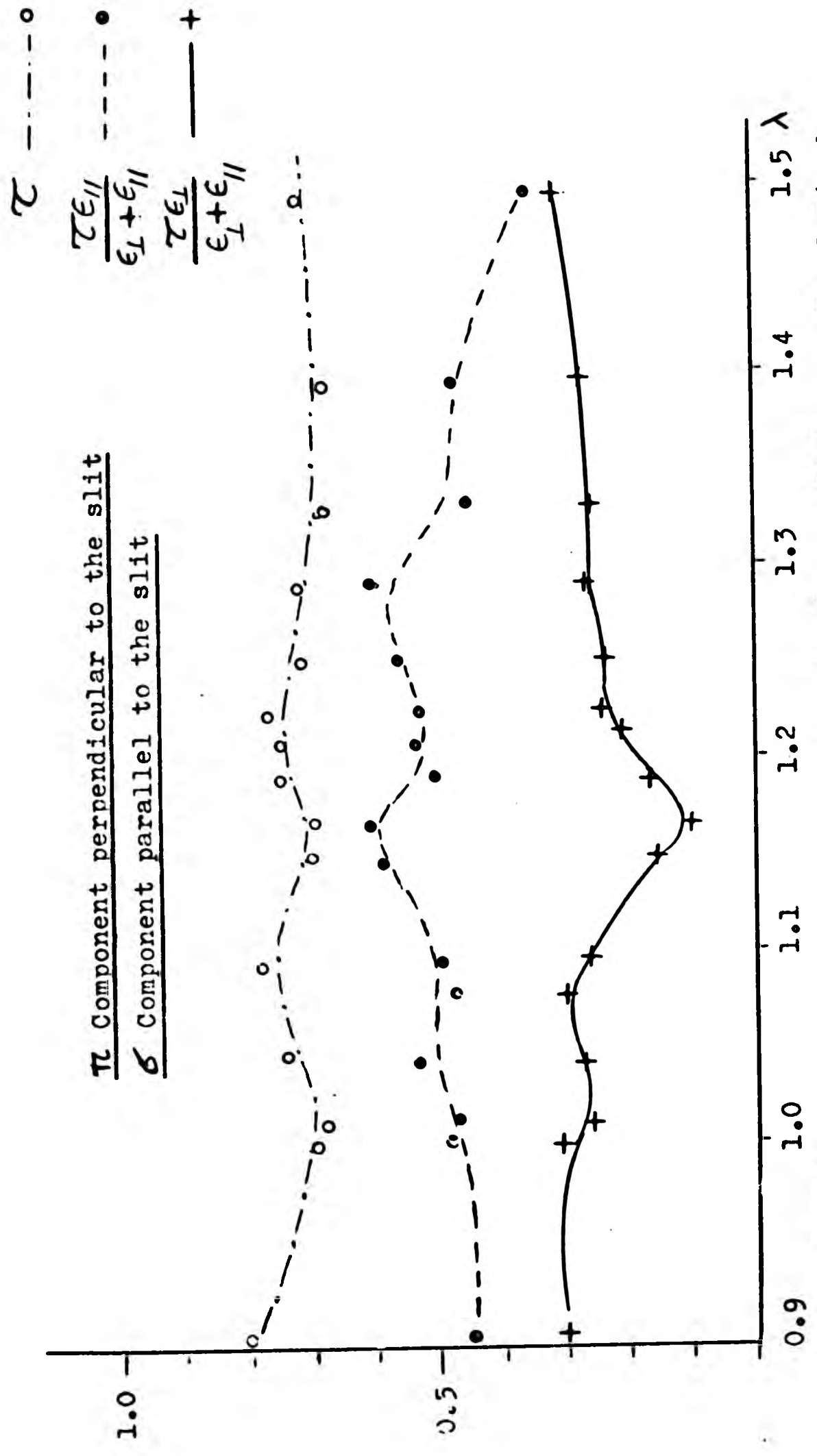
Figure 7-4: Optical arrangement for recording line profile

(a) Horizontal plane of the optical arrangement

(b) Vertical plane of the optical arrangement

the Fabry-Perot plates by the lens L_2 of focal length
30cm.

7-6 Effect of the polarization of the light on
the recorded signal

To isolate π or σ component of the light in zero
magnetic field, an infra-red plastic HR polaroid was
employed. A spectrum had been recorded without any
magnetic field to investigate the grating efficiency
($\epsilon_\perp$ and $\epsilon_{//}$) and transmissivity (τ) of the polaroid
for different components (electric vector perpendicular
and parallel to slit and grating rulings) over the whole
spectrum range of 0.79 - 2.7μm. The result of this
investigation is given in Graph 7-1 and 7-2 in
different orders of grating setting. The grating
efficiency for the electric vector perpendicular to the
slit is proportional to the height of the line signal
recorded when this component was selected by polaroid
positioned behind the diaphragm D in Figure 7-4.
The grating efficiency for the electric vector parallel
to the slit is similarly proportional to the appropriate
line signal. The ratio of $\tau\epsilon_\perp$ and $\tau\epsilon_{//}$ of a line
to the height of the line signal without polaroid
($\epsilon_\perp + \epsilon_{//}$) was calculated. The variation of these
ratios with wavelength in the first order 0.9μm to
1.5μ m and 1.7μm - 2.3μm and in the second order
0.9μm to 1.25μm of spectrum is shown in Graph 7-1
and 7-2. The Graph 7-1 and 7-2 shows a lower response

π Component perpendicular to the slit

σ Component parallel to the slit

τ

$\dfrac{2\varepsilon_{||}}{\varepsilon_{\perp}+\varepsilon_{||}}$
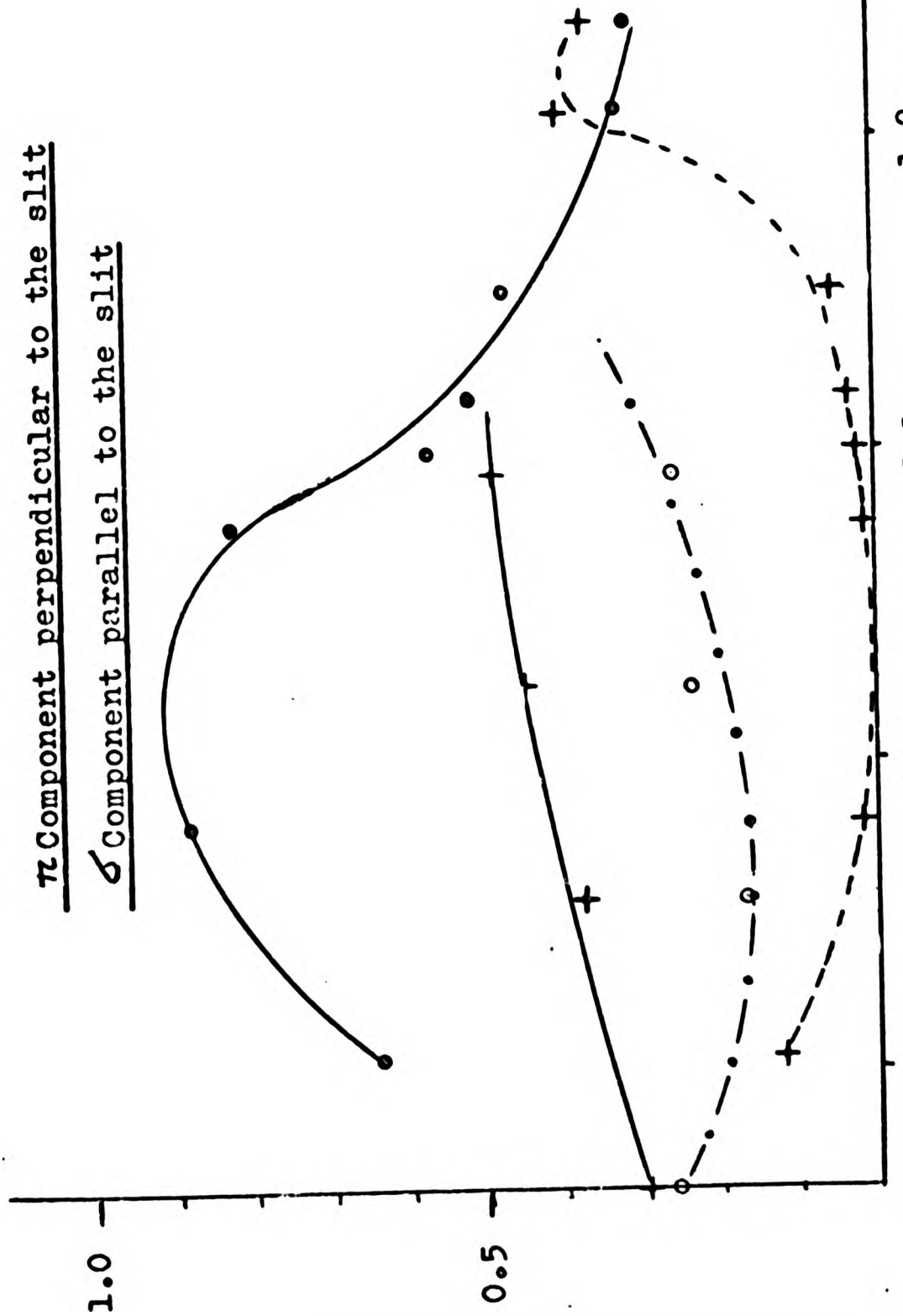
$\dfrac{\varepsilon_{\perp}+\varepsilon_{||}}{2}$

Graph 7-1: Transmissivity and grating efficiency ratio for polarized

Components in first order of wavelength 0.9 – 1.5 μ m.

$\dfrac{\tau \epsilon_{||}}{\epsilon_{||}+\epsilon_{\perp}}$

$\dfrac{\tau \epsilon_{||}}{\epsilon_{||}+\epsilon_{\perp}}$

$\dfrac{\tau \epsilon_{\perp}}{\epsilon_{||}+\epsilon_{\perp}}$

$\dfrac{\tau \epsilon_{\perp}}{\epsilon_{||}+\epsilon_{\perp}}$

π Component perpendicular to the slit

σ Component parallel to the slit

1.0

0.5

	1.0	1.1	1.2	1.3	λ
	2.0	2.2	2.4	2.6	

2nd Order 0.9

1st Order 1.8

Graph 7-2: Grating efficiency ratio for polarized components in first order 1.7-2.3μm and second order 0.9 - 1.25μm.

171

for the light with electric vector perpendicular to the slit. When the magnetic field is horizontal and the centre of the magnet is at the slit height, the π component of the zeeman pattern has its electric vector perpendicular to the slit, and therefore has a low response. However π components have a major role in the identification of line, whereas the σ components are less important since the overlapping orders is a major problem in the present technique.

To record the π components at maximum efficiency the system had to be arranged so that these components had their electric vector parallel to the slit. If the magnet and tube were retained at slit height this could only be achieved with a vertical field, i.e. the magnet on its side, which was not practical; however it could be achieved by holding the discharge tube in a horizontal position in the magnet below the main plane of the optical components. The vertical light beam then reflected by a mirror pivoted about a horizontal axis in the main optical plane. Maximum grating efficiency for the σ components could be achieved if required simply be rotating magnet and electrodeless discharge tube about a vertical axis. This rotation was already permitted by the stand for the magnet.

172

7-7 The Zeeman Effect Results

The results obtained in this investigation are classified due to the transitions involving the multiplets given in section 7-1. Seventeen lines in region 0.97μm to 1.25μm were investigated using plates A (section 7-3), three lines in region 1.25μm to 1.45μm using plates B, one line ($\lambda_{vac.} = 8196.95$ Å) using metallic coated quartz plates, and one line ($\lambda_{vac.} = 20429.84$ Å) was investigated without Fabry-Perot plates and pressure scanning, but the zeeman pattern was recorded by scanning the spectrum across the exit slit by rotating the grating, with the calibrating system.

Different magnetic field had to be applied due to the g value difference (Δg) and the overlapping of the σ component pattern in an individual transition. The results given in Table 7-1 for individual lines are average values obtained from various magnetic fields. The π components are given in brackets and the component separation from centre is listed in cm^{-1}. For some of the faint and overlapped patterns only π components were obtained; these are sufficient to support or reject the assignment made to a particular line. Table 7-2 gives the Landé g factors for the various levels involved.

The discussion of the observed zeeman patterns followed after the listed results in Table 7-1 and 7-2.

The patterns are listed in the following way:

TABLE 7-1:

Column (1)   the pattern number
Column (2)   the wavenumber of the line in cm^{-1}
Column (3)   the relative intensity
Column (4)   the quality and precision of the line
Column (5)   the Transition involved
Column (6)   the different magnetic field used
Column (7)   the pattern observed at present
             indicated by a (author), and the
             predicted pattern indicated by p

π Components are given in brackets.

TABLE 7-2:

Column (1)   the energy level involved in the
             assigned transition to the line
Column (2)   the theoretical g value
Column (3)   the previous observed g value listed
             in atomic energy level list of
             $ZrI^{(30)}$ indicated by NBS.
Column (4)   the observed g value in present
Column (5)   the wavenumber of the line in cm^{-1}

174

TABLE 7-1: Observed Zeeman Pattern of ZrI

Pat No.	Wave No in (cm^{-1})	Int.	Precision and Quality of the line	Transition	Magnetic field used in (T)	Zeeman Pattern
(1)	(2)	(3)	(4)	(5)	(6)	(7)
1	8091.00	290	A	$z^5D_0^o - a^5P_1$	0.41, 0.54, 0.65, 0.99	a – (0.00), 0.804 ± 0.01 p – (0.00), 0.756
2	8079.97	200	B	$z^5D_1^o - a^5P_2$	1.66	a – (0.00, 0.251 ± 0.01), 0.661 ± 0.01 p – (0.00, 0.209,), 0.63
3	8211.28	540	B	$z^5D_1^o - a^5P_1$	0.41, 0.65, 0.99	a – (0.322 ± 0.01), 0.815 ± 0.01, 0.483 ± 0.01 p – (0.288), 0.759, 0.470
4	8307.26	770	B	$z^5D_2^o - a^5P_2$	1.41, 1.66	a – (0.256 ± 0.005, 0.525 ± 0.005) p – (0.294 , 0.588)

TABLE 7-1 (Continued)

(1)	(2)	(3)	(4)	(5)	(6)	(7)
5	8367.25	580	B	$z^5D^o_3 - a^5P_3$	0.85, 1.73	a – (0.165 ± 0.02, 0.303 ± 0.02, 0.441 ± 0.01), p – (0.129, 0.258, 0.388)
6	8438.56	460	B	$z^5D^o_2 - a^5P_1$	0.65, 0.85, 0.99	a – (0.00, 0.305 ± 0.01), 0.139 ± 0.01, 0.444 + 0.01, 0.777 ± 0.01), 0.121 p – (0.00, 0.318), 0.440, 0.759
7	8608.92	900	A	$z^5D^o_3 - a^5P_2$	0.99, 1.45, 1.66	a – (0.00, 0.252 ± 0.01, 0.504 ± 0.01), p – (0.00, 0.248, 0.496)

TABLE 7-1 (Continued)

(1)	(2)	(3)	(4)	(5)	(6)	(7)
8	9760.25	110	A	$z^5G^o_2 - a^5F_2$	0.99, 1.45	a − (0.389 ± 0.01, 0.778 ± 0.01) − (0.372 , 0.745)
9	9913.14	380	A	$z^5G^o_2 - a^5F_1$	1.45, 1.73	a − (0.00, 0.297 ± 0.01), 0.293 ± 0.01, 0.566 ± 0.01 p − (0.00, 0.347), 0.347 , 0.695
10	7942.00	77	A	$x^5D^o_3 - a^5D_3$	0.65, 0.85	a − (0.00), 0.595 ± 0.005 p − ( ),
11	7986.52	185	A	$x^5D^o_4 - a^5D_4$	0.65, 0.85	a − (0.00), 0.452 ± 0.005 p − ( ),

177

TABLE 7-1 (Continued)

(1)	(2)	(3)	(4)	(5)	(6)	(7)
12	8046.47	54	A	$x^5D_2^o - a^5D_1$	0.65, 0.85	a – (0.00), 0.476 ± 0.005 p – ( ),
13	7086.92	55	A	$y^3D_1^o - b^3P_1$	0.65, 0.85, 0.99, 1.27	a – (0.383 ± 0.005), 0.256 ± 0.005, 0.604 ± 0.005 p – ( ),
14	7387.73	75	A	$y^3D_2^o - b^3P_1$	1.45, 1.6, 1.75	a – (0.00, 0.297 ± 0.005) 0.631 ± 0.01, ,), p – (, ,
15	7394.61	75	A	$y^3D_1^o - b^3P_0$	1.45, 1.75	a – (0.00), 0.338 ± 0.01 p – ( ),

178

TABLE 7-1 (Continued)

(1)	(2)	(3)	(4)	(5)	(6)	(7)
16	9196.70	115	A	$y^3D_2^0 - a^3D_1$	0.85, 0.99, 0.925	a – (0.00, 0.242 ± 0.001) p – (0.00, 0.229)
17	9309.24	460	A	$y^3F_4^0 - a^3D_3$	1.45, 1.75	a – (0.00, , , ,),0.791 ± 0.01 0.854 ± 0.01, 0.917 ± 0.01 p – (0.00,0.154,0.316,0.474), 0.467,0.616 0.765,0.914,1.06,1.212,1.361
18	9474.43	170	A	$y^3F_2^0 - a^3D_1$	1.45	a – (0.00, 0.296 ± 0.01) p – (0.00, 0.318)
19	9791.17	310	A	$z^3G_5^0 - a^3G_5$	0.99, 1.45	a – (0.00), 0.820 ± 0.005 p – (0.007), 0.819

179

TABLE 7-1 (Continued)

(1)	(2)	(3)	(4)	(5)	(6)	(7)
20	11916.47	86	C	$z^5F_1^o - a^5F_1$	1.79	a – (0.252 ± 0.01), 0.252 ± 0.005 p – (0.249), 0.249
21	12199.66	19	B	$z^5S_2^o - a^5P_1$	1.71	a – (0.00, 0.404 ± 0.01) p – (,)
22	4894.80	80	A	$z^3P_1^o - b^3P_0$	0.65, 0.85, 0.99, 1.45	a – (0.00), 1.024 ± 0.005 p – (0.00), 1.022

TABLE 7-2: Observed g values

Level involved	g_{L-S}	g_{NBS}	g_a	Wavenumber σ in cm^{-1}
(1)	(2)	(3)	(4)	(5)
a^5P_1	2.5	2.5	2.65 ± 0.03	8091.00
			2.67 ± 0.03	8211.28
			2.56 ± 0.01	8438.56
a^5P_2	1.83	1.82	1.85 ± 0.01	8079.97
$z^5D_1^o$	1.5	1.55	1.53 ± 0.01	8079.97
			1.59 ± 0.03	8211.28
$z^5D_2^o$	1.5	1.45	1.46 ± 0.01	8438.56
$z^5G_2^o$	0.33	0.43	0.362 ± 0.01	9913.14
a^5D_1	1.5	–	1.57 ± 0.02	8046.47
a^5D_3	1.5	–	1.5 ± 0.01	7942.00
a^5D_4	1.5	–	1.49 ± 0.02	7986.52
$x^5D_2^o$	1.5	1.54	1.57 ± 0.02	8046.47
$x^5D_3^o$	1.5	1.48	1.5 ± 0.01	7942.00
$x^5D_4^o$	1.5	1.46	1.49 ± 0.01	7986.52
$y^3D_1^o$	0.50	0.52	0.53 ± 0.01	7086.92
			0.498 ± 0.01	7394.61

181

TABLE 7-2:(Continued)

(1)	(2)	(3)	(4)	(5)
$y^3D^o_2$	1.16	1.14	1.139 ± 0.01	7387.73
b^3P_1	1.5	–	1.52 ± 0.01	7086.93
			1.504 ± 0.01	7387.73
$z^3G^o_5$	1.20	1.21	1.21 ± 0.005	9791.17
a^3G_5	1.20	1.20	1.21 ± 0.005	9791.17
$z^5F^o_1$	0.00	0.30	0.299 ± 0.005	11916.47
$z^5S^o_2$	2.00	–	1.99 ± 0.01	12199.66
$z^3P^o_1$	1.5	1.51	1.512 ± 0.005	4894.80

7-8 The Zeeman Effect – Discussion

Three lines (pattern 10, 11 and 12) of multiplet
x^5D^o – a^5D were all resolved to one sharp π component
at centre and only two sharp σ components symmetric
to the centre. No experimental g value is listed in
the atomic energy level list of the zirconium for
a^5D, but the theoretical value for all ^5D level is 3/2
and the observed value of g at present shows that the
actual value is not significantly different from this.
The assignment of the transitions x^5D^o – a^5D to the
above three lines are supported by their intensities

182

and since the g value for ^5D is equal to 3/2 independent of J value, the transition from ^5D to ^5D will give a triplet pattern in a magnetic field.

Two lines of multiplet $y^3D - b^3P$ (Pattern 13, and 14) were studied for zeeman effect. Both lines involve the level at 15932.10 cm^{-1} listed in Atomic Energy Levels [30] as b^3P_2, but the zeeman patterns obtained did not confirm involvement of a $^3P_2$ level. In transition $y^3D_2 - b^3P_2$ pattern 14 was obtained which had a central π component and two other π components symmetrical to the centre, and in transition $y^3D_1^o - b^3P_2$ the pattern 13 had only two π components symmetrical to the centre and no central component was observed. The patterns obtained clearly confirmed an involvement of $^3P_1$. The level 15932.10 cm^{-1} is involved in four observed transitions with levels J = 2:—

$$y^3F_2^o - 15932.10 \qquad \sigma = 7665.41 \text{ cm}^{-1} \quad \text{int} = 54 \text{ A}$$
$$z^3F_2^o - 15932.10 \qquad \sigma = 10129.24 \text{ cm}^{-1} \quad \text{int} = 8 \quad \text{B}$$
$$x^3D_2^o - 15932.10 \qquad \sigma = 10625.17 \text{ cm}^{-1} \quad \text{int} = 28 \text{ A}$$
$$y^3D_2^o - 15932.10 \qquad \sigma = 7387.73 \text{ cm}^{-1} \quad \text{int} = 75 \text{ A}$$

In each case a transition to the corresponding level with J = 3 would be expected but these were not observed; on the other hand, the transition from $z^3P_o^o$

183

(σ = 4301.87 cm^{-1}) was observed at 4301.93 cm^{-1}, intensity **6** B. The observed Landé factor for the disputed level was 1.504 $\pm$ 0.01; in many cases, the observed g values have been close to that for L-S coupling, and this again supports the case for assignment of 15932.10 cm^{-1} as b^{3}P$_1$ (L-S g value, 1.5).

The line σ = 7394.61 cm^{-1} (pattern 15) could not be assigned to any available transition when it was compared with the predicted lines from the energy levels. The zeeman pattern obtained had one sharp π component at centre (0.00) and two sharp σ components symmetrical to the centre. The result of the calculation suggested an involvement of:

(i) $A_1 - B_0$ with g = 0.498 $\pm$ 0.01

or (ii) $A_x - B_{x + 0, \pm 1}$ with g = g^1 = 0.498 $\pm$ 0.01

Since the value found for g resembles the g factors of y^{3}D$_1^0$ (0.52), one may suggest the involving transition to be y^{3}D$_1^0$ - b^{3}P$_0$ with b^{3}P$_0$ = 15624.31 cm^{-1} which is not quoted in the Atomic Energy Level list of zirconium. This was supported by assignment of three following observed lines to the transitions involving b^{3}P$_0$ and by studying of zeeman effect of one of these lines (pattern 22). The lines assigned

to the transitions involving b^3P_0 are given in
Table 7-3. The assignment is further supported by
the data in Table 7-4, giving the observed transitions
from the same upper levels to 15932.10 cm^{-1}, now
reclassified as b^3P_1.

TABLE 7-3: The assignment of the transitions
involving b^3P_0 to observed lines

Observed Wave No. in cm^{-1}	Relative intensity	Transition	Calculated wave No from energy levels in cm^{-1}
4894.80	80 A	$z^3P_1^o - b^3P_0$	4894.89
6349.90	15 A	$z^3S_1^o - b^3P_0$	6349.87
10529.76	23 B	$x^3D_1^o - b^3P_0$	10529.82
7394.61	75 A	$y^3D_1^o - b^3P_0$	7394.61

TABLE 7-4: Some lines assigned to the transitions
involving 15932.10 cm^{-1} (b^3P_1)

Observed Wave No in cm^{-1}	Relative intensity	Transition	Calculated wave No from energy levels in cm^{-1}
4534.94	19 A	$z^3P_2^o - b^3P_1$	4534.73
4587.17	15 A	$z^3P_1^o - b^3P_1$	4587.10
4301.93	6 B	$z^3P_0^o - b^3P_1$	4301.87

TABLE 7-4 (Continued)

Observed Wave No in cm^{-1}	Relative intensity	Transition	Calculated wave No from energy levels in cm^{-1}
6042.25	60 A	$z^3S_1^o - b^3P_1$	6042.08
7086.92	55 A	$y^3D_1^o - b^3P_1$	7086.82

The pattern 17 obtained for the line $\sigma = 9309.24$ cm^{-1} assigned to $y^3F_4^o - a^3D_3$ (with g_{NBS} for $y^3F_4^o$ 1.13 and g_{NBS} for a^3D_3 1.35), has a nearly sharp and strong central π component and was not resolved as expected. This pattern resembles a patters expected from multiplet $f^5G_2 - v^3P_1^o$ (9309.38 cm^{-1}) with both g and g' values to be found. If the transition involved can be considered to be $f^5G_2 - v^3P_1^o$ then, g value for f^5G_2 observed to be 1.26 and for $v^3P_1^o$, 1.36. But the other members of this multiplet ($f^5G - v^3P^o$) could not be found and the intensity of the line do not support the involvement of $f^5G_2 - v^3P_1^o$.

The line $\sigma = 7456.53$ cm^{-1} assigned to the transition $e^5F_4 - x^3G_3^o$ with g = 1.35 for e^5F_4 and g' = 0.75 for $x^3G_3^o$ was studied for zeeman effect. The pattern obtained had only a very sharp and strong central π component which is not an expected pattern

186

for this transition with such g values in a strong
magnetic field, therefore the assigned transition can
not be supported.

CHAPTER 8

CONCLUSIONS AND SUGGESTED FURTHER WORK

In Chapter 5, a line list of 218 manganese spectra lines in the region 0.8 - 1.97 μm is given. A number of these lines were observed with pronounced hyperfine structure. The total spread of the components may exceed 0.5 cm^{-1} in these lines. Lines in multiplet e^6S-y^6P^0 and w^6F^0-e^6D are even broader, and no hyperfine structure data is available for these lines. Fine structure components with intervals often less than 1 cm^{-1} have been observed in many terms. One example of this case is the broad lines of multiplet z^8F^0-e^8D, where it was impossible to separate the fine structure components. These results obtained in manganese spectrum measurements suggest a need of further investigation of the spectrum, particularly the hyperfine structure of the levels of this element. Pressure-scanning Fabry-Perot interferometer is a suitable technique for this investigation.

A few cases of high differences in the measured wavenumbers and the predicted wavenumbers from the energy levels of neutral manganese have been observed, particularly in multiplet y^8P^0-e^8S for the level $y^8P^0_{9/2}$ (0.79 cm^{-1}) which suggest a further work of checking the accuracy of some levels.

A repeated pattern of the group of lines has been observed in the region 10260 Å to 10492.7 Å which appears likely to be a band structure; this also needs a further

investigation into the cause, whether or not these are bands, by using electrodeless discharge tubes of manganese chloride or taking photographic plates of manganese arcs.

In Chapter 6 the zirconium lines in the spectral region of 0.8 - 2.7 µm have been re-measured and 181 new additional lines in this region have been observed. The comparison of the present measured wavenumbers with the measurements made in 1976 confirmed the accuracy of both measurements within the limitation of the precision assigned to the measurements. In view of the results obtained at the present time which support the measurements of 1976, this confirms the suggestion made in 1976 that all the zirconium spectra in the visible region should be re-measured and a position adjustment of the levels is desirable.

In Chapter 7 the investigation into the phenomenon of the Zeeman effect of the infrared lines of zirconium was carried out. In this investigation 22 lines in a limited bandwidth of 0.48 µm in the region 0.97 - 1.45 µm have been studied. It was limited to the region 0.97 - 1.45 µm due to the availability of the suitably coated F.P. plates. The result of the observation led to the calculation of a new level, 15624.31 cm^{-1} (b^{3}p^0) and confirmation of the level 15932.10 listed in MnI energy level to be b^{3}P$_1$ and not b^{3}P$_2$. In this limited region of investigation 5 new Landé g factors were also observed and, as the range of the spectrum extends to 2.7 µm, it is suggested by the results that a further investigation of

189

the Zeeman effect is desirable by using pressure-scanning
Fabry-Perot and suitable multi-layer dielectric coated
plates.

REFERENCES

(1)   AG Taklif (1976), M. Phil thesis, University of
       London.

(2)   M. Outred (1978), Journal of Physical and Chemical
       Reference Data, Volume 7, No. 1, pages 1-262 N.B.S

(3)   W.F. Meggers and F.O. Westfall (1950), Lamps and
       Wavelength of Mercury 198. J. Res. Nat. Bur. Std.
       44,447-455.

(4)   C.H. Corliss and W.F. Meggers (1958), Improved
       Description of Hafnium Spectra. J. Res. Nat. Bur.
       Std. 61,295-324.

(5)   W.F. Meggers and R.W. Stanley (1958), J. Res. Nat.
       Bur. Std. 61, 95.

(6)   R.M. Dagnall, K.C. Thomson and T.S. West (1967),
       Talanta, 14. 557

(7)   O. Giarcia-Riquelme (1949), Estructura y nuevos
       niveles energeticos del spectro arco del manganese
       Anales Soc. Espan. Fis. y Quim., 45A,435-448,547-576.

(8)   W.F. Meggers (1933), The Infra-red Arc Spectra of
       Manganese and Rhenium. J.R es. Nat. Bur. Std. 10,
       757-769.

(9)   H.M. Randall and E.F. Barker (1919), The Infra-red
       Arc Spectra of Cobalt, Nickel, Manganese and Chromium.
       Astrophys. J. 49,59-63.

(10)   C.E. Moore (1952), Atomic Energy Levels as Derived
       from the Analysis of Optical Spectra. N.B.S. Cir.
       467, Vol 2, 27-31.

(11)   O. Giarcia-Riquelme (1962), Unpublished Zeeman data
       for Mn I June 1962 (Paper 68 A1-252).

(12)   M.A. Catalon, W.F. Meggers and O. Giarcia-Riquelme
       (1964), J. of Res. Nat. Bur. Std. - A. Physics and
       Chemistry Vol. 68A, No.1.

(13)   C. Corliss and J. Sugar (1977), J. Phys. Chem. Ref.
       Data. Vol. 6, No. 4. Energy Levels of Manganese,
       Mn I Through Mn XXV.

(14)   W.F. Meggers (1931), B. S. Jour. Research Vol. 6
       (RP 322), P. 1027.

(15)   C.C. Kiess and H.K. Kiess (1931), J. Res. Bur. Std.
       6, 621-669.

(16)   Meggers and Kiess (1932), J. Res. Bur. Std., 9, 324-326.

(17)   Kiess and Lang (1930), J. Res. Bur. Std., 5, 305.

(18)   G.R. Harrison (1952), Massachusetts Institute of Technology Wavelength Tables (John Wiley and Sons, INC, New York).

(19)   E.H. Howe (1958), J. Opt. Soc. Am., 48, 28-30.

(20)   C.C. Kiess and H.K. Kiess (1931), Bur. Std. J. Research 6, 621, RP296.(IP)(T)(CL)(ZE)(ED).

(21)   P.M. Sancho (1932), Anal. Soc. Esp. de Fisca Y Quimica (Madrid) 30, 867 (ZE).

(22)   P. Jacquinot (1958), J. Phys. Radium 19,223.
       P. Jacquinot (1960), Rep. Progr. Physics 23,267.

(23)   R. Beer and J. Ring (1961), Vol. 1. PP.94-103 Pergamon Press Ltd. Printed in Great Britain.

(24)   K.L. Aldous, D. Alger, R.M. Dagnall and West (1970), Lab. Pract., 587.

(25)   M. Outred, C.B. Hamand (1980), J. Phys. D: Appl. Phys., 13. Printed in Great Britain.

(26)   C.G. Fastie (1952), J. Opt. Soc. Am., 42, 641.

(27)   R. Chabbal (1958), J. Phys. Radium. 19,295.

(28)   A.P. Thorne (1974), Spectrophysics, Chapman and Hall, London.

(29)   A. Giacchetti, J. Blaise, C.H. Corliss and R. Zalubas (1974), J. Res. Nat. Bur. Std., 78A, 247-281.

(30)   C.E. Moore (1952), Atomic Energy Levels. NBS, Circ 467, Vol. 1 (U.S. Government Printing Office, Washington DC).

(31)   H.E.White and R. Ritschl (1930), Phys. Rev 35, 1146

(32)   Fisher and Peck (1939), Phys. Rev 55, 270.

APPENDIX 1   A comparison of zirconium infra-red wavenumbers measured with accuracy of A (i.e. estimated error ± 0.02 cm⁻¹) in present time and measurements made in 1976

Zr tube in 1 in. diam. cavity σ cm⁻¹ (1)	Zr tube in 2 in. diam. cavity σ cm⁻¹ (2)	Average measured wave No. of Zr cm⁻¹ (3)	Previously measured wave No. of Zr cm⁻¹ (4)	Calculated wave No. of Zr from energy level cm⁻¹ (5)	Relative intensity (6)	Wave No. difference (7)
3793.27	3793.33	3793.30 A	3793.26 A		43	0.04
3944.73	3944.79	3944.76 A	3944.74 A		15	0.02
3980.08	3980.09	3980.08 A	3980.08 B		38	0.00
4083.41	4083.41	4083.41 A	4083.38 A	4083.27	42	0.03
4500.72	4500.67	4500.69 A	4500.70 A		22	−0.01
4507.76	4507.73	4507.74 A	4507.73 A		10	0.01
4521.56	4521.53	4521.54 A	4521.52 A	4521.57	25	0.02
4535.01	4534.96	4534.98 A	4534.94 A	4534.73	19	0.04
4565.25	4565.21	4565.23 A	4565.21 A	4565.27	10	0.02
4587.19	4587.16	4587.17 A	4587.17 A	4587.10	15	0.00

(1)	(2)	(3)	(4)	(5)	(6)	(7)
4656.04	4655.98	4656.01 A	4655.97 A	4655.79	170	0.04
4723.14	4723.10	4723.12 A	4723.10 A	4723.14	20	0.02
4795.70	4795.62	4795.66 B	4795.64 A	4795.60	100	0.02
4831.66	4831.61	4831.63 A	4831.63 A	4831.46	28	0.00
4884.08	4884.02	4884.05 A	4884.04 A	4884.13	18	0.01
4887.81	4887.74	4887.77 A	4887.74 A	4887.60	200	0.03
4946.61	4946.54	4946.57 A	4946.55 A		20	0.02
5014.12	5014.04	5014.07 A	5014.06 A	5014.28	14	0.01
5016.32	5016.27	5016.29 A	5016.27 A		12	0.02
5079.90	5079.94	5079.92 A	5079.89 A	5079.80	20	0.03
5548.68	5548.62	5548.65 A	5548.63 A		18	0.02
5562.83	5562.81	5562.82 A	5562.79 A	5562.51	20	0.03
5570.74	5570.69	5570.71 A	5570.71 A		23	0.00
7352.77	7352.72	7352.74 A	7352.79 A	7352.80	32	-0.05
7387.77	7387.71	7387.74 A	7387.74 A	7387.76	75	0.00

(1)	(2)	(3)	(4)	(5)	(6)	(7)
7394.66	7394.57	7394.61	B 7394.61 A		75	0.00
7406.99	7406.93	7406.96	A 7406.95 A		10	0.01
7444.28	7444.26	7444.27	A 7444.24 A	7444.24	310	0.03
7575.39	7575.38	7575.38	A 7575.36 A	7575.38	50	0.02
7585.95	7585.97	7585.96	A 7585.92 A		12	0.04
7586.98	7586.98	7586.98	A 7586.94 A		15	0.04
7602.72	7602.68	7602.70	A 7602.66 A		85	0.04
7665.46	7665.39	7665.42	A 7665.41 A		54	0.01
7828.23	7828.25	7828.24	A 7828.23 A		11	0.01
7876.09	7876.13	7876.11	A 7876.10 A		8	0.01
7903.75	7903.76	7903.77	A 7903.77 B		55	-0.02
7925.54	7925.53	7925.53	A 7925.52 B		5	0.01
7974.14	7974.22	7974.18	B 7974.17 A		5	0.01
7977.28	7977.29	7977.28	A 7977.27 A	7977.23	8	0.01
7988.60	7988.64	7988.62	A 7988.64 A		17	-0.02

(1)	(2)	(3)	(4)	(5)	(6)	(7)
8080.02	8080.01	8080.01 A	8079.97 B	8079.88	200	0.04
8091.06	8091.04	8091.05 A	8091.00 A	8091.00	290	0.05
8143.63	8143.57	8143.60 A	8143.56 A	8143.59	60	0.04
8188.65	8188.58	8188.61 B	8188.54 A		6	0.07
8192.55	8192.49	8192.52 A	8192.48 A	8192.41	310	0.04
8199.55	8199.52	8199.53 A	8199.51 A	8199.48	77	0.02
8211.35	8211.27	8211.31 B	8211.28 B	8211.17	540	0.03
8233.86	8233.84	8233.85 A	8233.81 B		23	0.04
8235.54	8235.50	8235.52 B	8235.46 A		20	0.06
8239.25	8239.21	8239.23 A	8239.19 A	8239.19	35	0.04
8307.29	8307.26	8307.27 A	8307.26 B	8307.19	770	0.01
8350.05	8350.11	8350.08 A	8350.04 A		20	0.04
8373.70	8373.72	8373.71 A	8373.68 A		26	0.03
8407.02	8407.05	8407.03 A	8307.01 A		30	0.02
8430.41	8430.41	8430.41 A	8430.39 A		11	0.02

(1)	(2)	(3)		(4)		(5)	(6)	(7)
8575.43	8575.44	8575.43	A	8575.40	A	8575.40	1500	0.03
8786.74	8786.78	8786.76	A	8786.71	A	8786.63	51	0.05
8870.21	8870.19	8870.20	B	8870.13	A	8870.09	29	0.07
8936.51	8936.47	8936.49	A	8936.49	B		70	0.00
8970.99	8970.83	8970.91	C	8970.92	A	8971.08	17	-0.01
9088.80	9088.64	9088.72	B	9088.74	A	9088.67	70	-0.02
9099.70	9099.57	9099.63	B	9099.66	A	9099.44	20	-0.03
9185.75	9185.59	9185.67	A	9185.70	A	9185.69	32	-0.03
9196.81	9196.61	9196.71	C	9196.70	A	9196.85	115	0.01
9199.36	9199.22	9199.29	B	9199.31	A		98	-0.02
9208.63	9208.48	9208.55	B	9208.53	A	9208.45	62	0.02
9248.66	9248.58	9248.62	A	9248.65	A	9248.69	51	-0.03
9309.33	9309.11	9309.22	A	9309.25	A	9309.27	460	-0.03
9346.09	9345.92	9345.99	B	9346.00	A	9345.89	550	-0.01
9366.52	9366.34	9366.43	C	9366.44	A	9366.42	123	-0.01

(1)	(2)	(3)		(4)		(5)	(6)	(7)
9383.53	9383.33	9383.43	C	9383.44	A	9383.42	570	-0.01
9474.52	9474.31	9474.41	C	9474.44	A	9474.46	17	-0.03
9581.65	9581.45	9581.55	C	9581.58	A	9581.47	54	-0.03
9633.88	9633.69	9633.78	C	9633.79	A	9633.84	21	-0.01
10986.19	10986.12	10986.15	A	10986.12	A	10985.99	50	0.03
11023.13	11023.05	11023.09	B	11023.07	B	11023.04	150	0.02
11089.47	11089.44	11089.45	B	11089.38	A	11089.36	120	0.07
11094.16	11094.12	11094.14	A	11094.09	B	11094.03	58	0.05
11180.51	11180.40	11180.45	B	11180.46	A	11180.43	40	-0.01
11220.25	11220.13	11220.19	B	11220.17	A	11220.27	12	0.02
11224.84	11224.83	11224.83	B	11224.75	A	11224.75	26	0.08
11233.54	11233.49	11233.51	A	11233.51	A	11233.52	170	0.00
11303.50	11303.51	11303.50	A	11303.47	C	11303.39	20	0.03
11314.11	11314.09	11314.10	A	11314.05	B	11314.22	130	0.05
11354.11	11354.10	11354.10	A	11354.06	B	11354.02	30	0.04

(1)	(2)	(3)	(4)	(5)	(6)	(7)
11378.25	11378.28	11378.26 A	11378.20 A	11378.20	21	0.06
11645.99	11646.05	11646.02 A	11345.98 A	11646.00	27	0.04
11667.31	11667.28	11667.29 A	11667.32 A	11667.33	30	−0.03
11820.50	11820.57	11820.53 B	11820.56 A	11820.52	17	−0.03
12015.63	12015.77	12015.70 B	12015.72 A	12015.72	13	−0.02
12068.32	12068.42	12068.37 B	12068.39 A	12068.41	32	−0.02
12173.04	12173.06	12173.05 A	12173.09 A	12173.10	58	−0.04
12387.97	12387.97	12387.97 A	12388.01 B	12387.99	30	−0.04

APPENDIX 2

<u>TABLE A$_2$-1:-</u> The measured values for reflectivity R, absorptivity A, and transmissivity, T in glass metallic coated plates.

Wavelength (nm)	Plate A			Plate B		
	R	A	T	R	A	T
400	82.8%	11.0%	6.2%	83.7%	10.5%	5.8%
500	84.4%	11.4%	4.2%	85.0%	11.0%	4.0%
600	85.0%	11.7%	3.3%	85.4%	11.3%	3.3%
700	83.8%	13.2%	3.0%	84.1%	12.9%	3.0%
800	81.3%	15.9%	2.8%	82.0%	15.2%	2.8%

<u>TABLE A$_2$-2:-</u> The measured values for reflectivity, R, absorptivity A, and transmissivity T in quartz metallic coated plates.

Wavelength (nm)	Plate A			Plate B		
	R	A	T	R	A	T
400	69.2%	16.7%	14.1%	70.9%	15.4%	13.7%
500	74.45%	15.75%	9.8%	75.9%	14.3%	9.8%
600	75.91%	16.49%	7.6%	77.29%	15.11%	7.6%
700	75.44%	18.16%	6.4%	76.79%	16.81%	6.4%
800	73.06%	20.74%	6.2%	74.33%	19.47%	6.2%

APPENDIX 3

TABLE A_3-1:— Half-width and intensity variation for zirconium 587.98 nm line profile vs. incident power in slab line and Broida Cavities for tube a (6 mm diam. and nearly 5 cm. length).

Slab line cavity			Small Broida cavity		
Photomultiplier voltage = 670 V			Photomultiplier voltage = 700 V		
Spacer = 6 mm. = 0.8333 cm^{-1}			Spacer = 1.5 mm. = 0.3333 cm^{-1}		
Incident Power (Watts)	Relative Intensity	Half Width (mK)	Incident Power (Watts)	Relative Intensity	Half Width (mK)
35	13	110±4	50	24	100±2
37.5	12	110±4	60	85	105±2
40	10	127±4	70	198	103±2
80	13.5	110±4	75	290	108±2
90	16.5	110±4	90	285	119±2
100	46	110±4			
110	144	149±5			

APPENDIX 3 (Continued)

TABLE A_3-2:- Half-width and intensity variation for zirconium 587.98 nm line profile vs. incident power in slab line and Broida Cavities for tube b (6 mm. diam. and nearly 3 cm. length).

Slab line Cavity

Photomultiplier
voltage = 670 V
Spacer = 6 mm.
    = 0.8333 cm^{-1}

Small Broida Cavity

Photomultiplier
voltage = 700 V
Spacer = 1.5 mm.
    = 0.3333 cm^{-1}

Incident Power (Watts)	Relative Intensity	Half Width (mK)	Incident Power (Watts)	Relative Intensity	Half Width (mK)
70	3	114±4	45	13	121±2
75	4	123±4	50	24	140±2
80	29	136±4	55	80	149±2
85	30	144±4	60	145	200±2

APPENDIX 3 (Continued)

TABLE A_3-3:- Half width and intensity variations for
zirconium 587.98 nm line profile vs.
incident power in slab line and Broida
Cavities for tube c (6 mm. diam. and
nearly 3 cm. length).

Slab line cavity			Small Broida Cavity		
Photomultiplier voltage = 670 V			Photomultiplier voltage = 700 V		
Spacer = 6 mm. = 0.8333 cm^{-1}			Spacer = 6 mm. = 0.8333 cm^{-1}		
Incident Power (Watts)	Relative Intensity	Half Width (mK)	Incident Power (Watts)	Relative Intensity	Half Width (mK)
30	23	114±4	35	8	119±4
42.5	20	114±4	40	6	119±4
47.5	31	114±4	42.5	11	119±4
50	53	119±4	45	45	127±4

IV